Universidade de São Paulo
Instituto de Astronomia, Geofísica e Ciências Atmosféricas
Departamento de Astronomia

Hugo Alberto Folonier

Maré em satélites planetários diferenciados. Aplicação à Titã.

Tide on differentiated planetary satellites. Application to Titan.

São Paulo
2016

Hugo Alberto Folonier

Maré em satélites planetários diferenciados. Aplicação à Titã.

Tide on differentiated planetary satellites. Application to Titan.

Tese apresentada ao Departamento de Astronomia do Instituto de Astronomia, Geofísica e Ciências Atmosféricas da Universidade de São Paulo como requisito parcial para a obtenção do título de Doutor em Ciências. Versão Corrigida. O original encontra-se disponível na Unidade.

Área de Concentração: Astronomia

Orientador: Prof. Dr. Sylvio Ferraz Mello

São Paulo

2016

Para mis amores

Euge y Lulita

por su amor y compañia

Acknowledgements

Eu gostaria muito de agradecer a todas as pessoas que de uma forma ou outra, ajudaram a que pudesse fazer esta tese. Dentre elas, quero mencionar especialmente:

A Sylvio Ferraz Mello, por me dar esta maravilhosa oportunidade de trabalhar com ele. Não tenho palavras para lhe agradecer a sua disposição, paciência e sabedoria compartida, sem a qual, esta tese não teria sido possível.

A Tatiana Michtchenko, pelo conhecimento adquirido pelas disciplinas, além de sua confiança, colaboração e apoio brindado durante todo este período.

Aos professores que participarom da comissão julgadora Adrian Rodríguez, Clodoaldo Ragazzo, Nelson Callegari Jr. e Lucas Ruis dos Santos pelas discussões e sugestões que ajudaram a enriquecer este trabalho.

A Konstantin V. Kholshevnikov, pela colaboração e sugestões no artículo apresentado.

A meus Profesores Ramachrisna Teixeira, Jorge Horvath, Ibere Luiz Caldas e Fábio Saltara, pelos excelentes cursos que me ministraram.

A meus colegas de trabalho e amigos do IAG: Alan, Eduardo, Marcos, Adrian, Jorge, Gleidson, Andres, Paulo, Douglas, Raphael e Elielson.

Ao grupo de Mecânica Celeste de Córdoba, especialmente a Cristián Beaugé, que me ajudou a poder vir a fazer a pós-graduação no IAG.

A Fernando Roig, pelos conselhos e experiências compartilhadas.

A meu amor Eugenia, pelo carinho, companheirismo e paciência ao longo de todos estes anos.

A toda minha família e da Eugenia, muito especialmente a meus pais Hugo e Silvia, por me ensinar o valor do sacrifício e do trabalho bem feito.

A todos aqueles amigos que conheci aqui no Brasil, especialmente ao Alan, Laura, Cintia, Daryel, Fara, Yumei, Ana, Elisa e Matthieu.

A meus amigos de Argentina, por não ter me esquecido a pesar da distância.

Às secretárias do departamento de Astronomia e da Pós-graduação do IAG.

Aos técnicos, funcionários e professores do IAG que fazem deste instituto.

À CNPq, pelo apoio financeiro fornecido sob o projeto n^o: 141684/2013-5, e à CAPES, pelo subsídio logo no início deste projeto.

"*...Caminante, son tus huellas*
el camino y nada más;
caminante, no hay camino,
se hace camino al andar.

Al andar se hace camino
y al volver la vista atrás
se ve la senda que nunca
se ha de volver a pisar.

Caminante no hay camino
sino estelas en la mar..."

Antonio Machado, *Cantares.*

Resumo

A maioria das teorias atuais de maré estão baseadas na teoria de Darwin, e tem como característica principal a introdução *ad hoc* do atraso tidal. Estas teorias predizem uma rotação estacionaria síncrona quando a órbita é circular, e um excesso de rotação (conhecido como super-sincronismo) quando a órbita é elíptica. Na teoria de Darwin, esse excesso é dado por $\sim 6ne^2$ (n é o movimento médio e e a excentricidade orbital), e é independente da natureza do corpo deformado. Recentemente, foi proposta uma nova teoria de maré, desenvolvida no IAG (Ferraz-Mello, Celest Mech Dyn Astron 116: 109, 2013). Usando uma linearização da equação de Navier-Stokes para um fluido com um número de Reynolds muito baixo, esta teoria estuda a deformação do corpo extenso, supondo que ela é proporcional ao stress. A constante de proporcionalidade γ (chamada fator de relaxação), depende inversamente da viscosidade. O excesso de rotação predito nesta teoria é $\sim 6ne^2\gamma^2/(n^2+\gamma^2)$. Todas estas teorias adotam a hipótese da homogeneidade do corpo deformado. Porém, corpos celestes reais, como os satélites do Sistema Solar Europa, Encélado ou Titã, apresentam uma estrutura de camadas, com um oceano interno que possibilita a rotação independente entre a crosta e o núcleo, impossibilitando aplicar as teorias atuais a este tipo de problemas. Nesta tese estendemos a teoria de maré por fluência, ou *creep tide theory*, para corpos não homogêneos diferenciados. Desenvolvendo um modelo para duas camadas, estudamos a evolução rotacional, assim como as soluções estacionárias quando, além das forças de maré, incluimos as possíveis forças de interação entre as camadas, como o acoplamento gravitacional e a fricção. Posteriormente, aplicamos a teoria a Titã, adicionando a interação crosta-atmosfera e considerando a existência de um oceano interno. Finalmente, desenvolvemos a teoria de maré de Darwin para corpos não homogêneos diferenciado e comparamos com a teoria de maré por fluência.

Abstract

Almost all existing tidal theories are based on the Darwin's theory, and have as main feature the introduction of the *ad hoc* tidal lag. These theories predict a synchronous stationary rotation when the orbit is circular, and an excess of rotation (known as super-synchronism), when the orbit is elliptical. In the Darwin's theory, this excess is given by $\sim 6ne^2$ (n is the mean motion and e is the orbital eccentricity), and is independent of the nature of the deformed body. Recently, a new theory was proposed, developed in the IAG (Ferraz-Mello, Celest Mech Dyn Astron 116: 109, 2013). Using a linearization of the Navier-Stokes equation for a fluid with a very low Reynolds number, this theory studies the deformation of the extense body, assuming that it is proportional to the stress. The constant of proportionality γ (called relaxation factor), depends inversely on the viscosity. The excess of rotation predicted in this theory is $\sim 6ne^2\gamma^2/(n^2+\gamma^2)$. All these theories adopt the hypothesis of homogeneity of the deformed body. However, real celestial bodies, as the satellites of the Solar System Europe, Enceladus or Titan, present a multi-layered structure, with an internal ocean that allows the independent rotation between the crust and the core, making impossible to apply the current theories to this kind of problems. In this thesis, we extend the *creep tide theory*, to a differentiated non-homogeneous body. Developing the two-layer model, we study the rotational evolution, as well as the stationary solutions when, besides the tidal forces, we include the interaction between the different layers, as the gravitational coupling and the friction. Then, we apply the theory to Titan, adding the crust-atmosphere exchange of angular momentum and considering the existence of a subsurface ocean. Finally, we develop the Darwin tidal theory to differentiated non-homogeneous bodies and compare with the creep tide theory.

List of Figures

2.1 Scheme of the differentiated body m 27
2.2 Density profile for the two-layer model. 36
2.3 Clairaut's numbers for the two-layer model. 36
2.4 Flattening profile for the two-layer model. 39
2.5 Fluid Love number for the two-layer model. 40
2.6 Density and flattening profiles for polynomial density distributions. 41
2.7 Calculated parameters with the polynomial density law. 42
2.8 Density and flattening profiles for the polytropic density distributions. . . . 43
2.9 Calculated parameters with the polytropic density law. 44
2.10 Polytropic density profile. 44
2.11 Polytropic flattening profile. 45

3.1 Elements of the model 48

4.1 Gravitational coupling: Equatorial section of the i-th and j-th layers. . . . 61
4.2 Scheme of the composition of the elastic and anelastic tides. 62
4.3 Evolution of y_s when $\gamma_c = \gamma_s$ 67
4.4 Evolution of ν_s/n when $\gamma_c = \gamma_s$ 67
4.5 Evolution of y_s when $\gamma_c \neq \gamma_s$ 68
4.6 Family of stationary rotation with $n/\gamma_c = n/\gamma_s = 0.01$ 68
4.7 Family of stationary rotation with $n/\gamma_c = n/\gamma_s = 1$ 69
4.8 Zoom of the family of stationary rotation with $n/\gamma_c = n/\gamma_s = 1$ 70
4.9 Basins of the attractors when $n/\gamma_c = n/\gamma_s = 0.01$ and $e = 0.4875$ 71
4.10 Attractors when $n/\gamma_c = n/\gamma_s = 10$ 72

4.11 Constants B_{ij} of the approximate solution 77
4.12 Comparison between the numerical and the analytical solutions 78

5.1 Reference model 80
5.2 Dependence of d_i, $\mathcal{H}_i$, $\mathcal{D}_i$ and C_i on the thickness of the ocean h 83
5.3 Dependence of T_{ij}, K_i and $n \times \mu_i$ on the thickness of the ocean h 84
5.4 Time evolution of $\Omega_s - n$ 85
5.5 Constants B_{ij} of the approximate solution 86
5.6 Amplitude of the shell rotation for $\eta_o = 10^{-3}$ Pa s 89
5.7 Amplitude of the shell rotation for $\eta_o = 10^{9}$ Pa s 90
5.8 Amplitude of the core rotation for $\eta_o = 10^{-3}$ Pa s 91
5.9 Approximate solutions with the atmospheric influence 94

6.1 Spherical coordinate system 96

A.1 Scheme for the calculation of the mass 125

C.1 Interface between two adjacent homogeneous layers of m 136

List of Tables

5.1 Basic data of Titan 81
5.2 Titan's four-layer reference model 81
5.3 Titan's two-layer equivalent model 82
5.4 Titan's calculated parameters in the two-layer model 83

F.1 Cayley coefficients $E_{0,k}$ 148
F.2 Cayley coefficients $E_{2,k}$ 148

Contents

1. Introduction 21

2. The static tide 25

2.1 Introduction 25

2.2 The equilibrium equations 26

2.3 Flattening of the layers 28

2.4 Extension to the continuous case 30

2.4.1 Boundary conditions. Radau transformation 33

2.5 Potential of the tidally deformed body 34

2.6 Two-layer Core-Shell model 35

2.6.1 Discrete model 35

2.6.2 Continuous model 37

2.6.3 Fluid Love number 40

2.7 Application to different density distribution laws 40

2.7.1 Polynomial density functions 41

2.7.2 Polytropics pressure-density laws 42

2.7.3 An analitical result: The politrope with n=1 43

3. Non-homogeneous creep tide theory 47

3.1 Introduction 47

3.2 Creep tide theory 47

3.3 The creep equation 48

3.4 The disturbing potential 50

3.5 Forces and torques . . . 52
3.6 Forces and torques acting on M . . . 54
3.7 Work done by the tidal forces acting on M . . . 55
3.8 Variations in semi-major axis and eccentricity . . . 56

4. The two-layer model . . . 59
4.1 The tidal torques . . . 59
4.2 The gravitational coupling . . . 60
4.3 Linear drag . . . 64
4.4 Rotational equations . . . 66
4.5 Comparison with the homogeneous case . . . 66
4.6 Near-synchronous solution of the rotational equations . . . 71
4.6.1 Tidal drift and the periodic terms . . . 75

5. Application to Titan's rotation . . . 79
5.1 Introduction . . . 79
5.2 The model . . . 80
5.3 Atmospheric influence on Titan's rotation . . . 82
5.4 The results . . . 83
5.5 Near-synchronous solution of the rotational equations . . . 92

6. Non-homogeneous Darwin theory . . . 95
6.1 Darwin tide theory . . . 95
6.2 The tidal phase lags . . . 97
6.3 The Love numbers . . . 97
6.4 Delayed potential, forces and torques . . . 99
6.5 Forces and torques acting on M . . . 101
6.6 Work done by the tidal forces acting on M . . . 101
6.7 Variations in semi-major axis and eccentricity . . . 103
6.8 Comparison with the creep tide theory . . . 103

7. Conclusion . . . 107

Bibliography . . . 111

Appendix 119

A. Shape and gravitational potential of one ellipsoid and one ellipsoidal layer . . . 121

A.1 Homogeneous ellipsoid 121

A.2 Ellipsoidal layer 123

B. The contribution of the gravitational potentials to the equilibrium equations . . 129

B.1 The equilibrium equations 129

B.2 The contribution of the outer layers 129

B.3 The contribution of the inner layers 131

B.4 The contribution of the tidal potential 132

C. The relaxation factor 135

D. The integral of section 3.7 139

E. Fluid Love's number of the i-th layer 143

E.1 The tidal fluid Love number of the i-th layer 143

E.2 The rotational fluid Love number of the i-th layer 144

E.3 Potential of the tidally deformed layer 144

F. The Cayley functions 145

F.1 Auxiliary formulas 145

F.2 Cayley coefficients 148

Chapter 1

Introduction

Tidal torques are a key physical agent controlling the rotational and orbital evolution of systems with close-in bodies and may give important clues on the physical conditions in which these systems are originated and evolved. The viscoelastic nature of a real body causes a non-instantaneous deformation, and the body continuously tries to recover the equilibrium figure corresponding to the varying gravitational potential due to the orbital companion. In standard Darwin's theory (e.g. Darwin, 1880; Kaula, 1964; Mignard, 1979; Efroimsky and Lainey, 2007; Ferraz-Mello et al., 2008), the gravitational potential of the deformed body is expanded in Fourier series, and the viscosity is introduced by means of *ad hoc* phase lags in the periodic terms.[1]

All these theories predict the existence of a stationary rotation. If the lags are assumed to be proportional to the tidal frequencies, the stationary rotation has the frequency $\Omega_{stat} \simeq n(1+6e^2)$, where n is the mean motion and e is the orbital eccentricity[2]. The synchronous rotation is only possible when the orbit is circular, but the stationary rotation becomes super-synchronous in the non-zero eccentricity case. In these theories, the excess of rotation $6ne^2$ does not depend on the rheology of the body. However, this prediction is not confirmed for Titan, where the excess provided by the theory is $\sim 38^\circ$ per year, and the Cassini mission, using radar measurement, has not showed discrepancy from synchronous motion larger than $\sim 0.02^\circ$ per year (Meriggiola, 2012; Meriggiola et al., 2016).

Recently, a new tidal theory for viscous homogeneous bodies has been developed by Ferraz-Mello (2013; 2015a) (hereafter FM13 and FM15, respectively). A Newtonian creep

[1] Mignard (1979), introduced an *ad hoc* constant time lag.

[2] If the tidal phase lags are assumed to be frequency independent, as in MacDonald (1964), the resulting stationary solution is $\Omega \simeq n(1+9.5e^2)$ (see Goldreich, 1966).

model, which results from a spherical approximate solution of the Navier-Stokes equation for fluids with very low Reynolds number, is used to calculate the surface deformation, due to an anelastic tide. This deformation is assumed proportional to the stress, and the proportionality constant γ, called the relaxation factor, is inversely proportional to the viscosity of the body. In the creep tide theory, the excess of synchronous rotation is roughly proportional to $6n\gamma^2e^2/(n^2+\gamma^2)$. A similar planar theory, using a Maxwell viscoelastic rheology, was developed by Correia et al. (2014) and generalized later to the spatial case by Boué et al. (2016). Despite the different methods used to introduce the elasticity of the body, this approach is virtually equivalent to the creep tide theory (Ferraz-Mello, 2015b). Other general rheologies were studied by Henning et al. (2009) and Frouard et al. (2016).

However, real celestial bodies are quite far from being homogeneous and how the tide influences its dynamic evolution is not entirely clear yet. Differentiation is common in our Solar System, and several satellites present evidence of a subsurface liquid ocean. We may cite, for instance, Europa (Wahr et al., 2006; Khurana et al., 1998) and Enceladus (Porco et al., 2006; Nimmo et al., 2007). One paradigmatic case is Titan, where, in addition, the exchange of a certain amount of angular momentum between the surface and the atmosphere may be important (Tokano and Neubauer, 2005; Richard et al., 2014), and the presence of an internal ocean (Tobie et al., 2005; Lorenz et al., 2008; Sohl et al., 2014) may decouple rotationally the crust from the interior (Karatekin et al., 2008). The rotation of the crust has been studied by Van Hoolst et al. (2009) using the static tide and internal effects, as gravitational coupling and pressure torques. They found that the crust rotation is influenced, mainly by the atmosphere and the Saturn torque, and claim that the viscous crust deformation and the non-hydrostatic effects, could play an important role in the amplitude of the crust oscillation.

The main objectives of this work are: i) To extend the creep tide theory for multi-layered bodies and to study their rotational evolution. ii) To apply the non-homogeneous tidal theory to Titan. This thesis is organized as follows: In Chap. 2 we generalize the linear Clairaut theory for one multi-layered body with differential rotation, adding a tidal potential due to the presence of an external body. We present and solve the $2N$ classical equations of equilibrium and extend the Clairaut's equation for the continuous problem and its solution. We calculate the potential at a point in the space due to the deformed

body and we calculate a generalized Love number for the differentiated non-homogeneous bodies. Finally, we apply the theory to a body composed of two homogeneous layers, and for several laws of density. The main results, for the particular case in that all the layers have the same angular velocity, were published in Folonier et al. (2015). In Chap. 3 we present the non-homogeneous creep tide theory for one body composed of N homogeneous layers. We compute the disturbing potential of the deformed body, as well as the forces, the toques and the work done by the tidal forces acting on the bodies. In addition, we calculate the variations in semi-major axis and eccentricity, produced by the tidal forces. In Chap. 4, we develop the two-layer model, adding the gravitational coupling between the core and the shell and the friction that occurs at interface in contact. We compare the two-layer model with the homogeneous theory and calculate the approximate near-synchronous rotation. In Chap. 5, we apply to Titan[3]. In Chap. 6 we extend the Darwin tide theory for multi-layered bodies and compare with the creep tide theory. Finally, the conclusions are presented in Chap. 7. The work is completed by several appendices where are given technical details of some of the topics presented in the forthcoming chapters.

[3] Chapters 3, 4 and 5 are the basis of one paper to be submitted soon to publication in the journal Celestial Mechanics and Dynamical Astronomy.

Chapter 2

The static tide

2.1 Introduction

Several theories of tidal evolution, since the theory developed by Darwin in the XIX century (Darwin, 1880), are based on the figure of equilibrium of an inviscid tidally deformed body (see e.g. Ferraz-Mello et al., 2008; Ferraz-Mello, 2013). The addition of the viscosity to the model is done at a later stage, but the way it is introduced is not unique and can vary when different tidal theories are considered. Frequently, the adopted figure is a Jeans prolate spheroid or, if the rotation is important, a Roche triaxial ellipsoid (Chandrasekhar, 1969). It is worth recalling that ellipsoidal figures are excellent first approximations, but not exact figures of equilibrium (Poincaré, 1902; Lyapunov, 1925; 1927). Besides, Maclaurin, Jacobi, Roche and Jeans ellipsoids are valid only for homogeneous bodies. Real celestial objects, however, are quite far from being homogeneous. This causes significant deviations which need to be taken into account in the astronomical applications.

The non-homogeneous problem, when we only consider the deformation by rotation, has been extensively studied. The problem of one body formed by n rotating homogeneous spheroidal layers as well as its extension to the continuous case was studied by Clairaut (1743) (revisited by Tisserand, 1891 and Wavre, 1932). Their works were based on the hypotheses of small deformations (linear theory for the polar flattenings) and constant angular velocity inside the body. The general case of homogeneous layers rotating with different angular velocities (non-linear theory) was studied by Montalvo et al. (1983) and Esteban and Vazquez (2001) (see Borisov et al., 2009 for a more detailed review), and was generalized to the continuous inviscid case by Bizyaev et al. (2014).

The case of uniformly rotating layers was studied by several authors. Kong et al.

(2010) discussed the particular case of a body formed by two homogeneous layers with same angular velocity. Hubbard (2013), with a recursive numerical form of the potential of a N-layers rotating planet, in hydrostatic equilibrium, showed a solution for the spheroidal shapes of the interfaces of the layers.

When the tidal forces acting on the body are taken into account along with the rotation, the literature is much less extensive. Usually the spin-orbit synchronism is assumed, so that the rotating body solution can be used (e.g. Van Hoolst et al., 2008). Tricarico (2014), assuming synchronism, found a recursive analytical solution for the shape of a body formed by an arbitrary number of layers. For this, he developed the potentials of homogeneous ellipsoids in terms of the polar and equatorial shape eccentricities. However, the results do not include tidally deformed bodies whose rotation is non-synchronous, as, for instance, the Earth, solar type stars hosting close-in planets and hot Jupiters in highly eccentric orbits. Recently, Wahl et al. (2016) extended the Concentric Maclaurin Spheroid method, presented in Hubbard (2013), to include the tidal forces.

In this chapter, we study the static equilibrium figure of one body composed of N homogeneous layers, deformed by a tidal potential and the differential rotation of its layers. The main results were published in Folonier et al. (2015).

2.2 The equilibrium equations

We consider one differentiated body m of mass m_T, disturbing to one mass point M of mass M orbiting at a distance r from the center of m. We assume that m is composed of N homogeneous layers of density d_i $(i = 1, \cdots, N)$ and angular velocity $\mathbf{\Omega}_i = \Omega_i \widehat{\mathbf{k}}$, perpendicular to the orbital plane. We also assume that each layer has an outer ellipsoidal shape with semi axes a_i, b_i and c_i, where the semi-major axis a_i is pointing towards M and c_i is the axis of rotation (Fig. 2.1).

If we consider one point on the outer surface of the i-th layer, with position vector $\mathbf{r}_i = (x_i, y_i, z_i)$ and velocity $\mathbf{v}_i = \mathbf{\Omega}_i \times \mathbf{r}_i$, respect of the center of m, we can use the same equation used in the study of equilibrium ellipsoids (see Tisserand, 1891, Chap. 8 and 13; Jeans, 1929, Sec. 215-216; Jardetzky, 1958; Chandrasekhar, 1969), which expresses the fact that the total force acting on a point of its surface must be perpendicular to the

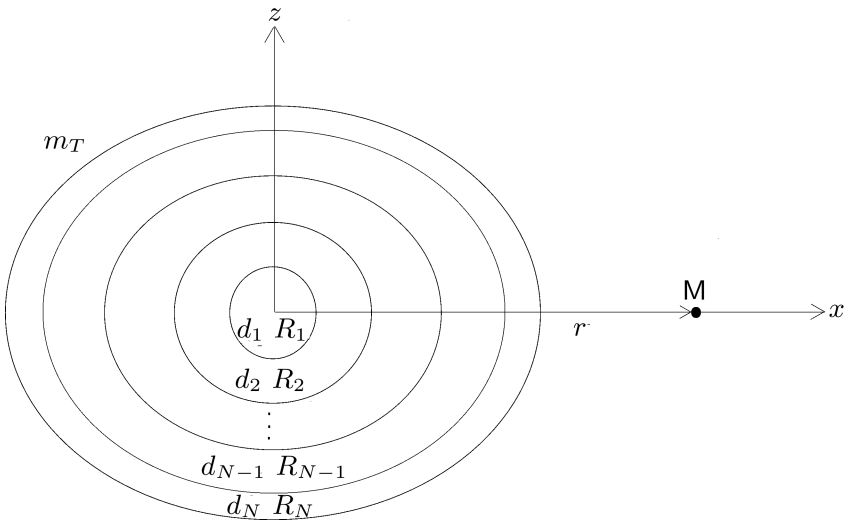

Figure 2.1: Body of mass m_T formed of N homogeneous layers of density d_i, where each layer has an outer mean equatorial radius R_i and an angular velocity $\mathbf{\Omega}_i$, and a point mass M orbiting at a distance r from its center in a plane perpendicular to the rotation axis. Figure extracted of Folonier and Ferraz-Mello (2015).

surface

$$\nabla_{\mathbf{r}_i}\Phi_i \propto \nabla_{\mathbf{r}_i}U_G + \mathbf{\Omega}_i \times (\mathbf{\Omega}_i \times \mathbf{r}_i), \tag{2.1}$$

where U_G is the total gravitational potential at $\mathbf{r}_i$, the term $\mathbf{\Omega}_i \times (\mathbf{\Omega}_i \times \mathbf{r}_i)$ corresponds to the centripetal acceleration and

$$\Phi_i(x_i, y_i, z_i) = \frac{x_i^2}{a_i^2} + \frac{y_i^2}{b_i^2} + \frac{z_i^2}{c_i^2} - 1 = 0, \tag{2.2}$$

is the ellipsoidal surface equation. The use of the above equilibrium equation in a case where the tidal force field is changing because of the external body needs a justification. Eq. (2.1) means that no change in the shape of the body occurs because of internal forces; the shape will change, but only because of the relative change of the position of the external body.

Hence, we obtain the equilibrium equations

$$\begin{aligned} \Omega_i^2 &= \frac{1}{x_i}\frac{\partial U_G}{\partial x_i} - \frac{\alpha_i}{z_i}\frac{\partial U_G}{\partial z_i} \\ \Omega_i^2 &= \frac{1}{y_i}\frac{\partial U_G}{\partial y_i} - \frac{\beta_i}{z_i}\frac{\partial U_G}{\partial z_i}, \end{aligned} \tag{2.3}$$

where

$$\alpha_i = \frac{c_i^2}{a_i^2}; \qquad \beta_i = \frac{c_i^2}{b_i^2}. \tag{2.4}$$

The problem of find the equilibrium figure (i.e. the values of the semi axes a_i, b_i and c_i) is equivalent to finding the equatorial and polar flattenings

$$\epsilon_\rho^{(i)} = \frac{a_i - b_i}{R_i} \approx \frac{1-\alpha_i}{2} - \frac{1-\beta_i}{2}; \qquad \epsilon_z^{(i)} = \frac{b_i - c_i}{R_i} \approx \frac{1-\beta_i}{2}, \tag{2.5}$$

where $R_i = \sqrt{a_i b_i}$ is the outer mean equatorial radius of the i-th layer. For this, we will use the $2N$ equilibrium equations (2.3).

If we denote U_j (with $j = 1, \cdots, N$) the potential of the j-th layer, and U_{tid} the tidal potential at $\mathbf{r}_i$, the total gravitational potential is

$$U_G = U_{tid} + \sum_{j=1}^{N} U_j. \tag{2.6}$$

As the equilibrium equations (2.3) are linear in the potential U, we can write

$$\Omega_i^2 = \chi_i^{(k)}(U_{tid}) + \sum_{j=1}^{N} \chi_i^{(k)}(U_j), \tag{2.7}$$

where $\chi_i^{(1)}$ and $\chi_i^{(2)}$ are the operators

$$\begin{aligned} \chi_i^{(1)} &= \frac{1}{x_i}\frac{\partial}{\partial x_i} - \frac{\alpha_i}{z_i}\frac{\partial}{\partial z_i} \\ \chi_i^{(2)} &= \frac{1}{y_i}\frac{\partial}{\partial y_i} - \frac{\beta_i}{z_i}\frac{\partial}{\partial z_i}. \end{aligned} \tag{2.8}$$

2.3 Flattening of the layers

The next step is to calculate the contribution of each gravitational potential to the equilibrium equations (2.7). If we consider separately the contributions to the potentials due to the inner and outer layers, and the tidal forces at a point on the i-th surface (see Appendix B), we obtain the equations

$$\begin{aligned} \Omega_i^2 &= -\frac{3GM}{r^3} + G\frac{4\pi}{3}\left[\frac{3m_T}{2\pi R_i^3} - \frac{6}{5}(d_i - d_{i+1}) - \sum_{j=i+1}^{N} 2(d_j - d_{j+1})\frac{R_j^3 - R_i^3}{R_i^3}\right]\left(\epsilon_\rho^{(i)} + \epsilon_z^{(i)}\right) - \\ &\quad -G\frac{4\pi}{3}\sum_{j=i+1}^{N}\frac{6}{5}(d_j - d_{j+1})\left(\epsilon_\rho^{(j)} + \epsilon_z^{(j)}\right) - G\frac{4\pi}{3}\sum_{j=1}^{i-1}\frac{6}{5}(d_j - d_{j+1})\frac{R_j^5}{R_i^5}\left(\epsilon_\rho^{(j)} + \epsilon_z^{(j)}\right) \\ \Omega_i^2 &= G\frac{4\pi}{3}\left[\frac{3m_T}{2\pi R_i^3} - \frac{6}{5}(d_i - d_{i+1}) - \sum_{j=i+1}^{N} 2(d_j - d_{j+1})\frac{R_j^3 - R_i^3}{R_i^3}\right]\epsilon_z^{(i)} - \\ &\quad -G\frac{4\pi}{3}\sum_{j=i+1}^{N}\frac{6}{5}(d_j - d_{j+1})\epsilon_z^{(j)} - G\frac{4\pi}{3}\sum_{j=1}^{i-1}\frac{6}{5}(d_j - d_{j+1})\frac{R_j^5}{R_i^5}\epsilon_z^{(j)}. \end{aligned} \tag{2.9}$$

The solution of this system can be written as

$$\epsilon_\rho^{(i)} = \mathcal{H}_i \epsilon_J; \qquad \epsilon_z^{(i)} = \mathcal{G}_i \bar{\epsilon}_M, \tag{2.10}$$

where $\bar{\epsilon}_M$ is the flattening of the equivalent MacLaurin homogeneous spheroid in synchronous rotation and ϵ_J are the flattening of the equivalent Jeans homogeneous spheroids

$$\bar{\epsilon}_M = \frac{5R_N^3 n^2}{4m_T G}; \qquad \epsilon_J = \frac{15MR_N^3}{4m_T r^3}, \tag{2.11}$$

G is the gravitational constant, n is the mean motion of M and $R_N = \sqrt{a_N b_N}$ is the outer mean equatorial radius of m.

The coefficients $\mathcal{H}_i$ and $\mathcal{G}_i$ are the Clairaut's numbers

$$\mathcal{H}_i = \sum_{j=1}^{N} (\mathsf{E}^{-1})_{ij} x_j^3 \qquad \mathcal{G}_i = \sum_{j=1}^{N} (\mathsf{E}^{-1})_{ij} x_j^3 \left(\frac{\Omega_j}{n}\right)^2, \tag{2.12}$$

where $(\mathsf{E}^{-1})_{ij}$ are the elements of the inverse of the matrix E, with elements

$$(\mathsf{E})_{ij} = \begin{cases} -\dfrac{3}{2f_N}(\widehat{d}_j - \widehat{d}_{j+1}) x_i^3, & i < j \\ -\dfrac{3}{2f_N}(\widehat{d}_i - \widehat{d}_{i+1}) x_i^3 + \dfrac{5}{2} - \dfrac{5}{2f_N} \displaystyle\sum_{k=i+1}^{N} (\widehat{d}_k - \widehat{d}_{k+1})(x_k^3 - x_i^3), & i = j \\ -\dfrac{3}{2f_N}(\widehat{d}_j - \widehat{d}_{j+1}) \dfrac{x_j^5}{x_i^2}, & i > j \end{cases} \tag{2.13}$$

where $x_i = R_i/R_N$ and $\widehat{d}_i = d_i/d_1$ are the normalized mean equatorial radius and density, respectively, and $f_N = 3\int_0^1 \widehat{d}(z) z^2 \, dz$, where $\widehat{d}(z)$ is the normalized density profile.

It is important to note that if the orbital motion is synchronous with the angular velocity of each layer, when the approximation $\epsilon_J \simeq 3\bar{\epsilon}_M$ is adopted[1], the system (2.9) is completely equivalent to that found by Tricarico (2014), where the square of the polar and equatorial "*eccentricities*" used there are related to the polar and equatorial flattenings through $e_{pi}^2 \approx 2\epsilon_z^{(i)}$ and $e_{qi}^2 \approx 2\epsilon_\rho^{(i)}$.

The calculations done are valid only for small flattenings, i.e. we assume that the perturbation due to the tide and the rotation are small enough so as not to deform too much the body (in the second order, the figure ceases to be an ellipsoid).

[1] The exact relation is $\epsilon_J = 3\bar{\epsilon}_M \frac{a^3}{r^3} \frac{M}{M+m_T}$. The aproximation is valid only if the mass of the deformed body and the eccentricity are small, that is $r \simeq a$ and $m_T \ll M$.

In the rigid rotation case, if the velocity of rotation of each layer is $\Omega_i = \Omega$, the polar flattening of the i-th layer, can be rewritten as

$$\epsilon_z^{(i)} = \mathcal{H}_i \epsilon_M, \tag{2.14}$$

where

$$\epsilon_M = \frac{5R_N^3\Omega^2}{4m_T G}, \tag{2.15}$$

is the non-synchronous flattening of the equivalent MacLaurin homogeneous spheroid.

2.4 Extension to the continuous case

In this section we extend the equilibrium figure to the continuous case. In order to calculate the first Clairaut function $\mathcal{H}(x)$, we follow the method showed in Tisserand (1891), Chap. 14, writing the first equation of (2.9), less the second equation, as

$$\sum_{j=1}^{i-1}(\mathsf{E})_{ij}\mathcal{H}_j + (\mathsf{E})_{ii}\mathcal{H}_i + \sum_{j=i+1}^{N}(\mathsf{E})_{ij}\mathcal{H}_j = x_i^3. \tag{2.16}$$

If we introduce the notation $\Delta(x_k) = x_k - x_{k-1}$ and the boundary values $x_0 = 0$ and $d_{N+1} = 0$, we may rewrite the terms on the left hand side of the last equation as

$$\begin{aligned}
\sum_{j=1}^{i-1}(\mathsf{E})_{ij}\mathcal{H}_j &= -\frac{3}{2f_N}\sum_{j=1}^{i-1}\widehat{d}_j\frac{x_j^5}{x_i^2}\mathcal{H}_j + \frac{3}{2f_N}\sum_{j=1}^{i-1}\widehat{d}_{j+1}\frac{x_j^5}{x_i^2}\mathcal{H}_j \\
&= -\frac{3}{2f_N}\sum_{j=1}^{i-1}\widehat{d}_j\frac{\Delta(x_j^5\mathcal{H}_j)}{x_i^2} + \frac{3}{2f_N}\widehat{d}_i\frac{x_{i-1}^5}{x_i^2}\mathcal{H}_{i-1} \\
\sum_{j=i+1}^{N}(\mathsf{E})_{ij}\mathcal{H}_j &= -\frac{3}{2f_N}\sum_{j=i+1}^{N}\widehat{d}_j x_i^3\mathcal{H}_j + \frac{3}{2f_N}\sum_{j=i+1}^{N}\widehat{d}_{j+1}x_i^3\mathcal{H}_j \\
&= -\frac{3x_i^3}{2f_N}\sum_{j=i+1}^{N}\widehat{d}_j\Delta(\mathcal{H}_j) - \frac{3}{2f_N}\widehat{d}_{i+1}x_i^3\mathcal{H}_i,
\end{aligned} \tag{2.17}$$

or

$$\begin{aligned}
\sum_{j=1}^{i-1}(\mathsf{E})_{ij}\mathcal{H}_j + \sum_{j=i+1}^{N}(\mathsf{E})_{ij}\mathcal{H}_j &= -\frac{3}{2f_N}\left[\sum_{j=1}^{i-1}\widehat{d}_j\frac{\Delta(x_j^5\mathcal{H}_j)}{x_i^2} + x_i^3\sum_{j=i+1}^{N}\widehat{d}_j\Delta(\mathcal{H}_j)\right] + \\
&\quad -\frac{3}{2f_N}\left[\widehat{d}_i\frac{\Delta(x_i^5\mathcal{H}_i)}{x_i^2} + \Delta(\widehat{d}_{i+1})x_i^3\mathcal{H}_i\right],
\end{aligned} \tag{2.18}$$

and

$$\begin{aligned}(\mathsf{E})_{ii}\mathcal{H}_i &= -\frac{3}{2f_N}\Delta(\widehat{d}_{i+1})x_i^3\mathcal{H}_i + \frac{5}{2}\mathcal{H}_i - \frac{5}{2f_N}\sum_{k=i+1}^{N}(\widehat{d}_k - \widehat{d}_{k+1})(x_k^3 - x_i^3)\mathcal{H}_i \\ &= -\frac{3}{2f_N}\Delta(\widehat{d}_{i+1})x_i^3\mathcal{H}_i + \frac{5\mathcal{H}_i}{2} - \frac{5\mathcal{H}_i}{2f_N}\sum_{k=i+1}^{N}\widehat{d}_k\Delta(x_k^3). \qquad (2.19)\end{aligned}$$

If we assume that the number of layers tends to infinity so that the increments $\Delta x_k = x_k - x_{k-1}$ are infinitesimal quantities, when $\Delta x_k \to 0$, the Eq. (2.16) becomes

$$\frac{5x^2}{3}f(x)\mathcal{H}(x) = \frac{2f_N}{3}x^5 + \int_{z=0}^{z=x}\widehat{d}(z)d(z^5\mathcal{H}(z)) + x^5\int_{z=x}^{z=1}\widehat{d}(z)d\mathcal{H}(z), \qquad (2.20)$$

where the function $f(x)$ is

$$f(x) \stackrel{\text{def}}{=} 3\int_0^x \widehat{d}(z)z^2dz, \qquad (2.21)$$

with $f(0) = 0$ and $f(1) = f_N$.

Deriving (2.20) with respect to x, we have

$$\frac{2f(x)}{3x^3}\mathcal{H}(x) + \frac{f(x)}{3x^2}\mathcal{H}'(x) = \frac{2f_N}{3} + \int_{z=x}^{z=1}\widehat{d}(z)d\mathcal{H}(z), \qquad (2.22)$$

and deriving once more we obtain the differential equation for the flattening profile

$$\mathcal{H}''(x) + \frac{6\widehat{d}(x)x^2}{f(x)}\mathcal{H}'(x) + \left(\frac{6\widehat{d}(x)x}{f(x)} - \frac{6}{x^2}\right)\mathcal{H}(x) = 0. \qquad (2.23)$$

It is a homogeneous linear differential equation of second order with non-constant coefficients for the first Clairaut function $\mathcal{H}(x)$, that represent the continuous counterpart of the first Clairaut coefficient $\mathcal{H}_i$. The differential equation (2.23) is the same expression found by Clairaut (Tisserand, 1891; Jeffreys, 1953).

The Eq. (2.20) allows us to calculate the limits that the Clairaut coeficient $\mathcal{H}_N$ can take at the surface. In the homogeneous case $\widehat{d}(x) = 1$, the integrals can be calculated trivially. At the surface $x = 1$, we obtain $\mathcal{H}_N = 1$. In the non-homogeneous case, if the density is a piecewise continuous non-increasing function ($\widehat{d}' \leqslant 0$), we have, at the surface

$$\begin{aligned}\mathcal{H}_N &= \frac{2}{5} + \frac{3}{5f_N}\int_{z=0}^{z=1}\widehat{d}(z)d(z^5\mathcal{H}(z)) \\ &= \frac{2}{5} + \frac{3}{5f_N}\left[\widehat{d}_N\mathcal{H}_N - \int_{z=0}^{z=1}z^5\mathcal{H}(z)d\widehat{d}(z)\right] \geqslant \frac{2}{5}. \qquad (2.24)\end{aligned}$$

Then, under the assumption of equilibrium, a non-homogeneous body will have equatorial flattenings on the surface with values between 0.4 and 1 times the values they would have if the body was homogeneous.

It is worth mentioning that Eq. (2.24) is valid if $\mathcal{H}(z) \geq 0$, that is, $a_i \geq b_i$. If $a_i < b_i$, we can redefine the equatorial flattening as $\epsilon_\rho^{(i)} = (b_i - a_i)/R_i = \mathcal{H}_i \epsilon_J \geq 0$.

In order to calculate the equation for the second Clairaut function $\mathcal{G}(x)$, we can proceed in the same way. Using the second equation of (2.9), we obtain

$$\frac{5x^2}{3} f(x)\mathcal{G}(x) = \frac{2f_N}{3} x^5 \widehat{\Omega}^2 + \int_{z=0}^{z=x} \widehat{d}(z) d(z^5 \mathcal{G}(z)) + x^5 \int_{z=x}^{z=1} \widehat{d}(z) d\mathcal{G}(z), \tag{2.25}$$

where $\widehat{\Omega} = \Omega(x)/n$. Deriving with respect to x, we have

$$\frac{2f(x)}{3x^3}\mathcal{G}(x) + \frac{f(x)}{3x^2}\mathcal{G}'(x) = \frac{2f_N}{3}\widehat{\Omega}^2 + \frac{4f_N}{15} x\widehat{\Omega}\widehat{\Omega}' + \int_{z=x}^{z=1} \widehat{d}(z) d\mathcal{G}(z), \tag{2.26}$$

and deriving once more we obtain the differential equation for the flattening profile

$$\mathcal{G}''(x) + \frac{6\widehat{d}(x)x^2}{f(x)}\mathcal{G}'(x) + \left(\frac{6\widehat{d}(x)x}{f(x)} - \frac{6}{x^2}\right)\mathcal{G}(x) = \frac{4f_N x^2}{5f(x)}\left(6\widehat{\Omega}\widehat{\Omega}' + x\widehat{\Omega}'^2 + x\widehat{\Omega}\widehat{\Omega}''\right). \tag{2.27}$$

It is a non-homogeneous linear differential equation of second order with non-constant coefficients. The homogeneous equation is equal to the differential equation of the first Clairaut equation (2.23). The non-homogeneity of Eq. (2.27) depend on the rotation profile $\widehat{\Omega}(x) = \Omega/n$, particularly depend on the $\widehat{\Omega}'$ and $\widehat{\Omega}''$, therefore, to rigid rotation $\widehat{\Omega}(x)$ is a constant function, and the Eq. (2.27) results equal to the differential equation (2.23).

In the homogeneous case $\widehat{d}(x) = 1$, the integral (2.25) can be calculated trivially

$$\mathcal{G}(x) = \frac{2}{5}\widehat{\Omega}^2 + \frac{3}{5}\mathcal{G}_N, \tag{2.28}$$

with $\mathcal{G}_N = \widehat{\Omega}_N^2$ at the surface $x = 1$. In the non-homogeneous case, if the density is a non-increasing function ($\widehat{d}' \leqslant 0$), we have, at the surface

$$\begin{aligned} \mathcal{G}_N &= \frac{2\widehat{\Omega}_N^2}{5} + \frac{3}{5f_N}\int_{z=0}^{z=1} \widehat{d}(z) d(z^5 \mathcal{G}(z)) \\ &= \frac{2\widehat{\Omega}_N^2}{5} + \frac{3}{5f_N}\left[\widehat{d}_N \mathcal{G}_N - \int_{z=0}^{z=1} z^5 \mathcal{G}(z) d\widehat{d}(z)\right] \geqslant \frac{2\widehat{\Omega}_N^2}{5}. \end{aligned} \tag{2.29}$$

Then, under the assumption of equilibrium, a non-homogeneous body will have flattenings on the surface with values between $0.4\widehat{\Omega}_n^2$ and $\widehat{\Omega}_n^2$ times the values they would have if the body was homogeneous.

2.4.1 Boundary conditions. Radau transformation

The differential equation (2.23) requires two boundary conditions to be solved. However, before attempting to find these boundary conditions, we will show two relationships that will turn out to be useful later. The first relationship is obtained from equation (2.22), where at $x = 1$ we have

$$\mathcal{H}'_N = 2(1 - \mathcal{H}_N). \tag{2.30}$$

The second relationship is obtained from the differential equation (2.23). If we note that $f(x) \sim x^3 + 3\widehat{d}'_0 x^4/4$ and $\widehat{d}(x) \sim 1 + \widehat{d}'_0 x$, in the neighborhood of $x = 0$, the Eq. (2.23) can be approximated by

$$\mathcal{H}'' + 6\frac{\mathcal{H}'}{x} + 6\widehat{d}'_0 \frac{\mathcal{H}}{x} = 0, \tag{2.31}$$

it is

$$\mathcal{H}'_0 = -\widehat{d}'_0 \mathcal{H}_0, \tag{2.32}$$

where $\widehat{d}'_0$ is the derivative of the density at $x = 0$.

In practical applications, it is convenient to introduce the Radau transformation

$$\eta(x) = \frac{x\mathcal{H}'(x)}{\mathcal{H}(x)}, \tag{2.33}$$

and rewritten Clairaut's equation as the Ricatti differential equation

$$\eta' + \frac{\eta^2}{x} + \left[q(x) + \frac{5}{x}\right]\eta + q(x) = 0, \tag{2.34}$$

where

$$q(x) \stackrel{\text{def}}{=} \frac{6}{x}\left(\frac{\widehat{d}(x)x^3}{f(x)} - 1\right). \tag{2.35}$$

In the new variables, using the relation (2.32), the boundary condition is

$$\eta(x = 0) = 0. \tag{2.36}$$

The variable η is sometimes referred to as *Radau's parameter* (Bullen, 1975). Defining $\eta(x = 1) = \eta_N$ and using the relationship (2.30) and the transformation (2.33), the boundary conditions of (2.23) are

$$\mathcal{H}_N = \frac{2}{2 + \eta_N}; \qquad \mathcal{H}'_N = \frac{2\eta_N}{2 + \eta_N}. \tag{2.37}$$

As a result of this relationship, if considering that $0.4 < \mathcal{H}_N < 1$, we recover the classical result $0 < \eta_N < 3$ (Tisserand, 1891).

Finally, it should be noted that once $\eta(x)$ is found, we may find the profile flattening from equation (2.33), whose solution is

$$\mathcal{H}(x) = \mathcal{H}_N e^{\int_1^x \eta(z)/z \ dz}. \tag{2.38}$$

The complete study of the differential equation for the second Clairaut function $\mathcal{G}(x)$ (Eq. 2.27), escapes from the objectives of this work. As we will show in the following Chapters, the axial terms of the potential of the deformed body, which involve Clairaut number $\mathcal{G}_i$, are torque free and do not contribute to the tidal rotational evolution of m.

2.5 Potential of the tidally deformed body

The disturbing potential of the i-th ellipsoidal layer at an external point $\mathbf{r}^*$ is given by (see Eq. A.33)

$$\delta U_2^{(i)}(\mathbf{r}^*) = -\frac{GC_i\mathcal{L}_i}{2r^{*3}}\epsilon_J\left(3\cos^2\Psi_x - 1\right) - \frac{GC_i\mathcal{L}'_i}{2r^{*3}}\bar{\epsilon}_M\left(3\cos^2\Psi_z - 1\right), \tag{2.39}$$

where Ψ_x and Ψ_z are the angles between the direction of the point where the potential is taken and the coordinate axes x and z, respectively, $C_i \simeq \frac{2}{5}m_i(R_i^5 - R_{i-1}^5)/(R_i^3 - R_{i-1}^3)$ is the axial moment of inertia of the i-th layer (see Eq. A.26) and the parameters

$$\mathcal{L}_i = \frac{\mathcal{H}_i R_i^5 - \mathcal{H}_{i-1}R_{i-1}^5}{R_i^5 - R_{i-1}^5}; \qquad \mathcal{L}'_i = \frac{\mathcal{G}_i R_i^5 - \mathcal{G}_{i-1}R_{i-1}^5}{R_i^5 - R_{i-1}^5}. \tag{2.40}$$

The total potential is the sum of the potentials of all layers:

$$U(\mathbf{r}^*) = -\frac{2k_f G m_T R_N^2}{15r^{*3}}\epsilon_J\left(3\cos^2\Psi_x - 1\right) - \frac{2k'_f G m_T R_N^2}{15r^{*3}}\bar{\epsilon}_M\left(3\cos^2\Psi_z - 1\right), \tag{2.41}$$

the constants k_f and k'_f are often called the tidal and rotational fluid Love number (Munk and MacDonald, 1960; Correia and Rodríguez, 2013). For a non-homogeneous body, by identification of the terms, we find

$$k_f \stackrel{\text{def}}{=} \frac{3}{2}\frac{1}{m_T R_N^2}\sum_{i=1}^{N}\frac{m_i\Delta(R_i^5\mathcal{H}_i)}{R_i^3 - R_{i-1}^3}; \qquad k'_f \stackrel{\text{def}}{=} \frac{3}{2}\frac{1}{m_T R_N^2}\sum_{i=1}^{N}\frac{m_i\Delta(R_i^5\mathcal{G}_i)}{R_i^3 - R_{i-1}^3}, \tag{2.42}$$

where $\Delta(f_i) = f_i - f_{i-1}$, denotes the increment of one function f_i, between the inner and the outer boundaries of this layer. Using the continuous model and the mass of the i-th

layer $m_i = \frac{4\pi}{3} d_i (R_i^3 - R_{i-1}^3)$, we obtain

$$k_f = \frac{3}{2f_N} \int_{z=0}^{z=1} \widehat{d}(z) d(z^5 \mathcal{H}(z)); \qquad k'_f = \frac{3}{2f_N} \int_{z=0}^{z=1} \widehat{d}(z) d(z^5 \mathcal{G}(z)). \tag{2.43}$$

Using the integral form of Clairaut's equations (2.20) and (2.25), and evaluating at $x = 1$, we obtain

$$k_f = \frac{5}{2}\mathcal{H}_N - 1; \qquad k'_f = \frac{5}{2}\mathcal{G}_N - \widehat{\Omega}_N^2. \tag{2.44}$$

which shows the link of the tidal fluid Love number k_f, with the coefficient $\mathcal{H}_N$. This relationship is based on the fact that both constants depend solely on the internal structure, characterizing the inhomogeneity of the body. In the homogeneous case $\mathcal{H}_N = 1$ thus recovering the classical result $k_f = 1.5$. If we also assume a synchronous rotation, $\mathcal{G}_N = \Omega_N/n = 1$ and $k'_f = k_f = 1.5$.

2.6 Two-layer Core-Shell model

2.6.1 Discrete model

In this section we consider the simple case of a body formed of two synchronous homogeneous layers: a core with density d_1 and mean radius R_1, and a shell with density $d_2 = \widehat{d}_1 d_1$ (with $\widehat{d}_1 < 1$) and mean outer radius R_2 (Fig. 2.2). If we define the normalized mean core radius $x_1 = R_1/R_2$, then, the parameter f_N can be written as

$$f_N = \widehat{d}_1 + (1 - \widehat{d}_1) x_1^3. \tag{2.45}$$

The linear system for the equatorial flattenings is

$$\begin{aligned} (\mathsf{E})_{11}\mathcal{H}_1 + (\mathsf{E})_{12}\mathcal{H}_2 &= x_1^3 \\ (\mathsf{E})_{21}\mathcal{H}_1 + (\mathsf{E})_{22}\mathcal{H}_2 &= 1, \end{aligned} \tag{2.46}$$

(see Eq. 2.16), where the elements of the matrix E are

$$\begin{aligned} (\mathsf{E})_{11} &= \frac{(2 + 3\widehat{d}_1)x_1^3}{2\widehat{d}_1 + 2(1 - \widehat{d}_1)x_1^3}; \qquad (\mathsf{E})_{12} = -\frac{3\widehat{d}_1 x_1^3}{2\widehat{d}_1 + 2(1 - \widehat{d}_1)x_1^3} \\ (\mathsf{E})_{21} &= -\frac{3(1 - \widehat{d}_1)x_1^5}{2\widehat{d}_1 + 2(1 - \widehat{d}_1)x_1^3}; \qquad (\mathsf{E})_{22} = \frac{2\widehat{d}_1 + 5(1 - \widehat{d}_1)x_1^3}{2\widehat{d}_1 + 2(1 - \widehat{d}_1)x_1^3}. \end{aligned} \tag{2.47}$$

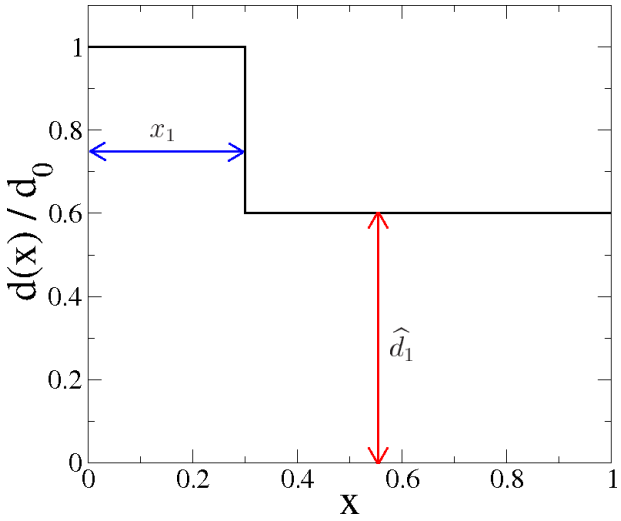

Figure 2.2: Density profile of a body formed by two homogeneous layers. x_1 is the mean radius of the core R_1 relative to the mean outer radius of the shell R_2. $\widehat{d}_1$ is the shell density d_2 relative to the core density d_1. Figure extracted of Folonier et al. (2015).

Hence, the first Clairaut's numbers are

$$\begin{aligned}\mathcal{H}_1 &= \frac{10\left(\widehat{d}_1+(1-\widehat{d}_1)x_1^3\right)^2}{\left(2+3\widehat{d}_1\right)\left(2\widehat{d}_1+5(1-\widehat{d}_1)x_1^3\right)-9\widehat{d}_1(1-\widehat{d}_1)x_1^5}\\ \mathcal{H}_2 &= \frac{2\left(\widehat{d}_1+(1-\widehat{d}_1)x_1^3\right)\left(2+3\widehat{d}_1+3(1-\widehat{d}_1)x_1^5\right)}{\left(2+3\widehat{d}_1\right)\left(2\widehat{d}_1+5(1-\widehat{d}_1)x_1^3\right)-9\widehat{d}_1(1-\widehat{d}_1)x_1^5}.\end{aligned} \tag{2.48}$$

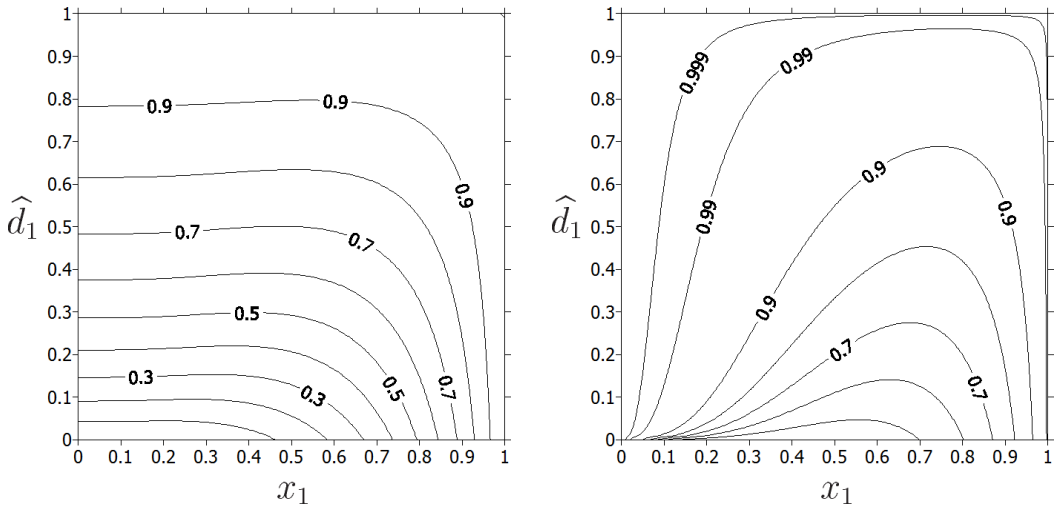

Figure 2.3: Possible values of $\mathcal{H}_1$ (core) and $\mathcal{H}_2$ (shell) as functions of the core size x_1 and of the relative density of the shell $\widehat{d}_1$. Figure extracted of Folonier et al. (2015).

Fig. 2.3 shows the results obtained for the constants $\mathcal{H}_1$ and $\mathcal{H}_2$. We see that:

- If $\widehat{d}_1 = 1$ or $x_1 = 1$, the constants are $\mathcal{H}_1 = \mathcal{H}_2 = 1$, that is the solution for a homogeneous body.

- When the core is denser than the shell, $\mathcal{H}_2 \geqslant \mathcal{H}_1$ and the flattening of the core are smaller than the equatorial flattening of the surface (where $\epsilon_\rho^{(1)} = \mathcal{H}_1\epsilon_J \leqslant \epsilon_\rho^{(2)} = \mathcal{H}_2\epsilon_J$).

- Since $\mathcal{H}_2 \leqslant 1$, the maximum surface flattening is given by the homogeneous solution. In presence of a core, the surface is always less flattened than it is in the homogeneous case.

- While $\mathcal{H}_1$ may take all possible values bettween 0 and 1, $\mathcal{H}_2$ is always larger than the critical limit 0.4, corresponding to the degenerate limit case in which the whole mass would tend to concentrate in the center and would be surrounded by a zero-density shell (case of Huygens-Roche). Therefore the flattenings of the outer surface can never be less than 40% of the homogeneous reference values. This is the same result given by Eq. (2.24) for the continuous case.

2.6.2 Continuous model

Now, we will consider the same problem, but using the continuous model. In this case, the normalized density profile is

$$\widehat{d}(x) = \begin{cases} 1 & 0 \leqslant x \leqslant x_1 \\ \widehat{d}_1 & x_1 < x \leqslant 1, \end{cases} \tag{2.49}$$

and the function $f(x)$ is

$$f(x) = \begin{cases} x^3 & 0 \leqslant x \leqslant x_1 \\ \widehat{d}_1 x^3 + (1-\widehat{d}_1)x_1^3 & x_1 < x \leqslant 1. \end{cases} \tag{2.50}$$

A simple treatment, without actually solving the differential equation, is to solve the integral equation (2.20), that can be calculated trivially since the density profile $\widehat{d}(x)$ is piecewise constant

$$\int_0^x \widehat{d}(z)d(z^5\mathcal{H}) = \begin{cases} x^5\mathcal{H}(x) - \Big[x^5\mathcal{H}(x)\Big]_{x=0} & 0 \leqslant x \leqslant x_1 \\ \widehat{d}_1 x^5\mathcal{H}(x) + (1-\widehat{d}_1)x_1^5\mathcal{H}_1 - \Big[x^5\mathcal{H}(x)\Big]_{x=0} & x_1 < x \leqslant 1, \end{cases} \tag{2.51}$$

and

$$\int_x^1 \widehat{d}(z)d\mathcal{H} = \begin{cases} (1-\widehat{d}_1)\mathcal{H}_1 + \widehat{d}_1\mathcal{H}_2 - \mathcal{H}(x) & 0 \leqslant x \leqslant x_1 \\ \widehat{d}_1\mathcal{H}_2 - \widehat{d}_1\mathcal{H}(x) & x_1 < x \leqslant 1, \end{cases} \tag{2.52}$$

where $\mathcal{H}_1 = \mathcal{H}(x_1)$ and $\mathcal{H}_2 = \mathcal{H}(1)$. We remind that, a priori, we do not know the form of the function $\mathcal{H}(x)$.

In the core, $0 \leqslant x \leqslant x_1$, the integral equation is

$$\frac{5x^5}{3}\mathcal{H}(x) = x^5\left(\frac{2f_N}{3} + \widehat{d}_1\mathcal{H}_2 + (1-\widehat{d}_1)\mathcal{H}_1\right) - \Big[x^5\mathcal{H}(x)\Big]_{x=0}, \tag{2.53}$$

which, for $x = 0$, gives the condition $\frac{5}{3}\Big[x^5\mathcal{H}(x)\Big]_{x=0} = -\Big[x^5\mathcal{H}(x)\Big]_{x=0}$ which may be fulfilled only if $\Big[x^5\mathcal{H}(x)\Big]_{x=0} = 0$. So in that interval, we have

$$\mathcal{H}(x) = \frac{2f_N}{5} + \frac{3}{5}\widehat{d}_1\mathcal{H}_2 + \frac{3}{5}(1-\widehat{d}_1)\mathcal{H}_1, \tag{2.54}$$

that is, the flattening profile in the core remains constant, although we do not know yet the boundary values $\mathcal{H}_1$ and $\mathcal{H}_2$. Particularly, if $x = x_1$, we obtain

$$(2+3\widehat{d}_1)\mathcal{H}_1 = 2f_N + 3\widehat{d}_1\mathcal{H}_2. \tag{2.55}$$

In the shell, $x_1 < x \leqslant 1$, the integral equation is

$$\frac{5x^2}{3}\left(\widehat{d}_1x^3 + (1-\widehat{d}_1)x_1^3\right)\mathcal{H}(x) = x^5\left(\frac{2f_N}{3} + \widehat{d}_1\mathcal{H}_2\right) + (1-\widehat{d}_1)x_1^5\mathcal{H}_1. \tag{2.56}$$

If we evaluate it at the boundary $x = 1$, we obtain

$$(1-\widehat{d}_1)x_1^5\mathcal{H}_1 = (2\widehat{d}_1 + 5(1-\widehat{d}_1)x_1^3)\mathcal{H}_2 - \frac{2f_N}{3}. \tag{2.57}$$

Since the function $\mathcal{H}(x)$ should be continuous at the boundary $x = x_1$, we may combine the equations (2.55) and (2.57), to obtain the boundary conditions:

$$\begin{aligned} \mathcal{H}_1 &= \frac{10\left(\widehat{d}_1 + (1-\widehat{d}_1)x_1^3\right)^2}{\left(2+3\widehat{d}_1\right)\left(2\widehat{d}_1 + 5(1-\widehat{d}_1)x_1^3\right) - 9\widehat{d}_1(1-\widehat{d}_1)x_1^5} \\ \mathcal{H}_2 &= \frac{2\left(\widehat{d}_1 + (1-\widehat{d}_1)x_1^3\right)\left(2+3\widehat{d}_1 + 3(1-\widehat{d}_1)x_1^5\right)}{\left(2+3\widehat{d}_1\right)\left(2\widehat{d}_1 + 5(1-\widehat{d}_1)x_1^3\right) - 9\widehat{d}_1(1-\widehat{d}_1)x_1^5}, \end{aligned} \tag{2.58}$$

which coincide with the results of the discrete model. The flattening profile can then be written as

$$\mathcal{H}(x) = \begin{cases} \mathcal{H}_1, & 0 \leqslant x \leqslant x_1 \\ \dfrac{3(1-\widehat{d}_1)x_1^5 + (2+3\widehat{d}_1)x^5}{5x^2\left(\widehat{d}_1 x^3 + (1-\widehat{d}_1)x_1^3\right)}\mathcal{H}_1, & x_1 < x \leqslant 1 \end{cases} .$$

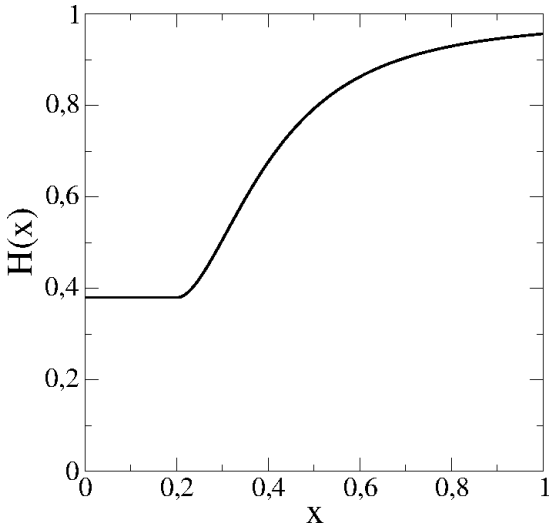

Figure 2.4: Example of flattening profile $\mathcal{H}(x)$ when $x_1 = 0.2$ and $\widehat{d}_1 = 0.2$.

The results obtained with the two models are in excellent agreement. In the discrete case, by construction, we only obtain the values of the flattening in the surface of the body and in the interface core-shell as a function of the relative density of both layers and the normalized mean radius of the nucleus. In the continuous model, however, we get a flattening profile which is continuous and coincides with those of the first model in the points $x = x_1$ and $x = 1$. So, the continuous model not only gives the flattening in the surfaces of the two parts, but also the flattening of the actual equipotentials within the fluid. Fig. 2.4 shows one example: we plot the flattening profile $\mathcal{H}(x)$ when $x_1 = 0.2$ and $\widehat{d}_1 = 0.2$. The values of the Clairaut function in the points $x = x_1$ and $x = 1$, coincides with the Clairaut's numbers in the discrete model: $\mathcal{H}(x_1) = \mathcal{H}_1 \simeq 0.379$ and $\mathcal{H}(1) = \mathcal{H}_2 \simeq 0.956$.

2.6.3 Fluid Love number

Using equation (2.44), together with the expression for $\mathcal{H}_2$ (Eqn. 2.48), the expression of the fluid Love number k_f is

$$k_f = \frac{5\left(\widehat{d}_1 + (1-\widehat{d}_1)x_1^3\right)\left(2 + 3\widehat{d}_1 + 3(1-\widehat{d}_1)x_1^5\right)}{\left(2+3\widehat{d}_1\right)\left(2\widehat{d}_1 + 5(1-\widehat{d}_1)x_1^3\right) - 9\widehat{d}_1(1-\widehat{d}_1)x_1^5} - 1. \tag{2.59}$$

Fig. 2.5 shows the possible value of k_f as a function of the core size x_1 and of the relative density of the shell $\widehat{d}_1$. If we obtain k_f, for example by determining $\mathcal{H}_N$ by direct observation of the surface flattenings, then equation (2.59) defines a continuous curve of possible values for the size of the nucleus x_1 and the relative density of the shell $\widehat{d}_1$ under the hypothesis of two homogeneous layers. Moreover, as can be seen in this figure, a maximum value for these physical parameters can be predicted.

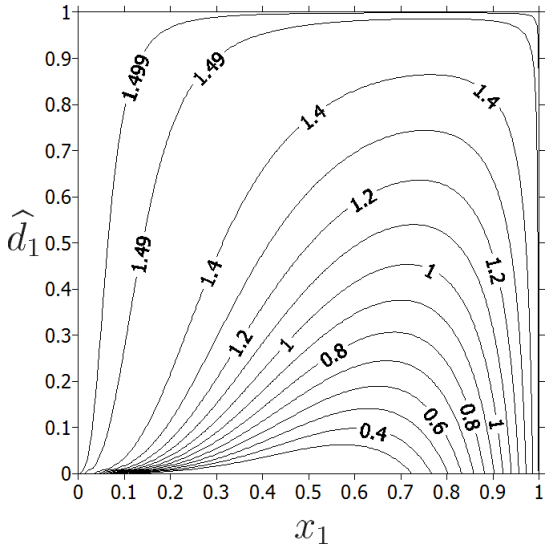

Figure 2.5: Possible values of k_f as functions of the core size x_1 and of relative density of the shell $\widehat{d}_1$. Figure extracted of Folonier et al. (2015).

2.7 Application to different density distribution laws

In this section, we present some applications of the theory developed in this chapter to bodies with continuous density distributions. For this we use two examples of density distributions: polynomial and polytropic density laws.

In both cases the Clairaut's equation is solved numerically after introduction of the variable defined by the Eq. (2.33). The flattening profile $\mathcal{H}(x)$ and the Love number are then obtained through the inverse transformation.

2.7.1 *Polynomial density functions*

We consider initially a simple polynomial density law:

$$\widehat{d}(x) = 1 - x^{\alpha}, \tag{2.60}$$

where $\alpha > 0$. The *left* panel of Fig. 2.6 shows the density functions for $\alpha = 0.1, 1, 2, 10$ and 100 as functions of the normalized mean radius x.

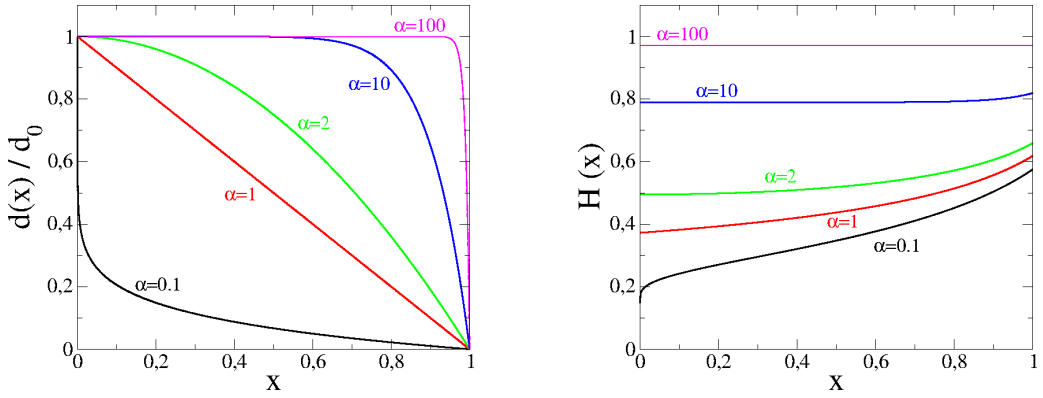

Figure 2.6: Left: Density profiles for polynomial density distributions with different values of α. *Right*: Flattening profile $\mathcal{H}(x)$ for the same density laws. $\alpha = 0.1$ (black), $\alpha = 1$ (red), $\alpha = 2$ (green), $\alpha = 10$ (blue) and $\alpha = 100$ (magenta). Figures extracted of Folonier et al. (2015).

The resulting flattening profiles $\mathcal{H}(x)$ are shown in the *right* panel of Fig. 2.6. In all cases, the flattening profile $\mathcal{H}(x)$ is an increasing monotonic function and, for all x, the values of $\mathcal{H}(x)$ increase when the power α increases.

Note that, as discussed in Section 2.4, the value of $\mathcal{H}_N$ is always greater than the limit value 0.4 and less than 1. Particularly $\mathcal{H}_N$ tends to 0.570 when α tends to 0 and $\mathcal{H}_N$ tends to 1 when α tends to ∞ (homogeneous case). The fluid Love number increases from 0.424 (when α tends to 0) to 1.5 (when α tends to ∞). These results can be seen in Fig. 2.7, where we also show the values of the flattening factor $\mathcal{H}_N$ at the surface and the dimensionless moment of inertia $C/m_T R_N^2$. This last parameter increases from 0.24 (when α tends to 0) to 0.4 (when α tends to ∞)[2].

[2] An elementary calculation allows one to find the relationship $\frac{C}{m_T R^2} \approx \frac{2}{3}\frac{\int_0^1 \widehat{dz}^4 dz}{\int_0^1 \widehat{dz}^2 dz} = \frac{2}{5} \times \frac{3+\alpha}{5+\alpha}$.

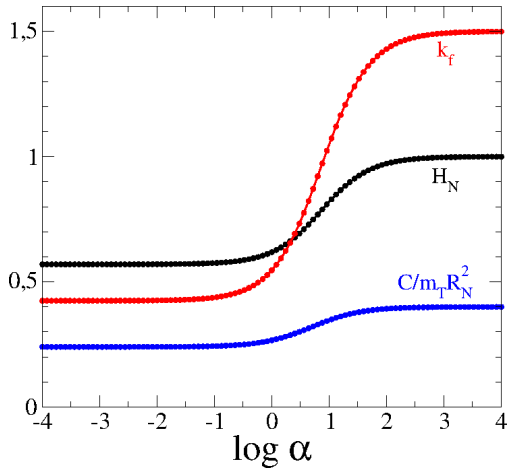

Figure 2.7: Values of $\mathcal{H}_N$ (black), k_f (red) and $C/m_T R_N^2$ (blue) for different values of the exponent of the polynomial density law. Figure extracted of Folonier et al. (2015).

2.7.2 *Polytropics pressure-density laws*

We may consider a self-gravitating body in hydrostatic equilibrium with a more general polytropic pressure-density law:

$$P = K d^{1+\frac{1}{n}}, \tag{2.61}$$

where P is the pressure, n is the polytropic index and K is constant. The differential equation for the density is then given by the *Lane-Emden equation* (Chandrasekhar, 1969)

$$\frac{1}{\xi^2}\frac{d}{d\xi}\left(x^2\frac{d\theta}{d\xi}\right) + \theta^n = 0, \tag{2.62}$$

where $\theta = \widehat{d}^{1/n}$ and $\xi = \alpha/R$, with $\alpha^2 = (n+1)K d_0^{\frac{1}{n}-1}/4\pi G$. The standard boundary conditions are $\theta(0) = 1$ and $\theta'(0) = 0$. If $0 \leq n < 5$ the solution $\theta(\xi)$ decreases monotonically and has a zero at a finite value $\xi = \xi_1$. This radius corresponds to the surface of the body where $P = \rho = 0$.

It is worth mentioning that several real cases exist that correspond to polytropes. For example, when convection is established in the interior of a star the resulting configuration is a polytrope; when the gas is degenerate, the corresponding equations of state have the same form as the polytropic equation of state, etc. (see Collins, 1989). We also mention recent results by Leconte et al. (2011) showing that the density profile of hot Jupiters is well approximated by a polytrope.

The *left* panel of the Fig. 2.8 shows the density functions for $n = 0.5, 1.0, 1.5, 3.0$ and

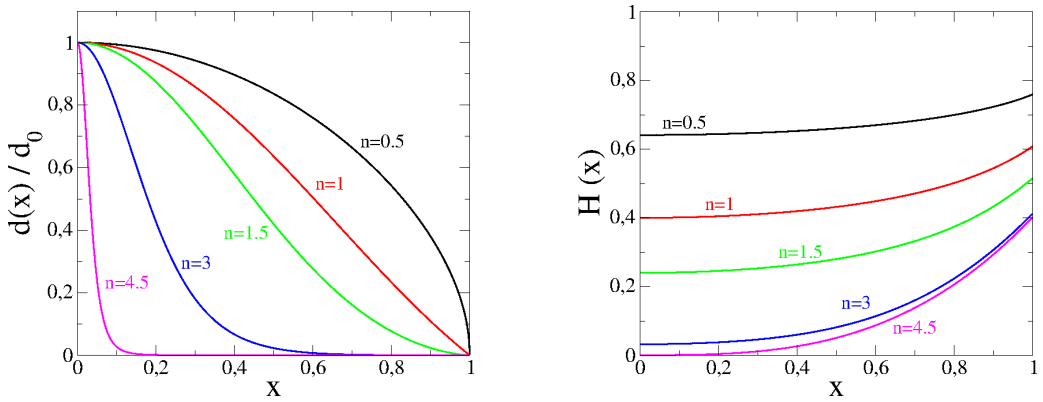

Figure 2.8: Left: Density profiles for different values of the polytropic index. *Right*: Flattening profile $\mathcal{H}(x)$ for these density laws. $n = 0.5$ (black), $n = 1$ (red), $n = 1.5$ (green), $n = 3$ (blue) and $n = 4.5$ (magenta). Figures extracted of Folonier et al. (2015).

4.5 as functions of the normalized mean radius $x = R/\alpha\xi_1$ obtained from the integration of the Lane-Emden equation.

The resulting flattening profiles $\mathcal{H}(x)$ are shown in the *right* panel of Fig. 2.8. In all cases, the flattening profile $\mathcal{H}(x)$ is an increasing monotonic function and for all x, the values of $\mathcal{H}(x)$ decrease when the polytropic index n increases.

As mentioned previously, the value of $\mathcal{H}_N$ is always greater than the limit value 0.4. Particularly $\mathcal{H}_N \to 0.4$ when $n \to 5$. The fluid Love number decreases from 1.5 for $n = 0$ (constant density) to 0 when n tends to the limit $n = 5$. These results can be seen in Fig. 2.9, where we also show the values of the flattening factor $\mathcal{H}_N$ and the dimensionless moment of inertia $C/m_T R_N^2$ for values of n below the limit $n = 5$. The adimensional moment of inertia decreases from 0.4 (when $n = 0$) and tends to 0 when $n \to 5$.

2.7.3 An analitical result: The politrope with n=1

The Clairaut differential equation (2.23) can be very difficult to solve analiticaly, even for very simple density profiles as linear or quadratic, which can only be solved numerically. However, for the particular case

$$\widehat{d}(x) = \frac{\sin \pi x}{\pi x}, \tag{2.63}$$

which corresponds to the density profile of degenerate gases with a polytropic index $n = 1$ (see Fig. 2.10) (de Pater et al. 2010, Chap. 6), the solution can be expressed analytically. This case is very useful since the state of the matter inside the gaseous planets is well

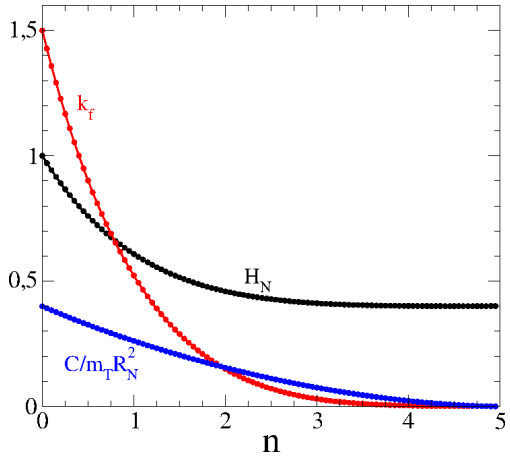

Figure 2.9: Values of $\mathcal{H}_N$ (black), k_f (red) and $C/m_T R_N^2$ (blue) for different polytropic indices $n < 5$. Figure extracted of Folonier et al. (2015).

approximated by this model.

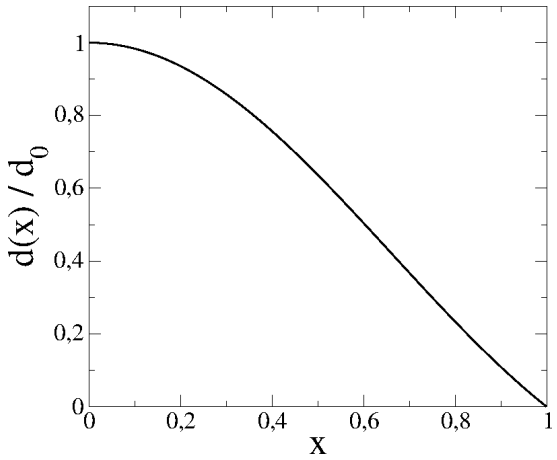

Figure 2.10: Polytropic density profile for $n = 1$.

In this case, the function $f(x)$ is

$$f(x) = \frac{3}{\pi^3}\big(\sin(\pi x) - \pi x \cos(\pi x)\big), \tag{2.64}$$

and the differential equation becomes

$$\mathcal{H}'' + \frac{2\pi^2 x}{1 - \pi x \cot(\pi x)}\mathcal{H}' + \left[\frac{2\pi^2}{1 - \pi x \cot(\pi x)} - \frac{6}{x^2}\right]\mathcal{H} = 0. \tag{2.65}$$

We can verify that the resulting equation has the linearly independent solutions

$$u(x) = \frac{3}{x^2} - \frac{\pi^2}{1 - \pi x \cot(\pi x)}; \qquad v(x) = \frac{(\pi^2 x^2 - 3)\cot(\pi x) + 3\pi x}{1 - \pi x \cot(\pi x)}, \tag{2.66}$$

and the flattening profile can be written as

$$\mathcal{H}(x) = C_1 u(x) + C_2 v(x), \tag{2.67}$$

where C_1 and C_2 are constants.

In order to calculate the integration constants, we introduce the solution (2.67) into the Eqs. (2.20) and (2.22). Evaluating at $x = 1$, we obtain the linear system

$$\begin{aligned} \frac{2f_N}{3} &= \left(\frac{5f_N u_N}{3} - \int_{z=0}^{z=1} \widehat{d}\, d(z^5 u)\right) C_1 + \left(\frac{5f_N v_N}{3} - \int_{z=0}^{z=1} \widehat{d}\, d(z^5 v)\right) C_2 \\ 1 &= \left(u_N + \frac{u'_N}{2}\right) C_1 + \left(v_N + \frac{v'_N}{2}\right) C_2, \end{aligned} \tag{2.68}$$

where $u_N = u(1)$, $v_N = v(1)$, $u'_N = u'(1)$ and $v'_N = v'(1)$. Replacing by the functions, the linear system becomes

$$\begin{aligned} \frac{2}{\pi^2} &= C_1 + \left(\frac{132}{\pi^5} - \frac{18}{\pi^3} - \frac{3}{\pi}\right) C_2 \\ 1 &= \frac{\pi^2}{2} C_1 + \left(\frac{3}{\pi} - \frac{7\pi}{2}\right) C_2. \end{aligned} \tag{2.69}$$

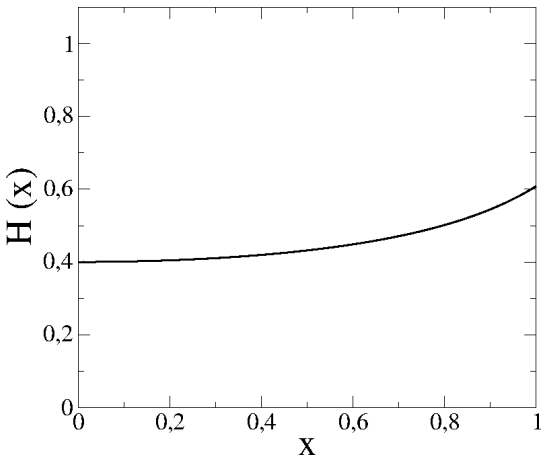

Figure 2.11: Polytropic flattening profile for $n = 1$.

Hence, the integration constants are

$$C_1 = \frac{2}{\pi^2}; \qquad C_2 = 0, \tag{2.70}$$

and the flattening profile is

$$\mathcal{H}(x) = \frac{6}{\pi^2 x^2} + \frac{2}{\pi x \cot(\pi x) - 1}, \tag{2.71}$$

which is the same strictly increasing function given in the *right* panel of Fig. 2.8, labeled $n = 1$ (see Fig. 2.11). A simple calculation allows us to find that the Clairaut numbers at the center and surface of m are

$$\begin{aligned} \mathcal{H}(0) &= \mathcal{H}_0 = 0.4 \\ \mathcal{H}(1) &= \mathcal{H}_N = \frac{6}{\pi^2} \approx 0.6, \end{aligned} \tag{2.72}$$

and the fluid Love number, using the Eq. (2.44), is

$$k_f = \frac{15}{\pi^2} - 1 \approx 0.52, \tag{2.73}$$

in excellent agreement with the classical value (Hubbard, 1975; Wahl et al., 2016).

Chapter 3

Non-homogeneous creep tide theory

3.1 Introduction

In this chapter, we extend the planar creep tide theory to the case of a viscoelastic body formed by N homogeneous layers, using the multi-layered static figure calculated in the above chapter. Solving the creep tide equation for each layer interface, we compute the disturbing potential of the deformed body, as well as the forces, the torques, the work done by the tidal forces acting on the bodies and the variations in semi-major axis and eccentricity.

3.2 Creep tide theory

Let us consider one differentiated body m of mass m_T, disturbed by one mass point M of mass M orbiting at a distance r from the center of m. We assume that the body is composed of N homogeneous layers of densities d_i $(i = 1, \cdots, N)$ and angular velocities $\mathbf{\Omega}_i$, perpendicular to the orbital plane.

The outer surface of the i-th layer is $\zeta_i(\widehat{\varphi}_i, \widehat{\theta}_i, t)$, where ζ_i is the distance of the surface points to the center of gravity of m and the angles $\widehat{\varphi}_i, \widehat{\theta}_i$ are their longitudes and co-latitudes in a fixed inertial reference system. At each instant, we assume that the static equilibrium figure of each layer under the action of the tidal potential and the rotation may be approximated by a triaxial ellipsoidal equilibrium surface $\rho_i(\widehat{\varphi}_i, \widehat{\theta}_i, t)$, whose semi-major axis is oriented towards M (see Fig. 3.1).

The adopted rheophysical approach is founded on the simple law

$$\dot{\zeta}_i = \gamma_i(\rho_i - \zeta_i), \tag{3.1}$$

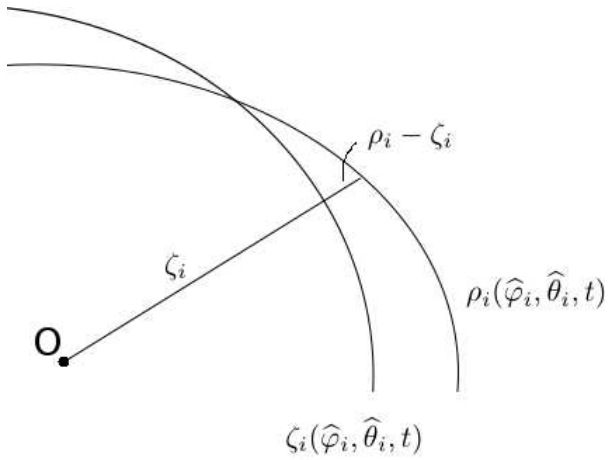

Figure 3.1: $\zeta_i(\widehat{\varphi}_i, \widehat{\theta}_i, t)$ is a section of the surface of the body at the time t; $\rho_i(\widehat{\varphi}_i, \widehat{\theta}_i, t)$ is a section of the surface of the equilibrium ellipsoid at the same time.

where γ_i is the relaxation factor at the outer surface of the i-th layer. This is a radial deformation rate gradient related to the viscosity through (see Appendix C)

$$\gamma_i = \frac{(d_i - d_{i+1}) g_i R_i}{2\eta_i}, \tag{3.2}$$

where R_i and g_i are the equatorial mean radius and the gravity acceleration at the outer surface of the i-th layer. η_i is the viscosity of the inner layer (assumed to be larger than that of the outer layer).

Although the creep equation is valid in a reference system co-rotating with the body, we can use the coordinates in a fixed reference system. This is due to the fact that only relative positions appear in the right-hand side of the creep equation. If $\widehat{\varphi}_F$ is the longitude of a point in one frame fixed in the body, then we have

$$\widehat{\varphi}_i = \widehat{\varphi}_F + \Omega_i t. \tag{3.3}$$

3.3 The creep equation

As shown in the Chap. 2, the static equilibrium figure of each layer under the action of the tidal potential and the rotation may be approximated by a triaxial ellipsoidal surface. Using that the equatorial and the polar flattenings of the outer boundary of the i-th layer are given by Eq. (2.10), the ellipsoidal surface equation of this layer, to first order in the

flattenings, can be written as (see Eq. (A.15) in the Appendix A)

$$\rho_i = R_i \left(1 + \frac{1}{2}\mathcal{H}_i\epsilon_J \sin^2\widehat{\theta}\cos\left(2\widehat{\varphi}_i - 2\varphi_M\right) - \left[\frac{1}{2}\mathcal{H}_i\epsilon_J + \mathcal{G}_i\bar{\epsilon}_M\right]\cos^2\widehat{\theta}\right), \tag{3.4}$$

where φ_M is the longitude of M fixed inertial reference system. Then, the creep equation (3.1) with the static equilibrium surface (3.4) is

$$\dot{\zeta}_i + \gamma_i\zeta_i = \gamma_i R_i \left(1 + \frac{1}{2}\mathcal{H}_i\epsilon_J \sin^2\widehat{\theta}\cos\left(2\widehat{\varphi}_i - 2\varphi_M\right) - \left[\frac{1}{2}\mathcal{H}_i\epsilon_J + \mathcal{G}_i\bar{\epsilon}_M\right]\cos^2\widehat{\theta}\right). \tag{3.5}$$

In order to solve the creep differential equation, we consider the two-body motion. The equations of the Keplerian motion to M, orbiting to m, are

$$r = \frac{a(1-e^2)}{1 + e\cos v}, \tag{3.6}$$

and

$$v = \ell + \left(2e - \frac{e^3}{4}\right)\sin\ell + \frac{5e^2}{4}\sin 2\ell + \frac{13e^2}{12}\sin 3\ell + \mathcal{O}(e^4), \tag{3.7}$$

where a is the semi-major axis, e is the eccentricity and the angles v and ℓ are the true and mean anomaly, respectively, of the body M. In the planar case, we have that $\varphi_M = v + \varpi$, where ϖ is the longitude of the periapsis.

Then, the creep equation becomes an ordinary differential equation of first order with periodic forced terms, that may be written as

$$\dot{\zeta}_i + \gamma_i\zeta_i = \gamma_i R_i \left[1 + \sum_{k\in\mathbb{Z}}\left(\mathcal{Z}_{ik}\sin^2\widehat{\theta}\cos\widehat{\Theta}_{ik} - \mathcal{Z}''_{ik}\cos^2\widehat{\theta}\cos\widehat{\Theta}''_{ik}\right)\right], \tag{3.8}$$

where the arguments of the cosines Θ_{ik}, Θ''_{ik} are linear functions of the time

$$\begin{aligned} \widehat{\Theta}_{ik} &= 2\widehat{\varphi}_i - 2\varpi + (k-2)\ell \\ \widehat{\Theta}''_{ik} &= k\ell. \end{aligned} \tag{3.9}$$

The constants $\mathcal{Z}_{ik}, \mathcal{Z}''_{ik}$ are

$$\begin{aligned} \mathcal{Z}_{ik} &= \frac{1}{2}\mathcal{H}_i\bar{\epsilon}_J E_{2,k} \\ \mathcal{Z}''_{ik} &= \frac{1}{2}\mathcal{H}_i\bar{\epsilon}_J E_{0,k} + \delta_{0,k}\mathcal{G}_i\bar{\epsilon}_M, \end{aligned} \tag{3.10}$$

where $\delta_{0,k}$ is the Kronecker delta ($\delta_{0,k} = 1$ when $k = 0$ and $\delta_{0,k} = 0$ when $k \neq 0$), the constant $\bar{\epsilon}_J$ is

$$\bar{\epsilon}_J = \frac{15MR_N^3}{4m_T a^3}, \tag{3.11}$$

and the coefficients of the Fourier series $E_{q,p}$ are eccentricity functions called the Cayley functions (Cayley, 1861)

$$E_{q,p}(e) = \frac{1}{2\pi}\int_0^{2\pi}\left(\frac{a}{r}\right)^3 \cos\left(qv + (p-q)\ell\right)\, d\ell. \tag{3.12}$$

After integration we obtain the forced terms

$$\delta\zeta_i = R_i \sum_{k\in\mathbb{Z}} \left(\mathcal{Z}_{ik} \sin^2\widehat{\theta} \cos\sigma_{ik} \cos\left(\widehat{\Theta}_{ik} - \sigma_{ik}\right) - \mathcal{Z}''_{ik} \cos^2\widehat{\theta} \cos\sigma''_{ik} \cos\left(\widehat{\Theta}''_{ik} - \sigma''_{ik}\right)\right). \tag{3.13}$$

The phases σ_{ik} and σ''_{ik} are

$$\tan\sigma_{ik} = \frac{\dot{\widehat{\Theta}}_{ik}}{\gamma_i} = \frac{\nu_i + kn}{\gamma_i}; \qquad \tan\sigma''_{ik} = \frac{\dot{\widehat{\Theta}}''_{ik}}{\gamma_i} = \frac{kn}{\gamma_i}, \tag{3.14}$$

where $\nu_i = 2\Omega_i - 2n$ is the semi-diurnal frequency. These phases are introduced during the exact integration of the creep equation (3.8).

If we define the angles

$$\begin{aligned} \delta_{ik} &= 2\varpi - (k-2)\ell + \sigma_{ik} \\ \delta''_{ik} &= k\ell - \sigma''_{ik}, \end{aligned} \tag{3.15}$$

the solution (3.13) can be writen as

$$\delta\zeta_i = R_i \sum_{k\in\mathbb{Z}} \left(\mathcal{Z}_{ik} \cos\sigma_{ik} \sin^2\widehat{\theta} \cos\left(2\widehat{\varphi}_i - \delta_{ik}\right) - \mathcal{Z}''_{ik} \cos\sigma''_{ik} \cos\delta''_{ik} \cos^2\widehat{\theta}\right), \tag{3.16}$$

which has a simple geometric interpretation: using Eq. (A.22), we can identify each term of the Fourier expansion of the height $\delta\zeta_i$, with one ellipsoidal surface, with equatorial and polar flattenings

$$\epsilon_\rho^{(ik)} = 2\mathcal{Z}_{ik}\cos\sigma_{ik}; \qquad \epsilon_z^{(ik)} = \mathcal{Z}''_{ik}\cos\sigma''_{ik}\cos\delta''_{ik} - \frac{\epsilon_\rho^{(ik)}}{2}, \tag{3.17}$$

and rotated at an angle $\delta_{ik}/2$, with respect to the axis x.

3.4 The disturbing potential

The potential of the i-th layer of m at a generic point $\mathsf{M}^*(r^*, \theta^*, \varphi^*)$ external to this layer, can be written as the potential of one spherical shell of outer and inner radii R_i and R_{i-1}, respectively, plus the disturbing potential due to the mass excess or deficit corresponding

to the outer and the inner boundary heights $\delta\zeta_i$ and $\delta\zeta_{i-1}$. It is important to note that since these excesses or deficits are very small, we may calculate the contribution of each term of the Fourier expansion separately and then sum them to obtain the total contribution.

In this way, we assume that the i-th layer has an outer and an inner boundary heights given by the k-th term of the Fourier expansion. The equatorial and polar flattenings of the outer boundary, $\epsilon_\rho^{(ik)}$ and $\epsilon_z^{(ik)}$, are given by Eq. (3.17), and the bulge is rotated at an angle $\delta_{ik}/2$ with respect to the axis x. Similarly, the inner boundary height $\delta\zeta_{i-1}^{(1)}$, can be identified with the boundary height of one ellipsoidal surface, with equatorial and polar flattenings

$$\epsilon_\rho^{(i-1k)} = 2\mathcal{Z}_{i-1k}\cos\sigma_{i-1k}; \qquad \epsilon_z^{(i-1k)} = \mathcal{Z}''_{i-1k}\cos\sigma''_{i-1k}\cos\delta''_{i-1k} - \frac{\epsilon_\rho^{(i-1k)}}{2}, \tag{3.18}$$

rotated at an angle $\delta_{i-1k}/2$, with respect to the axis x.

The disturbing potential at an external point $\mathsf{M}(r^*,\theta^*,\varphi^*)$, due to the mass excess or deficit, corresponding to the k-th term of the Fourier expansion of the outer and the inner boundary heights $\delta\zeta_i$ and $\delta\zeta_{i-1}$, is

$$\begin{aligned}\delta U_{ik}(\mathbf{r}^*) &= -\frac{3GC_i}{2r^{*3}}\sin^2\theta^*\frac{\Delta(R_i^5\mathcal{Z}_{ik}\cos\sigma_{ik}\cos(2\varphi^*-\delta_{ik}))}{R_i^5-R_{i-1}^5} + \\ &\quad +\frac{GC_i}{2r^{*3}}(3\cos^2\theta^*-1)\frac{\Delta\left(R_i^5\mathcal{Z}''_{ik}\cos\sigma''_{ik}\cos\delta''_{ik}\right)}{R_i^5-R_{i-1}^5},\end{aligned} \tag{3.19}$$

where C_i is the axial moment of inertia of the i-th layer (see Appendix A) and $\Delta(f_i) = f_i - f_{i-1}$, denotes the increment of one function f_i, between the inner and the outer boundaries of this layer.

Taking into account that the total disturbing potential of the i-th layer, can be approximated by the sum of the contribution of each term of the Fourier expansion, we obtain

$$\delta U_i(\mathbf{r}^*) = \sum_{k\in\mathbb{Z}}\delta U_{ik}(\mathbf{r}^*), \tag{3.20}$$

and replacing the coefficients $\mathcal{Z}_{ik}$ and $\mathcal{Z}''_{ik}$, given by Eq. (3.10), and the angles δ_{ik} and δ''_{ik},

given by Eq. (3.15), we obtain

$$\begin{aligned}\delta U_i(\mathbf{r}^*) &= -\frac{45GMR_N^3C_i}{16m_Tr^{*3}a^3}\sin^2\theta^*\sum_{k\in\mathbb{Z}}E_{2,k}\Big(\mathcal{C}_{ik}\sin\Theta_k^*+\mathcal{D}_{ik}\cos\Theta_k^*\Big)+\\ &+\frac{15GMR_N^3C_i}{16m_Tr^{*3}a^3}(3\cos^2\theta^*-1)\sum_{k\in\mathbb{Z}}E_{0,k}\Big(\mathcal{C}''_{ik}\sin k\ell+\mathcal{D}''_{ik}\cos k\ell\Big)+\\ &+\frac{5R_N^3n^2\mathcal{L}'_iC_i}{8m_Tr^{*3}}(3\cos^2\theta^*-1),\end{aligned}\tag{3.21}$$

where the argument Θ_k^*, is

$$\Theta_k^*=2\varphi^*-2\varpi+(k-2)\ell,\tag{3.22}$$

and the coefficient $\mathcal{L}'_i$, is

$$\mathcal{L}'_i=\frac{\mathcal{G}_iR_i^5-\mathcal{G}_{i-1}R_{i-1}^5}{R_i^5-R_{i-1}^5}.\tag{3.23}$$

The functions $\mathcal{C}_{ik}$, $\mathcal{D}_{ik}$ are defined as

$$\mathcal{C}_{ik}=\frac{1}{2}\frac{\Delta\big(\mathcal{H}_iR_i^5\sin 2\sigma_{ik}\big)}{R_i^5-R_{i-1}^5};\qquad \mathcal{D}_{ik}=\frac{\Delta\big(\mathcal{H}_iR_i^5\cos^2\sigma_{ik}\big)}{R_i^5-R_{i-1}^5},\tag{3.24}$$

and the coefficients $\mathcal{C}''_{ik}$, $\mathcal{D}''_{ik}$ are

$$\mathcal{C}''_{ik}=\frac{1}{2}\frac{\Delta\big(\mathcal{H}_iR_i^5\sin 2\sigma''_{ik}\big)}{R_i^5-R_{i-1}^5};\qquad \mathcal{D}''_{ik}=\frac{\Delta\big(\mathcal{H}_iR_i^5\cos^2\sigma''_{ik}\big)}{R_i^5-R_{i-1}^5},\tag{3.25}$$

and do not depend where the potential is calculated.

Furthermore, using the definitions of σ_{ik} and σ''_{ik}, given by Eqs. (3.14), we can write the trigonometric functions as

$$\sin 2\sigma_{ik}=\frac{2\gamma_i(\nu_i+kn)}{\gamma_i^2+(\nu_i+kn)^2};\qquad \cos^2\sigma_{ik}=\frac{\gamma_i^2}{\gamma_i^2+(\nu_i+kn)^2},\tag{3.26}$$

and

$$\sin 2\sigma''_{ik}=\frac{2\gamma_ikn}{\gamma_i^2+(kn)^2};\qquad \cos^2\sigma''_{ik}=\frac{\gamma_i^2}{\gamma_i^2+(kn)^2}.\tag{3.27}$$

These trigonometric expressions show the difference between the frequency functions $\mathcal{C}_{ik}(\nu_i,\nu_{i-1})$, $\mathcal{D}_{ik}(\nu_i,\nu_{i-1})$ and the coefficients $\mathcal{C}''_{ik}=\mathcal{C}_{ik}(0,0)$, $\mathcal{D}''_{ik}=\mathcal{D}_{ik}(0,0)$.

3.5 Forces and torques

To calculate the force and torque due to the i-th layer of m, acting on one mass M^* located in $\mathsf{M}^*(r^*,\theta^*,\varphi^*)$, we take the negative gradient of the potential of the i-th layer

at the point M^* and multiply it by the mass placed in the point $\mathbf{F}_i = -M^* \nabla_{\mathbf{r}^*} \delta U_i$. In spherical coordinates, we obtain

$$\begin{aligned}
F_{1i} &= -\frac{135GMM^*R_N^3C_i}{16m_Ta^3r^{*4}}\sin^2\theta^* \sum_{k\in\mathbb{Z}} E_{2,k}\Big(\mathcal{C}_{ik}\sin\Theta_k^* + \mathcal{D}_{ik}\cos\Theta_k^*\Big) + \\
&\quad + \frac{45GMM^*R_N^3C_i}{16m_Ta^3r^{*4}}(3\cos^2\theta^* - 1)\sum_{k\in\mathbb{Z}} E_{0,k}\Big(\mathcal{C}''_{ik}\sin k\ell + \mathcal{D}''_{ik}\cos k\ell\Big) + \\
&\quad + \frac{15M^*R_N^3n^2\mathcal{L}'_iC_i}{8m_Tr^{*4}}(3\cos^2\theta^* - 1) \\
F_{2i} &= \frac{45GMM^*R_N^3C_i}{16m_Ta^3r^{*4}}\sin 2\theta^* \sum_{k\in\mathbb{Z}} E_{2,k}\Big(\mathcal{C}_{ik}\sin\Theta_k^* + \mathcal{D}_{ik}\cos\Theta_k^*\Big) + \\
&\quad + \frac{45GMM^*R_N^3C_i}{16m_Ta^3r^{*4}}\sin 2\theta^* \sum_{k\in\mathbb{Z}} E_{0,k}\Big(\mathcal{C}''_{ik}\sin k\ell + \mathcal{D}''_{ik}\cos k\ell\Big) + \\
&\quad + \frac{15M^*R_N^3n^2\mathcal{L}'_iC_i}{8m_Tr^{*4}}\sin 2\theta^* \\
F_{3i} &= \frac{45GMM^*R_N^3C_i}{8m_Ta^3r^{*4}}\sin\theta^* \sum_{k\in\mathbb{Z}} E_{2,k}\Big(\mathcal{C}_{ik}\cos\Theta_k^* - \mathcal{D}_{ik}\sin\Theta_k^*\Big),
\end{aligned} \tag{3.28}$$

and the corresponding torque is $\mathbf{M}_i = \mathbf{r}^* \times \mathbf{F}_i$, or, since, $\mathbf{r}^* = (r^*, 0, 0)$:

$$M_{1i} = 0; \qquad M_{2i} = -r^*F_{3i}; \qquad M_{3i} = r^*F_{2i}, \tag{3.29}$$

that is

$$\begin{aligned}
M_{2i} &= -\frac{45GMM^*R_N^3C_i}{8m_Ta^3r^{*3}}\sin\theta^* \sum_{k\in\mathbb{Z}} E_{2,k}\Big(\mathcal{C}_{ik}\cos\Theta_k^* - \mathcal{D}_{ik}\sin\Theta_k^*\Big) \\
M_{3i} &= \frac{45GMM^*R_N^3C_i}{16m_Ta^3r^{*3}}\sin 2\theta^* \sum_{k\in\mathbb{Z}} E_{2,k}\Big(\mathcal{C}_{ik}\sin\Theta_k^* + \mathcal{D}_{ik}\cos\Theta_k^*\Big) + \\
&\quad + \frac{45GMM^*R_N^3C_i}{16m_Ta^3r^{*3}}\sin 2\theta^* \sum_{k\in\mathbb{Z}} E_{0,k}\Big(\mathcal{C}''_{ik}\sin k\ell + \mathcal{D}''_{ik}\cos k\ell\Big) + \\
&\quad + \frac{15M^*R_N^3n^2\mathcal{L}'_iC_i}{8m_Tr^{*3}}\sin 2\theta^*.
\end{aligned} \tag{3.30}$$

3.6 Forces and torques acting on M

Since we are interested in the force acting on M due to the tidal deformation of the i-th layer of m, we must substitute $(M^*, r^*, \theta^*, \varphi^*)$ by $(M, r, \frac{\pi}{2}, \varpi + v)$. The forces, then are

$$\begin{aligned} F_{1i} &= -\frac{135GM^2R_N^3C_i}{16m_Ta^3r^4}\sum_{k\in\mathbb{Z}} E_{2,k}\Big(\mathcal{C}_{ik}\sin\Upsilon_k + \mathcal{D}_{ik}\cos\Upsilon_k\Big) - \\ &\quad -\frac{45GM^2R_N^3C_i}{16m_Ta^3r^4}\sum_{k\in\mathbb{Z}} E_{0,k}\Big(\mathcal{C}''_{ik}\sin k\ell + \mathcal{D}''_{ik}\cos k\ell\Big) - \frac{15MR_N^3n^2\mathcal{L}'_iC_i}{8m_Tr^4} \\ F_{2i} &= 0 \\ F_{3i} &= \frac{45GM^2R_N^3C_i}{8m_Ta^3r^4}\sum_{k\in\mathbb{Z}} E_{2,k}\Big(\mathcal{C}_{ik}\cos\Upsilon_k - \mathcal{D}_{ik}\sin\Upsilon_k\Big), \end{aligned} \tag{3.31}$$

where the angle Υ_k, is defined as

$$\Upsilon_k = 2v + (k-2)\ell. \tag{3.32}$$

The corresponding torques are

$$\begin{aligned} M_{2i} &= -\frac{45GM^2R_N^3C_i}{8m_Ta^3r^3}\sum_{k\in\mathbb{Z}} E_{2,k}\Big(\mathcal{C}_{ik}\cos\Upsilon_k - \mathcal{D}_{ik}\sin\Upsilon_k\Big) \\ M_{3i} &= 0, \end{aligned} \tag{3.33}$$

After Fourier expansion, the torque along to the axis z ($M_{zi} = -M_{2i}$), can be written as

$$M_{zi} = \frac{45GM^2R_N^3C_i}{8m_Ta^6}\sum_{k,j\in\mathbb{Z}} E_{2,k}E_{2,k+j}\Big(\mathcal{C}_{ik}\cos j\ell + \mathcal{D}_{ik}\sin j\ell\Big). \tag{3.34}$$

Finally, the time average of the total torque over one period is $\langle M_{zi}\rangle = \frac{1}{2\pi}\int_0^{2\pi} M_{zi}d\ell$, therefore

$$\langle M_{zi}\rangle = \frac{45GM^2R_N^3C_i}{8m_Ta^6}\sum_{k\in\mathbb{Z}} E_{2,k}^2\mathcal{C}_{ik}. \tag{3.35}$$

The above expression for the time average, which is equivalent to take into account only the terms with $j = 0$, only is valid if ν_i is constant. This condition is satisfied, for example, by homogeneous bodies with $\gamma \gg n$, as stars and giant gaseous planets, where its stationary rotation is $\sim 6n\gamma e^2/(n^2+\gamma^2)$. However, the final rotation of the homogeneous rocky bodies, with $\gamma \ll n$, as satellites and Earth-like planets, is dominated by a forced libration $\sim B_1\cos(\ell+\phi_1)$ with the same period as the orbital motion of the system (see Chap. 3 of FM15). In this case, any time average that involves the rotation, should take

into account this oscillation. It is worth emphasizing that in this paper we calculate the time average of some quantities, as the work done by the tidal forces and the variations in semi-major axis and eccentricity, assuming which ν_i is constant, which is valid only for bodies with low viscosity. The applications to Titan in this paper were done using the complete equations, where the distinction between these extreme cases is not necessary.

3.7 Work done by the tidal forces acting on M

The time rate of the work done by the tidal forces due to the i-th layer is $\dot{W}^{(i)}_{orb} = \mathbf{F}_i \cdot \mathbf{v}$, where $\mathbf{v}$ is the relative velocity vector of the external body, whose components in spherical coordinates are

$$v_1 = \frac{nae\sin v}{\sqrt{1-e^2}}; \qquad v_2 = 0; \qquad v_3 = \frac{na^2\sqrt{1-e^2}}{r}. \tag{3.36}$$

Using the tidal force, given by the Eq. (3.31), the rate of the work corresponding to the i-th layer is

$$\begin{aligned}
\frac{dW^{(i)}_{orb}}{dt} &= -\frac{45GM^2R_N^3C_in}{8m_Ta^6}\sum_{k\in\mathbb{Z}}\Bigg\{E_{2,k}\times \\
&\times\Bigg[\mathcal{C}_{ik}\left(\frac{3e}{2\sqrt{1-e^2}}\left(\frac{a}{r}\right)^4\sin v\sin\Upsilon_k - \sqrt{1-e^2}\left(\frac{a}{r}\right)^5\cos\Upsilon_k\right)+ \\
&+\mathcal{D}_{ik}\left(\frac{3e}{2\sqrt{1-e^2}}\left(\frac{a}{r}\right)^4\sin v\cos\Upsilon_k + \sqrt{1-e^2}\left(\frac{a}{r}\right)^5\sin\Upsilon_k\right)\Bigg]+ \\
&+\frac{E_{0,k}}{3}\frac{3e}{2\sqrt{1-e^2}}\left(\frac{a}{r}\right)^4\sin v\Big(\mathcal{C}''_{ik}\sin k\ell + \mathcal{D}''_{ik}\cos k\ell\Big)\Bigg\}- \\
&-\frac{15MC_iR_N^3ne}{8m_Ta^3\sqrt{1-e^2}}n^2\mathcal{L}'_i\left(\frac{a}{r}\right)^4\sin v,
\end{aligned} \tag{3.37}$$

or after Fourier expansion[1]

$$\begin{aligned}
\frac{dW^{(i)}_{orb}}{dt} &= \frac{45GM^2R_N^3C_in}{16m_Ta^6}\sum_{k,j\in\mathbb{Z}}\Bigg((2-k-j)E_{2,k}E_{2,k+j}\Big(\mathcal{C}_{ik}\cos j\ell + \mathcal{D}_{ik}\sin j\ell\Big)- \\
&-\frac{(k+j)}{3}E_{0,k}E_{0,k+j}\Big(\mathcal{C}''_{ik}\cos j\ell + \mathcal{D}''_{ik}\sin j\ell\Big)\Bigg)- \\
&-\frac{15MC_iR_N^3ne}{8m_Ta^3\sqrt{1-e^2}}n^2\mathcal{L}'_i\left(\frac{a}{r}\right)^4\sin v.
\end{aligned} \tag{3.38}$$

[1] For the details of this calculation, see Appendix F.

The time-average over one period is

$$\left\langle \frac{dW_{orb}^{(i)}}{dt} \right\rangle_{tide} = \frac{45GM^2R_N^3C_in}{16m_Ta^6} \sum_{k\in\mathbb{Z}} \left((2-k)E_{2,k}^2\mathcal{C}_{ik} - \frac{k}{3}E_{0,k}^2\mathcal{C}''_{ik} \right). \tag{3.39}$$

The average of the last term of Eq. (3.38) is

$$\frac{1}{2\pi}\int_0^{2\pi} n^2\mathcal{L}'_i \left(\frac{a}{r}\right)^4 \sin v \; d\ell = \sum_{j=1}^{N} \frac{\Delta\left(R_i^5(\mathsf{E}^{-1})_{ij}x_j^3\right)}{R_i^5 - R_{i-1}^5} \frac{1}{2\pi}\int_0^{2\pi} \Omega_j^2 \left(\frac{a}{r}\right)^4 \sin v \; d\ell = 0, \tag{3.40}$$

(see Appendix D).

3.8 Variations in semi-major axis and eccentricity

In this section, we calculate the variation in semi-major axis and eccentricity. For this, we use the energy and angular momentum definitions. If we differentiate the equation

$$W_{orb} = -\frac{GMm_T}{2a},$$

where a is the semi-major axis of the relative orbit, we obtain the equation for the rate of variation in semi-major axis:

$$\dot{a} = \frac{2a^2\dot{W}_{orb}}{GMm_T}. \tag{3.41}$$

In the same way, if we differentiate the angular momentum equation, we obtain

$$L = \frac{Mm_T}{M+m_T} na^2\sqrt{1-e^2} = \frac{GMm_T}{na}\sqrt{1-e^2},$$

where e is the eccentricity of the relative orbit, and using $\dot{n}/n = -3\dot{a}/2a$, we obtain the equation for the rate of variation in eccentricity

$$\frac{e\dot{e}}{1-e^2} = -\frac{\dot{L}}{L} - \frac{\dot{W}_{orb}}{2W_{orb}}, \tag{3.42}$$

where $\dot{L} = \mathcal{M}_z$ is the total torque exerted by the tidal forces. The internal torques between the different layers of m, such as the friction forces and to the gravitational coupling, cancel themselves and do not affect the orbital motion.

Using Eqs. (3.41) and (3.34) and summing over all layers, we obtain the equation for

the variation in semi-major axis:

$$\begin{aligned}\dot{a} &= \sum_{i=1}^{N}\frac{45MR_N^3C_in}{8m_T^2a^4}\sum_{k,j\in\mathbb{Z}}\Bigg((2-k-j)E_{2,k}E_{2,k+j}\Big(\mathcal{C}_{ik}\cos j\ell+\mathcal{D}_{ik}\sin j\ell\Big)-\\ &-\frac{(k+j)}{3}E_{0,k}E_{0,k+j}\Big(\mathcal{C}''_{ik}\cos j\ell+\mathcal{D}''_{ik}\sin j\ell\Big)\Bigg)-\\ &-\frac{15R_N^3n^3e}{4Gm_T^2a\sqrt{1-e^2}}\left(\frac{a}{r}\right)^4\sin v\sum_{i=1}^{N}C_i\mathcal{L}'_i. \end{aligned}\tag{3.43}$$

After the time-average over one period, we obtain that the variation in semi-major axes is

$$\langle\dot{a}\rangle = \sum_{i=1}^{N}\frac{45MR_N^3C_in}{8m_T^2a^4}\sum_{k\in\mathbb{Z}}\left((2-k)E_{2,k}^2\mathcal{C}_{ik}-\frac{k}{3}E_{0,k}^2\mathcal{C}''_{ik}\right),\tag{3.44}$$

or

$$\langle\dot{a}\rangle = \frac{45MR_N^3Cn}{16m_T^2a^4}\sum_{i=1}^{N}\sum_{k\in\mathbb{Z}}\mathcal{Q}_i\left((2-k)E_{2,k}^2\sin 2\sigma_{ik}-\frac{k}{3}E_{0,k}^2\sin 2\sigma''_{ik}\right),\tag{3.45}$$

where the parameter $\mathcal{Q}_i$ is defined as

$$\mathcal{Q}_i=\Delta\left(\frac{-C_{i+1}}{R_{i+1}^5-R_i^5}\right)\frac{R_i^5\mathcal{H}_i}{C},\tag{3.46}$$

where $C_{N+1}=0$ (since $d_{N+1}=0$) and $R_0=0$. An elementary calculation using the axial moment of inertia of the i-th-layer C_i (see Section A) and the total axial moment of inertia $C=\frac{8\pi}{15}d_1R_N^5g_N$, with $g_N=5\int_0^1\widehat{d}(z)z^4\,dz$, gives

$$\mathcal{Q}_i=\frac{1}{g_N}(\widehat{d}_i-\widehat{d}_{i+1})x_i^5\mathcal{H}_i>0,\tag{3.47}$$

or, using the Eq. (2.42),

$$\sum_{i=1}^{N}\mathcal{Q}_i=\frac{2f_N}{3g_N}k_f,\tag{3.48}$$

where k_f is the tidal fluid Love number.

In the same way, using the Eq. (3.42), replacing $\mathcal{M}_z$ and $\dot{W}_{orb}$ by the Eqs. (3.34) and (3.38), and summing over all layers, we obtain

$$\begin{aligned}\dot{e} &= -\sum_{i=1}^{N}\frac{45MR_N^3C_in}{8m_T^2a^4}\frac{(1-e^2)}{2ae}\sum_{k,j\in\mathbb{Z}}\Bigg(\Big(\frac{2}{\sqrt{1-e^2}}-(2-k-j)\Big)E_{2,k}E_{2,k+j}\times\\ &\times\Big(\mathcal{C}_{ik}\cos j\ell+\mathcal{D}_{ik}\sin j\ell\Big)+\frac{(k+j)}{3}E_{0,k}E_{0,k+j}\Big(\mathcal{C}''_{ik}\cos j\ell+\mathcal{D}''_{ik}\sin j\ell\Big)\Bigg)-\\ &-\frac{15R_N^3n^3}{8Gm_T^2a^2}\sqrt{1-e^2}\left(\frac{a}{r}\right)^4\sin v\sum_{i=1}^{N}C_i\mathcal{L}'_i.\end{aligned}\tag{3.49}$$

After the time-average over one period, we obtain that the variation in eccentricity is

$$\langle \dot{e} \rangle = -\sum_{i=1}^{N} \frac{45 M R_N^3 C_i n}{8 m_T^2 a^4} \frac{(1-e^2)}{2ae} \sum_{k,j \in \mathbb{Z}} \left(\left(\frac{2}{\sqrt{1-e^2}} - (2-k) \right) E_{2,k}^2 \mathcal{C}_{ik} + \frac{k}{3} E_{0,k}^2 \mathcal{C}_{ik}'' \right), \tag{3.50}$$

or

$$\begin{aligned} \langle \dot{e} \rangle = & -\frac{45 M R_N^3 C n}{16 m_T^2 a^4} \frac{(1-e^2)}{2ae} \times \\ & \times \sum_{i=1}^{N} \sum_{k \in \mathbb{Z}} \mathcal{Q}_i \left[\left(\frac{2}{\sqrt{1-e^2}} - (2-k) \right) E_{2,k}^2 \sin 2\sigma_{ik} + \frac{k}{3} E_{0,k}^2 \sin 2\sigma_{ik}'' \right]. \end{aligned} \tag{3.51}$$

It is important to note that the parameter $\mathcal{Q}_i$ only depends on the internal structure. When $N = 1$, we obtain $\mathcal{Q}_1 = 1$, and recover the same differential equations of the homogeneous case given in FM15. In the general case, the variations in semi-major axis and eccentricity can be expressed as the sum of the contribution of each layer weighed by this parameter.

Chapter 4

The two-layer model

In the previous chapters we have studied the tidal effect on one body composed of N homogeneous layers. However, in contrast with a homogeneous body, in one differentiated body we must also take into account the interaction between the different layers. In this chapter, we consider two important interaction effects: the gravitational coupling and the friction that occurs at each interface of two layers in contact.

An important point to keeping mind is the number of layers to consider, because the number free parameters increases significantly as the number of layers is increased. For this reason, here, we study the simplest non-homogeneous problem: one body formed by two independent rotating parts. The inner layer, or *core*, is denoted with the subscript c and the outer layer, or *shell*, is denoted with the subscript s. Despite its simplicity, the two-layer model allows to study the main features, introducing a minimum number of free parameters.

4.1 The tidal torques

The tidal torques due to the core and the shell, along the axis z, are (see Eq. (3.34))

$$\begin{aligned} M_{zc} &= T_{cc} C_c \mathcal{T}_c \\ M_{zs} &= T_{ss} C_s \mathcal{T}_s - T_{sc} C_s \mathcal{T}_c, \end{aligned} \tag{4.1}$$

where the function $\mathcal{T}_i$ (with $i = c, s$) is

$$\mathcal{T}_i = \sum_{k,j \in \mathbb{Z}} E_{2,k} E_{2,k+j} \frac{\gamma_i (\nu_j + kn) \cos j\ell + \gamma_i^2 \sin j\ell}{\gamma_i^2 + (\nu_i + kn)^2}, \tag{4.2}$$

the constants T_{ij} are

$$T_{cc} = \mathcal{T}\mathcal{H}_c; \qquad T_{sc} = \frac{\mathcal{T}\mathcal{H}_c R_c^5}{R_s^5 - R_c^5}; \qquad T_{ss} = \frac{\mathcal{T}\mathcal{H}_s R_s^5}{R_s^5 - R_c^5}, \tag{4.3}$$

and the tidal parameter $\mathcal{T}$, is defined as

$$\mathcal{T} = \frac{45GM^2R_s^3}{8m_T a^6} \approx \frac{3n^2\bar{\epsilon}_\rho}{2}. \tag{4.4}$$

R_c, C_c are the mean outer radius and moment of inertia of the core, and R_s, C_s are the mean outer radius and moment of inertia of the shell. The parameters $\mathcal{H}_c$, γ_c are the Clairaut parameter and the relaxation factor at the core-shell interface and $\mathcal{H}_s$, γ_s are the Clairaut parameter and the relaxation factor at the body's surface.

4.2 The gravitational coupling

When the principal axes of inertia of two layers are not aligned, a restoring gravitational torque which tends to align these axes appears. This torque was calculated by several authors (e.g. Buffett, 1996; Van Hoolst et al., 2008; Karatekin et al., 2008; Callegari et al., 2015) when the layers are rigid. Here, we use one similar expression for this torque adapted to a body assumed as formed by two layers whose boundaries are prolate ellipsoids, whose flattenings are defined by the composition of the main elastic and anelastic tidal components.

In the case of one body composed by N homogeneous layers, the torque acting on the inner i-th layer due to the outer j-th layer (not necessarily contiguous) is

$$\mathbf{\Gamma}_{ij} = \int_{m_j} (\mathbf{r} \times \nabla \delta U_i)\, dm_j = \int_0^{2\pi} \int_0^{\pi} \int_{\zeta'_{j-1}}^{\zeta'_j} d_j\, (\mathbf{r} \times \nabla \delta U_i)\, r^2 \sin\theta\, dr\, d\theta\, d\varphi, \tag{4.5}$$

where d_j, m_j are the density and the mass in the j-th layer and δU_i is the disturbing potential of the i-th layer at an external point.

The limits of the integral in Eq. (4.5), ζ'_{j-1} and ζ'_j, are the *real* outer and inner boundaries of the j-th layer, respectively. In our model we have to consider the actual flattening of the surfaces, which is the composition of the main elastic and anelastic tidal components (see Sec. 10 of Ferraz-Mello, 2013). The addition of the two components is virtually equivalent to the use ab initio of the Maxwell viscoelastic model as done by Correia et al. (2014) (Ferraz-Mello, 2015b).

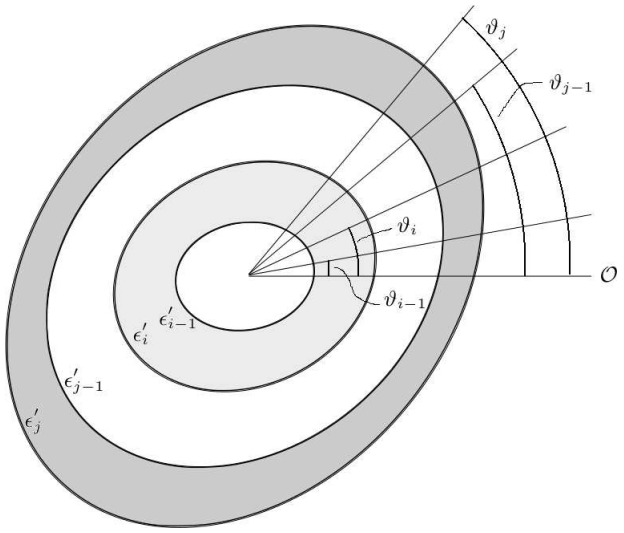

Figure 4.1: Equatorial section of the i-th and j-th layers. ϵ'_i and ϵ'_{i-1} are the outer and the inner equatorial flattenings of the i-th layer and the angles ϑ_i and ϑ_{i-1} are its outer and inner geodetic lags. Similarly, ϵ'_j and ϵ'_{j-1} are the outer and the inner equatorial flattenings and ϑ_j and ϑ_{j-1} are the equatorial flattenings and the geodetic lags of the j-th layer.

Assuming that the elastic and the tidal components have ellipsoidal surfaces (not aligned), the resulting surface can be approximated by a prolate ellipsoid with equatorial flattening ϵ' and rotated by an angle ϑ with respect to M. For the sake of simplicity, we also assume that the relative motion of the outer body M is circular. Then, neglecting the axial term does not contribute to the calculation of the gravitational coupling, the height of the outer surface of the j-th layer with respect to the one sphere of radius R_j, in polar coordinates, rotated by an angle ϑ_j with respect to M and to first order in the flattenings (see Fig. 4.2), is

$$\begin{aligned}\delta\zeta'_j &= \frac{1}{2}R_j\epsilon'_j\sin^2\theta\cos\left(2\varphi-2\vartheta_j\right)=\frac{1}{2}R_j\mathcal{H}_j\bar{\epsilon}_J\lambda_j\sin^2\theta\cos 2\varphi+\\ &+\frac{1}{2}R_j\mathcal{H}_j\bar{\epsilon}_J\cos\sigma_{j0}\sin^2\theta\cos\left(2\varphi-\sigma_{j0}\right),\end{aligned}\tag{4.6}$$

where $0<\lambda_j<1$ is a relative measurement of the maximum height of the elastic tides of the outer boundary of the j-th layer. The angle ϑ_j is often called the *geodetic lag* of the surface.

If we open the trigonometric functions, by identification of the terms with same trigonometric arguments, the resulting equatorial flattening of the outer boundary of the j-th layer is

$$\epsilon'_j=\mathcal{H}_j\bar{\epsilon}_J\sqrt{\lambda_j^2+\cos^2\sigma_{j0}(1+2\lambda_j)},\tag{4.7}$$

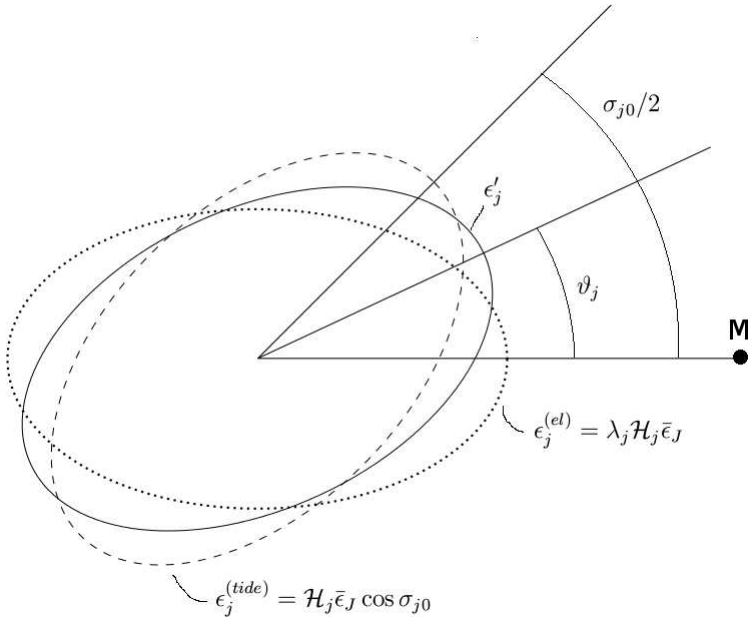

Figure 4.2: Scheme of the composition of the elastic and anelastic tides of the outer boundary of the j-th layer. $\epsilon_j^{(el)}$ (dotted ellipsoid) and $\epsilon_j^{(tide)}$ (dashed ellipsoid) are the equatorial flattenings of the main elastic and anelastic tides, respectively, and ϵ'_j is the equatorial flattening of the ellipsoidal surface which result of this composition (solid ellipsoid). The semi-major axis of the elastic ellipsoid is oriented towards M.

and the geodetic lag is

$$\vartheta_j = \frac{1}{2}\tan^{-1}\left(\frac{\sin 2\sigma_{j0}}{1+2\lambda_j+\cos 2\sigma_{j0}}\right). \tag{4.8}$$

The height of the inner boundary of the j-th layer, taking into account the composition of the main elastic and anelastic tides has an identical expression:

$$\begin{aligned}\delta\zeta'_{j-1} &= \frac{1}{2}R_{j-1}\epsilon'_{j-1}\sin^2\theta\cos\left(2\varphi-2\vartheta_{j-1}\right) = \frac{1}{2}R_{j-1}\mathcal{H}_{j-1}\bar{\epsilon}_J\lambda_{j-1}\sin^2\theta\cos 2\varphi + \\ &+\frac{1}{2}R_{j-1}\mathcal{H}_{j-1}\bar{\epsilon}_J\cos\sigma_{j-1,0}\sin^2\theta\cos\left(2\varphi-\sigma_{j-1,0}\right),\end{aligned} \tag{4.9}$$

where $0<\lambda_{j-1}<1$ is a relative measurement of the maximum height of the elastic tides of the inner boundary of the j-th layer. Then, the resulting equatorial flattening is

$$\epsilon'_{j-1} = \mathcal{H}_{j-1}\bar{\epsilon}_J\sqrt{\lambda_{j-1}^2+\cos^2\sigma_{j-1,0}(1+2\lambda_{j-1})}, \tag{4.10}$$

and the geodetic lag is

$$\vartheta_{j-1} = \frac{1}{2}\tan^{-1}\left(\frac{\sin 2\sigma_{j-1,0}}{1+2\lambda_{j-1}+\cos 2\sigma_{j-1,0}}\right). \tag{4.11}$$

In the same way, we assume that the ellipsoidal shape of this layer is also given by the composition of the main elastic and anelastic tidal components. Then, the inner and outer

equatorial flattenings, respectively, are

$$\epsilon'_{i-1} = \mathcal{H}_{i-1}\bar{\epsilon}_J\sqrt{\lambda_{i-1}^2 + \cos^2\sigma_{i-1,0}(1+2\lambda_{i-1})}; \qquad \epsilon'_i = \mathcal{H}_i\bar{\epsilon}_J\sqrt{\lambda_i^2 + \cos^2\sigma_{i0}(1+2\lambda_i)}, \tag{4.12}$$

and the corresponding geodetic lags are

$$\vartheta_i = \frac{1}{2}\tan^{-1}\left(\frac{\sin 2\sigma_{i0}}{1+2\lambda_i+\cos 2\sigma_{i0}}\right); \qquad \vartheta_{i-1} = \frac{1}{2}\tan^{-1}\left(\frac{\sin 2\sigma_{i-1,0}}{1+2\lambda_{i-1}+\cos 2\sigma_{i-1,0}}\right), \tag{4.13}$$

where $0 < \lambda_i, \lambda_{i-1} < 1$ are relative measurements of the maximum heights of the elastic tides of the outer and inner boundaries of the i-th layer.

Using the expression of the disturbing portential, given by Eq. (A.36), and neglecting the axial term, we obtain

$$\delta U_i = -\frac{3GC_i}{4r^3}\sin^2\theta\frac{\Delta\left(R_i^5\epsilon'_i\cos\left(2\varphi-2\vartheta_i\right)\right)}{R_i^5 - R_{i-1}^5}, \tag{4.14}$$

where $\Delta(f_i) = f_i - f_{i-1}$, denotes the increment of one function f_i between the inner and the outer boundaries of this layer. Then, the vectorial product in Eq. (4.5) is

$$\mathbf{r}\times\nabla\delta U_i = -\frac{2\pi G d_i}{5r^3}\Big(2\sin\theta\Delta\left(R_i^5\epsilon'_i\sin\left(2\varphi-2\vartheta_i\right)\right)\widehat{\boldsymbol{\theta}} + \sin 2\theta\Delta\left(R_i^5\epsilon'_i\cos\left(2\varphi-2\vartheta_i\right)\right)\widehat{\boldsymbol{\varphi}}\Big). \tag{4.15}$$

Using the polar unitary vectors in Cartesian coordinates

$$\begin{aligned}\widehat{\boldsymbol{\theta}} &= \cos\theta\cos\varphi\ \widehat{\mathbf{x}} + \cos\theta\sin\varphi\ \widehat{\mathbf{y}} - \sin\theta\ \widehat{\mathbf{z}}\\ \widehat{\boldsymbol{\varphi}} &= -\sin\varphi\ \widehat{\mathbf{x}} + \cos\varphi\ \widehat{\mathbf{y}},\end{aligned} \tag{4.16}$$

and the approximation of $\ln\zeta_j/\zeta_{j-1}$ to first order in the flattenings

$$\ln\frac{\zeta_j}{\zeta_{j-1}} \approx \ln\frac{R_j}{R_{j-1}} + \frac{1}{2}R_j\epsilon'_j\sin^2\theta\cos\left(2\varphi-2\vartheta_j\right) - \frac{1}{2}R_{j-1}\epsilon'_{j-1}\sin^2\theta\cos\left(2\varphi-2\vartheta_{j-1}\right), \tag{4.17}$$

then, the torque acting on the inner i-th layer due to the outer j-th layer is

$$\boldsymbol{\Gamma}_{ij} = \frac{32\pi^2 G}{75}d_i d_j\Delta_{ij}\left(R_i^5\epsilon'_i\epsilon'_j\sin\left(2\vartheta_j-2\vartheta_i\right)\right)\widehat{\mathbf{z}}, \tag{4.18}$$

where $\Delta_{ij}(f_{ij}) \stackrel{\text{def}}{=} \Delta(f_{ij}) - \Delta(f_{i,j-1}) = f_{ij} - f_{i-1,j} - f_{i,j-1} + f_{i-1,j-1}$.

As the torque acting on the outer j-th layer, due to the inner i-th layer, is the reaction

$$\boldsymbol{\Gamma}_{ji} = -\boldsymbol{\Gamma}_{ij}, \tag{4.19}$$

then, the total gravitational coupling, acting on the i-th layer can be written as

$$\mathbf{\Gamma}_i = \sum_{p=1;\ p\neq i}^{N} \mathbf{\Gamma}_{ip} = -\sum_{p=1}^{i-1} \mathbf{\Gamma}_{pi} + \sum_{p=i+1}^{N} \mathbf{\Gamma}_{ip}. \tag{4.20}$$

If we consider the two-layer model, the torques acting on the core and the shell are

$$\begin{aligned} \Gamma_c &= K \sin\left(2\vartheta_s - 2\vartheta_c\right) \\ \Gamma_s &= -K \sin\left(2\vartheta_s - 2\vartheta_c\right), \end{aligned} \tag{4.21}$$

where the gravitational coupling parameter K is

$$K = \frac{32\pi^2 G}{75} d_c d_s \epsilon_c' \epsilon_s' R_c^5. \tag{4.22}$$

The equatorial flattenings are

$$\epsilon_c' = \mathcal{H}_c \bar{\epsilon}_J \sqrt{\lambda_c^2 + \cos^2\sigma_{c0}(1+2\lambda_c)}; \qquad \epsilon_s' = \mathcal{H}_s \bar{\epsilon}_J \sqrt{\lambda_s^2 + \cos^2\sigma_{s0}(1+2\lambda_s)}, \tag{4.23}$$

and the geodetic lags are

$$\vartheta_c = \frac{1}{2}\tan^{-1}\left(\frac{\sin 2\sigma_{c0}}{1+2\lambda_c+\cos 2\sigma_{c0}}\right); \qquad \vartheta_s = \frac{1}{2}\tan^{-1}\left(\frac{\sin 2\sigma_{s0}}{1+2\lambda_s+\cos 2\sigma_{s0}}\right). \tag{4.24}$$

The parameters $0 < \lambda_c, \lambda_s < 1$ are relative measurements of the heights of the elastic tides of the outer surfaces of the core and the shell, respectively. The trigonometric $\sin 2\sigma_{i0}$ and $\cos^2\sigma_{i0}$ are frequency functions given in Eq. (3.26). An elementary calculation shows that

$$\cos 2\sigma_{i0} = \frac{\gamma_i^2 - \nu_i^2}{\gamma_i^2 + \nu_i^2}. \tag{4.25}$$

4.3 Linear drag

The model considered here also assumes that a linear friction occurs between two contiguous layers. We assume that between two contiguous layers (for instance, the inner boundary of the i-th layer and the outer boundary of the $(i+1)$-th layer) exists a thin liquid boundary with viscosity $\widehat{\eta}_i$ and thickness h_i.

We assume that the torque, along to the axis z, acting on the inner i-th layer due to the outer $(i+1)$-th layer is

$$\Phi_{i,i+1} = \mu_i(\Omega_{i+1} - \Omega_i), \tag{4.26}$$

and vice-versa. The friction coefficient μ_i of the i-th boundary is an undetermined constant.

Let $d\mathbf{F}_{i,i+1}$ be the force acting tangentially on the area element of an sphere of radius R_i. If the fluid in contact with the surface of the sphere is a Newton fluid, the modulus of the force is (Papanastasious et al., 2000, Chap. 6)

$$dF_{i,i+1} = \frac{\widehat{\eta}_i}{h_i} V_i R_i^2 \sin\theta \; d\phi \; d\theta \tag{4.27}$$

where $V_i = R_i \sin\theta(\Omega_{i+1} - \Omega_i)$ is the relative velocity of the $(i+1)$-th layer with respect to the i-th layer at the latitude θ and R_i, ϕ, θ are the spherical coordinates of the center of the area element. The modulus of the torque of the force $d\mathbf{F}_{i,i+1}$, along to the axis z, is

$$d\Phi_{i,i+1} = R_i \sin\theta \; dF_{i,i+1}. \tag{4.28}$$

The element of area is $R_i d\theta \times R_i \sin\theta d\phi$. The integral of $d\Phi_{i,i+1}$ over the sphere is easy to calculate giving

$$\Phi_{i,i+1} = \int_0^{2\pi} \int_0^{\pi} \frac{\widehat{\eta}_i}{h_i} R_i^4 \sin^3\theta(\Omega_{i+1} - \Omega_i) d\theta \; d\phi = \frac{8\pi}{3} \; \frac{\widehat{\eta}_i}{h_i} R_i^4 (\Omega_{i+1} - \Omega_i) \tag{4.29}$$

If we compare with the law used to introduce the friction, we obtain

$$\mu_i = \frac{8\pi}{3} \; \frac{\widehat{\eta}_i}{h_i} R_i^4. \tag{4.30}$$

This is the law corresponding to a liquid-solid boundary for low speeds.

The torque, along to the axis z, acting on the inner $(i+1)$-th layer due to the outer i-th layer is

$$\Phi_{i+1,i} \;\; = \;\; -\Phi_{i,i+1} = -\mu_i(\Omega_{i+1} - \Omega_i). \tag{4.31}$$

Then, the total torque, due to the friction, acting on the i-th layer is the sum of the torque due to the outer $(i+1)$-th layer plus the the torque due to the inner $(i-1)$-th layer

$$\Phi_i = \Phi_{i,i-1} + \Phi_{i,i+1} = \mu_{i-1}(\Omega_{i-1} - \Omega_i) - \mu_i(\Omega_i - \Omega_{i+1}). \tag{4.32}$$

In the two-layer model, the torque acting on the core due to the shell and the torque acting on the shell due to the core are, respectively

$$\begin{aligned} \Phi_c &= \mu(\Omega_s - \Omega_c) \\ \Phi_s &= -\mu(\Omega_s - \Omega_c), \end{aligned} \tag{4.33}$$

where η_o and h are the viscosity and the thickness, respectively, of the core-shell boundary and

$$\mu = \frac{8\pi}{3} \; \frac{\eta_o}{h} R_c^4. \tag{4.34}$$

4.4 Rotational equations

Putting together all contributions to the torque, we obtain the rotational equations

$$\begin{aligned} C_c\dot{\Omega}_c &= \mathcal{M}_z^{core} = -M_{zc} + \Gamma_c + \Phi_c \\ C_s\dot{\Omega}_s &= \mathcal{M}_z^{shell} = -M_{zs} + \Gamma_s + \Phi_s, \end{aligned} \tag{4.35}$$

where $\mathcal{M}_z^{core}$ and $\mathcal{M}_z^{shell}$ are the z-components of the total torque acting on the core and on the shell. These torques include the reaction of the tidal torque M_{zi} acting on the i-th layer, the gravitational coupling Γ_i and the friction Φ_i.

4.5 Comparison with the homogeneous case

In this section, we compare some of the main features of the homogeneous creep tide theory, developed in FM15, with the non-homogeneous creep tide theory for the two-layer model developed in this article. The main difficulty lies in the number of free parameters in these approaches. In the homogeneous case, with a suitable choice of dimensionless variables, the final state of rotation depends only on the ratio n/γ and on the eccentricity e (Eq. (42) of FM15). However, even in the most simple non-homogeneous case (the two-layer model), we need to set 12 free parameters. In order to proceed, we use the typical values for Titan and also Titan's eccentricity $e = 0.028$ (see Tables 5.1-5.4 in Sec. 5.2), and let as free parameters, only n/γ_i, e and μ.

Following FM15, we indroduce the adimensional variables $y_i = \nu_i/\bar{\gamma}$ and the scaled time $x = \ell/\bar{\gamma}$, where $\bar{\gamma} = 2\gamma_c\gamma_s(\gamma_c + \gamma_s)^{-1}$. If we consider the case in which $\gamma_c = \gamma_s$, the behavior of the evolutions of y_c and y_s is similar to that observed in the homogeneous case. Fig. 4.3 shows the time evolution of y_s, with inital conditions $y_c = 0.3$, $y_s = 0.15$ and differents values of $\alpha = \log_{10}(n/\gamma_c) = \log_{10}(n/\gamma_s)$. When $\gamma_i \ll n$ (i.e. rocky bodies), after a transient, the solution oscillates around zero, independently of the inital conditions (*left* panel), and the amplitude of oscillation decreases when α decreases. In the case $\alpha = 4$, we also plot the solution with initial conditions $y_c = 0.3$ and $y_s = -0.15$ (dashed black line). This solution increases quickly, becoming indistinguishable of the solution with initial value $y_s = 0.15$. When $\gamma_i \sim n$, the stationary solution becomes a super-synchronous rotation with the amplitude of the oscillation tending to zero. Finally, when $\gamma_i \gg n$, the stationary

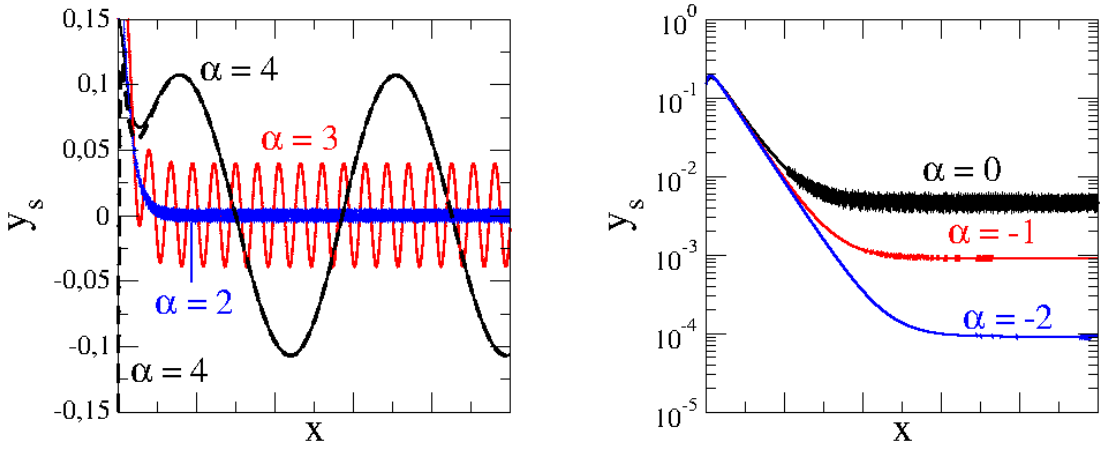

Figure 4.3: Evolution of y_s for the case $\gamma_c = \gamma_s$ with initial conditions $y_c = 0.3$ and $y_s = 0.15$ and several values of $\alpha = \log_{10}(n/\gamma_c) = \log_{10}(n/\gamma_s)$. For $\alpha = 4$, we also plot the initial conditions $y_s = 0$ and $y_s = -0.15$. *Left*: $\alpha = 4, 3, 2$. *Right*: $\alpha = 0, -1, -2$.

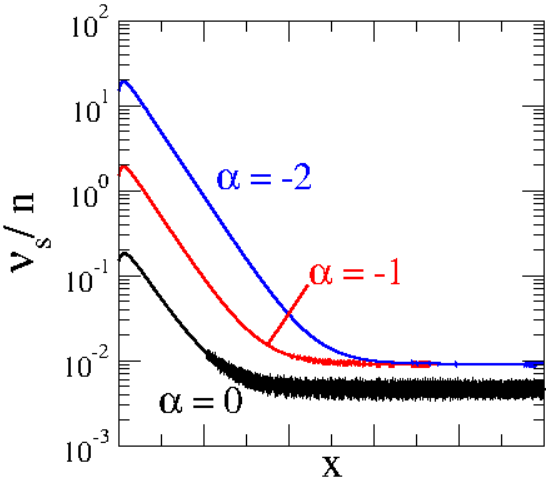

Figure 4.4: Same as Fig. (4.3), with ν_s/n instead of y_s.

solution of y_s becomes closer zero (*right* panel), but $\nu_s = \bar{\gamma} y_s$ tends to $12e^2$, independently of the value of α (Fig. 4.4). The evolution of y_c is very similar and the friction does not have any relevant role.

When $\gamma_c \neq \gamma_s$, we can have a different behavior of the core and shell rotations. In Fig. 4.5, we show the core and shell rotation (*left* and *right*, respectively) for $\log_{10}(n/\gamma_c) = 2$ and $\log_{10}(n/\gamma_s) = 4$. We also set two very differents values for the friction: the frictionless case $\mu = 0$ (black) and a very high value of friction $\mu = 10^{28}$ kg km^{2}s^{-1} (red lines), larger than the expected value in the case of Titan ($\mu = 10^{11} - 10^{13}$ kg km^{2}s^{-1}), which corresponds to a typical ocean viscosity $\eta_o = \eta_{H_2O} \approx 10^{-3}$ Pa s and a large range for the

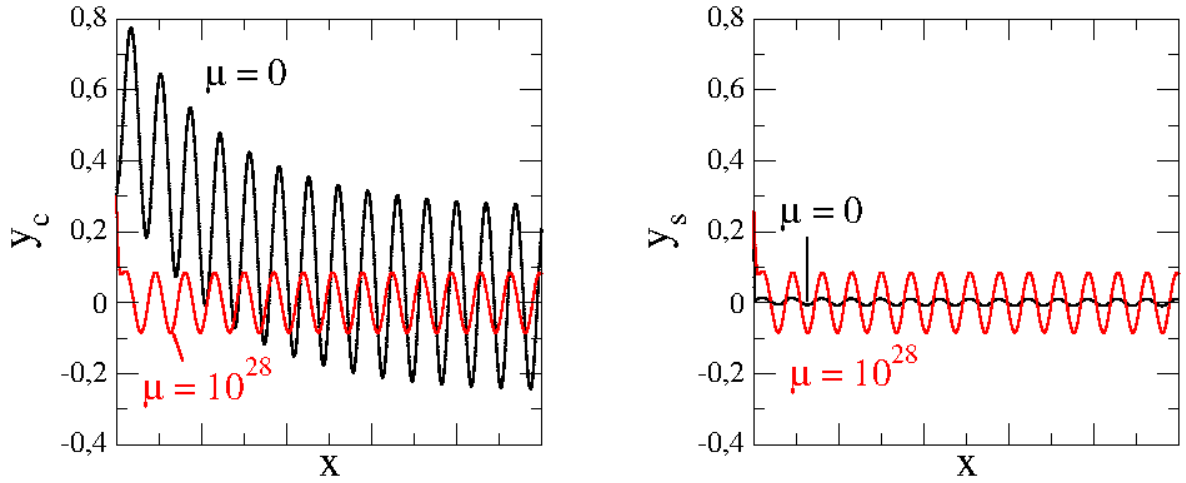

Figure 4.5: Evolution of y_c and y_s for initial conditions $y_c = 0.3$ and $y_s = 0.15$, relaxation factors such that $\log_{10}(n/\gamma_c) = 2$ and $\log_{10}(n/\gamma_s) = 4$, and two values of the friction parameter: $\mu = 0$ (black) and $\mu = 10^{28}$ kg km^{2}s^{-1} (red).

ocean thickness h (see Eq. 4.34). In the frictionless case, we can observe the differential rotation between the core and the shell. After a transient, both solutions oscillate around zero with very different amplitudes, depending on the value of γ of each surface. For very high friction parameter, both layers rotate with the same angular velocity. The core and the shell have the same amplitude of oscillation and phase, keeping the relative velocity equal to zero.

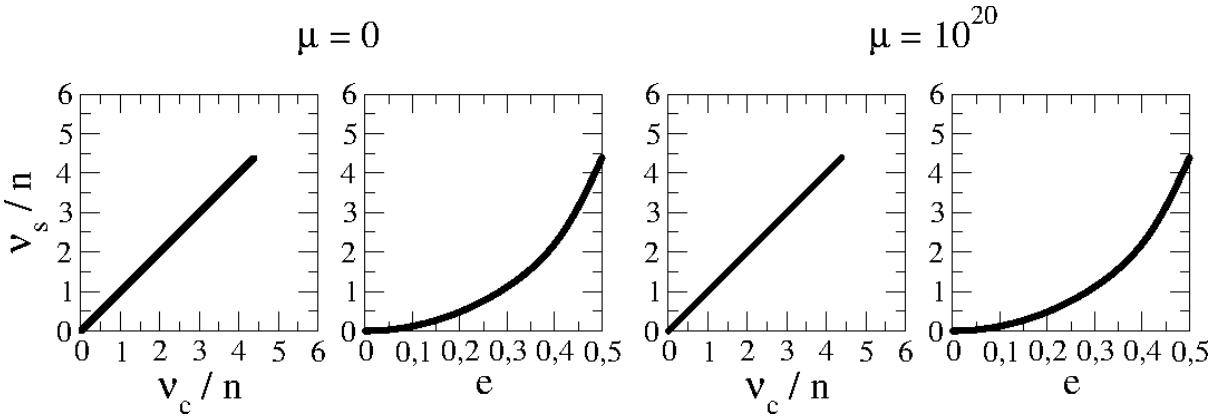

Figure 4.6: Family of stationary super-synchronous with rotations relaxation factors equal and such that $n/\gamma_c = n/\gamma_s = 0.01$ and $0 \leq e \leq 0.5$. *Left*: $\mu = 0$. *Right*: $\mu = 10^{20}$ kg km^{2}s^{-1}.

Finally, we study the dependence of the stationary solutions on the eccentricity. For that sake, we choose a grid of initial conditions ν_c/n and ν_s/n, and integrate the system (4.35) until the stationary solution is reached. When $n/\gamma_c = n/\gamma_s \ll 1$, all initial conditions

lead to the same equilibrium point (a super-synchronous rotation), independently of the value of the friction parameter. The value of the excess of rotation depends only on the eccentricity. In the *left* panels of Fig. 4.6, we show the family of stationary solutions, where each point corresponds to a different eccentricity value in $0 \leq e \leq 0.5$. If the eccentricity is zero, the rotations are synchronous to the orbital motion. When the eccentricity increases, the rotations become super-synchronous, and the excess of rotation ν_i/n is proportional to e^2 (*right* panels).

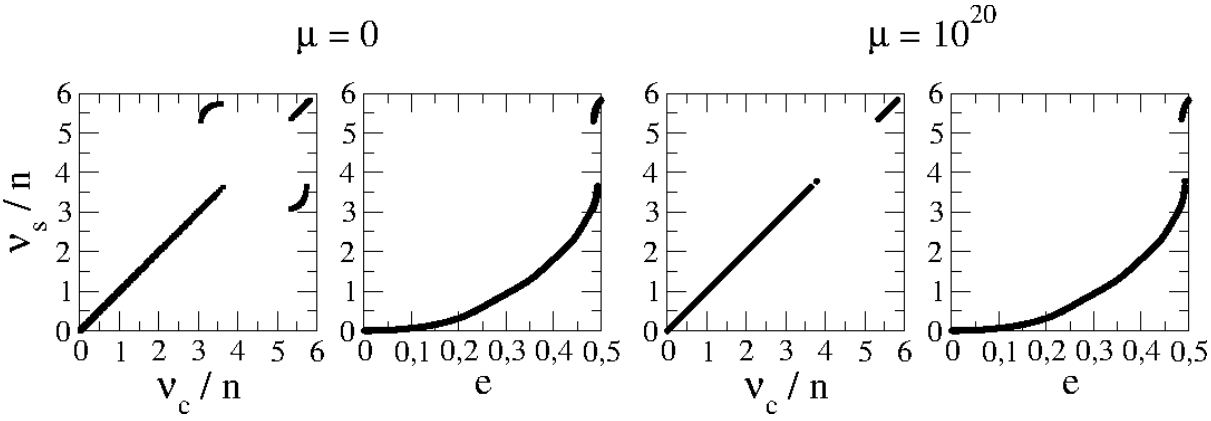

Figure 4.7: Families of stationary rotations for $n/\gamma_c = n/\gamma_s = 1$ and $0 \leq e \leq 0.5$. *Top*: $\mu = 0$. *Bottom*: $\mu = 10^{20}$ kg km^{2}s^{-1}.

When n/γ_c and n/γ_s increase, that is, when the viscosities increase, the excess in the super-synchronous rotation decreases. If the eccentricity is low, the only attractor is the super-synchronous solution. When the eccentricity increases, captures in other attractors $\nu_i \simeq n, 2n, 3n, \ldots$ appear gradually. This behavior was largely studied in FM15 and also in Correia et al. (2014).

Fig. 4.7 shows the families of stationary rotation for $n/\gamma_c = n/\gamma_s = 1$, $0 \leq e \leq 0.5$ and two values of the friction parameter: the frictionless case, with $\mu = 0$ (*top* panels), and a very high friction case, with $\mu = 10^{20}$ kg km^{2}s^{-1} (*bottom* panels). In the frictionless case, when the eccentricity is smaller than ~ 0.48, only the super-synchronous solution is possible. If the eccentricity is larger than 0.48, besides the super-synchronous solution, three new stationary configurations appear: The core and the shell in the 3/2 commensurability ($\nu_c \simeq n$ and $\nu_s \simeq n$), the core in super-synchronous rotation and the shell in the 3/2 commensurability ($\nu_c \simeq 0$ and $\nu_s \simeq n$) and the core in the 3/2 commensurability and the shell in super-synchronous rotation ($\nu_c \simeq n$ and $\nu_s \simeq 0$). Fig. 4.8 shows in more

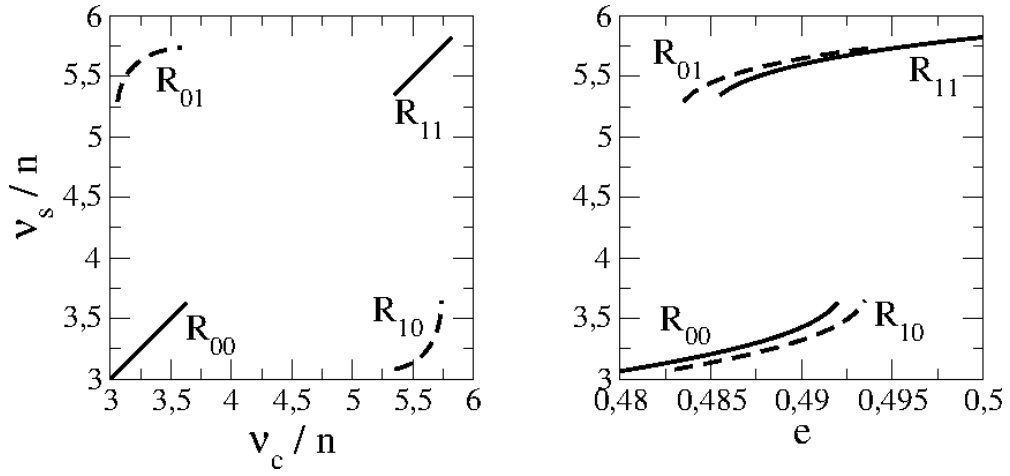

Figure 4.8: Families of stationary rotations with rotations relaxation factors equal and such that $n/\gamma_c = n/\gamma_s = 1$, $0 \leq e \leq 0.5$ and $\mu = 0$. Labels R_{pq} indicates the two frequencies: $\nu_c = pn$ and $\nu_s = qn$.

detail these stationary solutions. The labels R_{pq} denote the stationary families indicating the resonances $\nu_c = pn$ and $\nu_s = qn$. It is important to note that the excess in the rotations are large because the eccentricity is high. In the high friction case (*bottom* panels of Fig. 4.7), only the stationary solutions with the same commensurabilities survive because in these configurations, the relative velocity of rotation between the core and the shell is zero. Fig. 4.9 shows the four basins of each equilibrium point (red crosses, denoted by the label P_{pq}), when the eccentricity is such that $e = 0.4875$ and the friction parameter is $\mu = 0$. The basins are shown in white (P_{00} attractor), cyan (P_{01} attractor), yellow (P_{10} attractor) and green (P_{11} attractor). All the initial conditions in any of these regions, are reached to the corresponding attractor. Due to the inital rotations expected are such that $\nu_c(t = 0) \sim \nu_s(t = 0)$, the attractors with differential rotation zero are more probable than the attractors with higher differential rotation.

If n/γ_c and n/γ_s continue to increase and the friction parameter is low (not necessarily zero), the core and the shell may tend to differents resonances, depending on the eccentricity. If the friction increases, the attractors with higher differential rotation, begin to disappear, until eventually, as from a certain value limit of μ only survive the attractors with differential rotation zero Fig. 4.10.

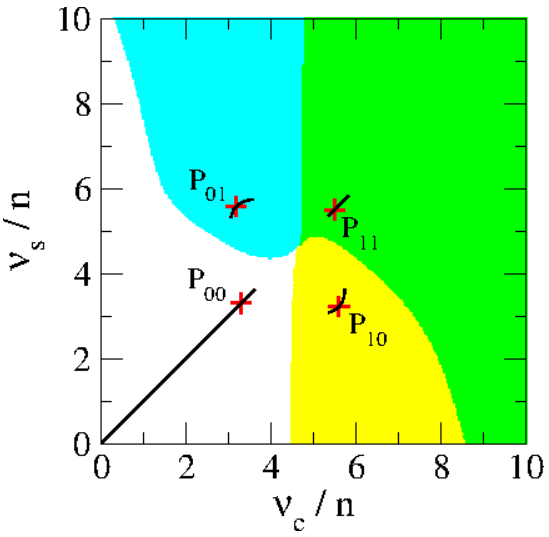

Figure 4.9: Basins of the attracting stationary rotations for $n/\gamma_c = n/\gamma_s = 1$, $e = 0.4875$ and $\mu = 0$. We plot the families of stationary rotations, corresponding to these relaxation factors and friction (solid black lines) and the four stationary solutions, corresponding this eccentricity (red crosses). The basins are shown in white (the core and the shell in super-synchronous rotation), cyan (the core in super-synchronous rotation and the shell in the 3/2 commensurability), yellow (the core in the 3/2 commensurability and the shell in the 3/2 commensurability) and green (the core and the shell in the 3/2 commensurability).

4.6 *Near-synchronous solution of the rotational equations*

Using the convention 1 = *core* and 2 = *shell*, the rotational system of the two-layer model, given by Eq. (4.35), can be written as

$$\begin{aligned} \dot{y}_1 &= -T^*_{11}\mathcal{T}_1 + \mathcal{K}_1 \sin 2\xi + \mathcal{F}_1(\gamma_2 y_2 - \gamma_1 y_1) \\ \dot{y}_2 &= T^*_{21}\mathcal{T}_1 - T^*_{22}\mathcal{T}_2 - \mathcal{K}_2 \sin 2\xi - \mathcal{F}_2(\gamma_2 y_2 - \gamma_1 y_1), \end{aligned} \tag{4.36}$$

where, the rotational variables are

$$y_1 = \frac{\nu_1}{\gamma_1} = \frac{2\Omega_1}{\gamma_1} - \frac{2n}{\gamma_1}; \qquad y_2 = \frac{\nu_2}{\gamma_2} = \frac{2\Omega_2}{\gamma_2} - \frac{2n}{\gamma_2}, \tag{4.37}$$

the tidal function $\mathcal{T}_i$ is

$$\mathcal{T}_i = \sum_{k,j\in\mathbb{Z}} E_{2,k}E_{2,k+j}\frac{(y_i + P_{ik})\cos(jnt) + \sin(jnt)}{1 + (y_i + P_{ik})^2}, \tag{4.38}$$

with $P_{ik} = kn/\gamma_i = kp_i$. The constants are

$$T^*_{ij} = \frac{2T_{ij}}{\gamma_i}; \qquad \mathcal{K}_i = \frac{2K}{\gamma_i C_i}; \qquad \mathcal{F}_i = \frac{\mu}{\gamma_i C_i}. \tag{4.39}$$

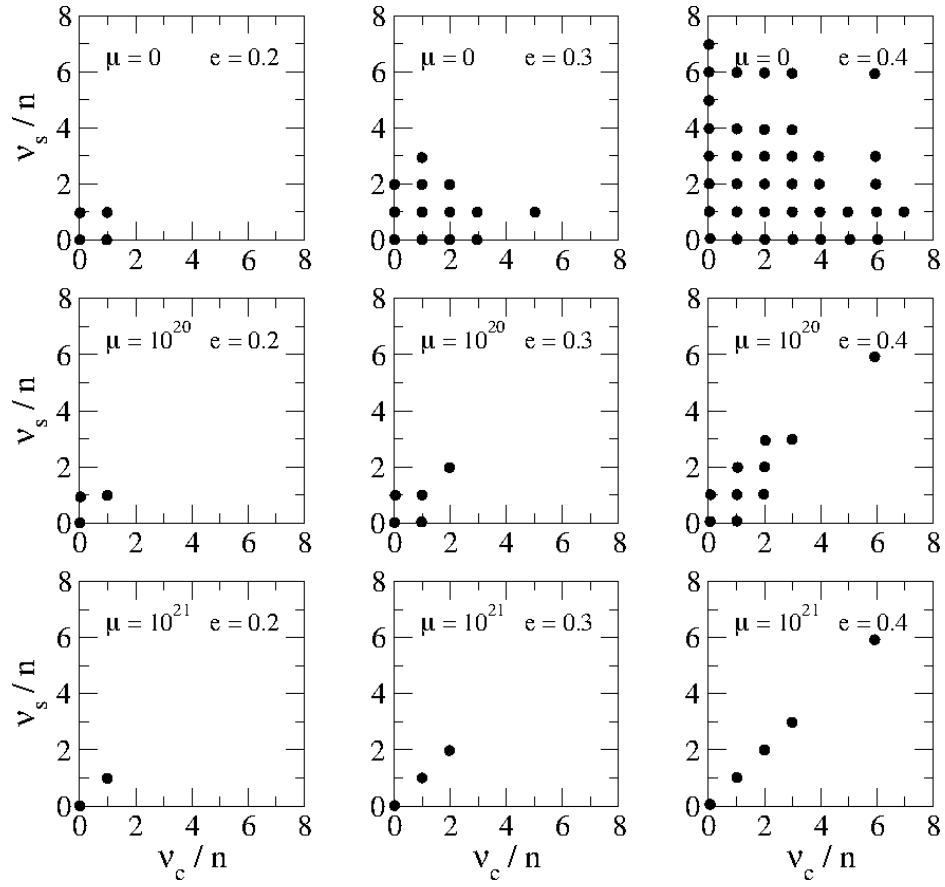

Figure 4.10: Attractors when the relaxation factors are equal and such that $n/\gamma_c = n/\gamma_s = 10$. The friction μ increases from *top* to *bottom* and the eccentricity e increases from *left* to *right*. The units of μ are kg km^{2}s^{-1}.

We assume that the solution, to second order in eccentricity, can be written as

$$\begin{aligned} y_1 &= b_{10}e^2 + c_{11}e\cos\ell + s_{11}e\sin\ell + c_{12}e^2\cos 2\ell + s_{12}e^2\sin 2\ell \\ y_2 &= b_{20}e^2 + c_{21}e\cos\ell + s_{21}e\sin\ell + c_{22}e^2\cos 2\ell + s_{22}e^2\sin 2\ell, \end{aligned} \tag{4.40}$$

where k_{i0}, c_{ij} and s_{ij} are undetermined coefficients. Introducing the solution (4.40) into the rotational system (4.36) and expanding to second order in eccentricity, by identification of the terms with same trigonometric argument, we can calculate these coefficients.

The derivatives of (4.40) are

$$\begin{aligned} \dot{y}_1 &= ns_{11}e\cos\ell - nc_{11}e\sin\ell + 2ns_{12}e^2\cos 2\ell - 2nc_{12}e^2\sin 2\ell \\ \dot{y}_2 &= ns_{21}e\cos\ell - nc_{21}e\sin\ell + 2ns_{22}e^2\cos 2\ell - 2nc_{22}e^2\sin 2\ell, \end{aligned} \tag{4.41}$$

To second order in eccentricity, the tidal function $\mathcal{T}_i$ is

$$\begin{aligned}\mathcal{T}_i \simeq\ & \frac{y_i}{1+y_i^2}+\frac{e^2}{4}\left(-\frac{20y_i}{1+y_i^2}+\frac{(y_i+p_i)}{1+(y_i+p_i)^2}+\frac{49(y_i-p_i)}{1+(y_i-p_i)^2}\right)+\\ &+\frac{e}{2}\left(\frac{6y_i}{1+y_i^2}-\frac{(y_i+p_i)}{1+(y_i+p_i)^2}+\frac{7(y_i-p_i)}{1+(y_i-p_i)^2}\right)\cos\ell+\\ &+\frac{e}{2}\left(-\frac{8}{1+y_i^2}+\frac{1}{1+(y_i+p_i)^2}+\frac{7}{1+(y_i-p_i)^2}\right)\sin\ell+\\ &+\frac{e^2}{4}\left(\frac{34y_i}{1+y_i^2}-\frac{7(y_i+p_i)}{1+(y_i+p_i)^2}-\frac{7(y_i-p_i)}{1+(y_i-p_i)^2}+\frac{34(y_i-2p_i)}{1+(y_i-2p_i)^2}\right)\cos 2\ell+\\ &+\frac{e^2}{4}\left(-\frac{34}{1+y_i^2}+\frac{7}{1+(y_i+p_i)^2}-\frac{7}{1+(y_i-p_i)^2}+\frac{34}{1+(y_i-2p_i)^2}\right)\sin 2\ell,\end{aligned} \tag{4.42}$$

and, using the proposed solution (4.40), can be approximated by

$$\begin{aligned}\mathcal{T}_i \simeq\ & \left(b_{i0}-\frac{12p_i}{1+p_i^2}+q_{i1}c_{i1}+q_{i2}s_{i1}\right)e^2+\left(c_{i1}-\frac{4p_i}{1+p_i^2}\right)e\cos\ell+\\ &+\left(s_{i1}-\frac{4p_i^2}{1+p_i^2}\right)e\sin\ell+\left(c_{i2}-\frac{17p_i}{1+4p_i^2}+q_{i1}c_{i1}-q_{i2}s_{i1}\right)e^2\cos 2\ell+\\ &+\left(s_{i2}-\frac{34p_i^2}{1+4p_i^2}+q_{i2}c_{i1}+q_{i1}s_{i1}\right)e^2\sin 2\ell,\end{aligned} \tag{4.43}$$

where the coefficients q_{i1} and q_{i2} are

$$q_{i1}=\frac{3(2+p_i^2+p_i^4)}{2(1+p_i^2)^2};\qquad q_{i2}=\frac{3p_i}{(1+p_i^2)^2}. \tag{4.44}$$

In the same way, the trigonometric function of the gravitational coupling can be approximated by

$$\begin{aligned}\sin 2\xi &= \sin\left[\tan^{-1}\left(\frac{y_2}{1+\lambda_2(1+y_2^2)}\right)-\tan^{-1}\left(\frac{y_1}{1+\lambda_1(1+y_1^2)}\right)\right]\\ &\simeq \left(\frac{b_{20}}{1+\lambda_2}-\frac{b_{10}}{1+\lambda_1}\right)e^2+\left(\frac{c_{21}}{1+\lambda_2}-\frac{c_{11}}{1+\lambda_1}\right)e\cos\ell+\\ &\quad+\left(\frac{s_{21}}{1+\lambda_2}-\frac{s_{11}}{1+\lambda_1}\right)e\sin\ell+\left(\frac{c_{22}}{1+\lambda_2}-\frac{c_{12}}{1+\lambda_1}\right)e^2\cos 2\ell+\\ &\quad+\left(\frac{s_{22}}{1+\lambda_2}-\frac{s_{12}}{1+\lambda_1}\right)e^2\sin 2\ell,\end{aligned} \tag{4.45}$$

and the amplitude of oscillation is

$$\begin{aligned}K &= \frac{32\pi^2G}{75}\mathcal{H}_1\mathcal{H}_2\bar{\epsilon}_\rho^2 d_1d_2R_1^5\sqrt{\lambda_1^2+\frac{1+2\lambda_1}{1+y_1^2}}\sqrt{\lambda_2^2+\frac{1+2\lambda_2}{1+y_2^2}}\\ &\simeq \frac{32\pi^2G}{75}(1+\lambda_1)(1+\lambda_2)\mathcal{H}_1\mathcal{H}_2\bar{\epsilon}_\rho^2 d_1d_2R_1^5.\end{aligned} \tag{4.46}$$

The friction term is

$$\begin{aligned}\gamma_2 y_2 - \gamma_1 y_1 \;\simeq\; & (\gamma_2 b_{20} - \gamma_1 b_{10})\, e^2 + (\gamma_2 c_{21} - \gamma_1 c_{11})\, e\cos\ell + (\gamma_2 s_{21} - \gamma_1 s_{11})\, e\sin\ell + \\ & + (\gamma_2 c_{22} - \gamma_1 c_{12})\, e^2\cos 2\ell + (\gamma_2 s_{22} - \gamma_1 s_{12})\, e^2\sin 2\ell. \end{aligned} \tag{4.47}$$

Replacing (4.41)-(4.47) into (4.36) and colecting the terms with same trigonometric argument, we can find three linear sub-systems for the undetermined b_{i0}, c_{ij} and s_{ij},which can be written in vectorial notation as

$$\begin{aligned} \mathsf{D}_1\Lambda_1 &= \mathsf{P}_1 \\ \mathsf{D}_2\Lambda_2 &= \mathsf{P}_2 - \mathsf{R}_2 \\ \mathsf{D}\Lambda_0 &= \mathsf{TP} - \mathsf{TR}, \end{aligned} \tag{4.48}$$

where

$$\Lambda_0 = \begin{bmatrix} b_{10} \\ b_{20} \end{bmatrix}; \qquad \Lambda_1 = \begin{bmatrix} c_{11} \\ s_{11} \\ c_{21} \\ s_{21} \end{bmatrix}; \qquad \Lambda_2 = \begin{bmatrix} c_{12} \\ s_{12} \\ c_{22} \\ s_{22} \end{bmatrix}, \tag{4.49}$$

are the undetermined coefficients vectors. The constants matrices are defined as

$$\mathsf{D} = \begin{bmatrix} a_{11} & a_{12} \\ a_{21} & a_{22} \end{bmatrix}; \qquad \mathsf{T} = \begin{bmatrix} T^*_{11} & -T^*_{12} \\ -T^*_{21} & T^*_{22} \end{bmatrix}; \qquad \mathsf{Q} = \begin{bmatrix} q_{11} & -q_{12} \\ -q_{21} & q_{22} \end{bmatrix}; \tag{4.50}$$

$$\mathsf{D}_1 = \begin{bmatrix} a_{11} & n & a_{12} & 0 \\ -n & a_{11} & 0 & a_{12} \\ a_{21} & 0 & a_{22} & n \\ 0 & a_{21} & -n & a_{22} \end{bmatrix}; \qquad \mathsf{D}_2 = \begin{bmatrix} a_{11} & 2n & a_{12} & 0 \\ -2n & a_{11} & 0 & a_{12} \\ a_{21} & 0 & a_{22} & 2n \\ 0 & a_{21} & -2n & a_{22} \end{bmatrix}, \tag{4.51}$$

where the constant a_{ij} is

$$a_{ij} = (-1)^{i+j}\left(T^*_{ij} + \frac{\mathcal{K}_i}{1+\lambda_j} + \mathcal{F}_i\gamma_j\right), \tag{4.52}$$

and the terms with $T^*_{12} = 0$, were added to make symmetrical the linear equations. Finally, the vectors P_i and R_i are

$$\mathsf{P} = 12\begin{bmatrix} p_1/(1+p_1^2) \\ p_2/(1+p_2^2) \end{bmatrix}; \qquad \mathsf{R} = \begin{bmatrix} q_{11}c_{11} + q_{12}s_{11} \\ q_{21}c_{21} + q_{22}s_{21} \end{bmatrix}; \tag{4.53}$$

$$\mathsf{P}_1 = 4\begin{bmatrix} T^*_{11}p_1/(1+p_1^2) - T^*_{12}p_2/(1+p_2^2) \\ T^*_{11}p_1^2/(1+p_1^2) - T^*_{12}p_2^2/(1+p_2^2) \\ -T^*_{21}p_1/(1+p_1^2) + T^*_{22}p_2/(1+p_2^2) \\ -T^*_{21}p_1^2/(1+p_1^2) + T^*_{22}p_2^2/(1+p_2^2) \end{bmatrix}; \tag{4.54}$$

$$\mathsf{P}_2 = 17\begin{bmatrix} T^*_{11}p_1/(1+4p_1^2) - T^*_{12}p_2/(1+4p_2^2) \\ T^*_{11}2p_1^2/(1+4p_1^2) - T^*_{12}2p_2^2/(1+4p_2^2) \\ -T^*_{21}p_1/(1+4p_1^2) + T^*_{22}p_2/(1+4p_2^2) \\ -T^*_{21}2p_1^2/(1+4p_1^2) + T^*_{22}2p_2^2/(1+4p_2^2) \end{bmatrix}; \tag{4.55}$$

$$\mathsf{R}_2 = \begin{bmatrix} T^*_{11}(q_{11}c_{11} - q_{12}s_{11}) - T^*_{12}(q_{21}c_{21} - q_{22}s_{21}) \\ T^*_{11}(q_{12}c_{11} + q_{11}s_{11}) - T^*_{12}(q_{22}c_{21} + q_{12}s_{11}) \\ -T^*_{21}(q_{11}c_{11} - q_{12}s_{11}) + T^*_{22}(q_{21}c_{21} - q_{22}s_{21}) \\ -T^*_{21}(q_{12}c_{11} + q_{11}s_{11}) + T^*_{22}(q_{22}c_{21} + q_{12}s_{11}) \end{bmatrix}. \tag{4.56}$$

The solution of these sub-systems are

$$\begin{aligned} \mathsf{\Lambda}_1 &= \mathsf{D}_1^{-1}\mathsf{P}_1 \\ \mathsf{\Lambda}_2 &= \mathsf{D}_2^{-1}\mathsf{P}_2 - \mathsf{D}_2^{-1}\mathsf{R}_2 \\ \mathsf{\Lambda}_0 &= \mathsf{D}^{-1}\mathsf{TP} - \mathsf{D}^{-1}\mathsf{TR}. \end{aligned} \tag{4.57}$$

Finally, the rotational solutions can be written as

$$\begin{aligned} \nu_1 &= B_{10} + B_{11}\sin(\ell + \phi_{11}) + B_{12}\sin(2\ell + \phi_{12}) \\ \nu_2 &= B_{20} + B_{21}\sin(\ell + \phi_{21}) + B_{22}\sin(2\ell + \phi_{22}), \end{aligned} \tag{4.58}$$

where the constants B_{ij} and the phases ϕ_{ij} are

$$\begin{aligned} B_{i0} &= \gamma_i b_{i0} e^2 \\ B_{ij} &= \gamma_i \sqrt{c_{ij}^2 + s_{ij}^2}\; e^j \\ \phi_{ij} &= \tan^{-1}(c_{ij}/s_{ij}). \end{aligned} \tag{4.59}$$

4.6.1 Tidal drift and the periodic terms

The tidal drift is the term B_{i0} of the solution (4.58). It is

$$\begin{aligned} \nu_1^{(stat)} &= B_{10} = \gamma_1 b_{10} e^2 + \mathcal{O}(e^3) \\ \nu_2^{(stat)} &= B_{20} = \gamma_2 b_{20} e^2 + \mathcal{O}(e^3). \end{aligned} \tag{4.60}$$

This result can be rewritte as

$$\begin{aligned}\nu_1^{(stat)} &= \frac{12n\kappa_{11}\gamma_1^2e^2}{\gamma_1^2+n^2}+\frac{12n\kappa_{12}\gamma_2^2e^2}{\gamma_2^2+n^2}- \\ &\quad -\kappa_{11}\gamma_1(q_{11}c_{11}+q_{12}s_{11})e^2-\kappa_{12}\gamma_2(q_{21}c_{21}+q_{22}s_{21})e^2+\mathcal{O}(e^3) \\ \nu_2^{(stat)} &= \frac{12n\kappa_{21}\gamma_1^2e^2}{\gamma_1^2+n^2}+\frac{12n\kappa_{22}\gamma_2^2e^2}{\gamma_2^2+n^2}- \\ &\quad -\kappa_{21}\gamma_1(q_{11}c_{11}+q_{12}s_{11})e^2-\kappa_{22}\gamma_2(q_{21}c_{21}+q_{22}s_{21})e^2+\mathcal{O}(e^3). \qquad (4.61)\end{aligned}$$

The coefficient κ_{ij} can be written as $\kappa_{ij}=f_{ij}/g$, where f_{ij} is

$$f_{ij}=\delta_{i,j}\frac{\mathcal{T}C_1C_2}{C}\frac{\mathcal{H}_1\mathcal{H}_2R_2^5}{R_2^5-R_1^5}+\frac{\mathcal{D}_j\gamma_i}{\gamma_j}\frac{(1+\lambda_i)K}{(1+\lambda_1)(1+\lambda_2)}+\mathcal{D}_j\gamma_i\frac{\mu}{2}, \qquad (4.62)$$

$\delta_{i,j}$ is the Kronecker delta ($\delta_{1,1}=\delta_{2,2}=1$ and $\delta_{1,2}=\delta_{2,1}=0$) and the constant g is

$$g=f_{11}+f_{22}-\frac{\mathcal{T}C_1C_2}{C}\frac{\mathcal{H}_1\mathcal{H}_2R_2^5}{R_2^5-R_2^5}. \qquad (4.63)$$

The two first terms of each Eq. (4.61)

$$N_i = \frac{12n\kappa_{i1}\gamma_1^2e^2}{\gamma_1^2+n^2}+\frac{12n\kappa_{i2}\gamma_2^2e^2}{\gamma_2^2+n^2} \qquad (4.64)$$

come from the non-periodic terms with $|j|=0$, while the terms that involve c_{i1} and s_{i1}.

$$P_i = -\kappa_{i1}\gamma_1(q_{11}c_{11}+q_{12}s_{11})e^2-\kappa_{i2}\gamma_2(q_{21}c_{21}+q_{22}s_{21})e^2, \qquad (4.65)$$

come from the periodic terms with $|j|=1$. The harmonic terms with $|j|=2$, do not contribute to the stationary rotation at order e^2.

It is worth emphasizing that in the absence of friction and gravitational coupling, that is, $K=\mu=0$, the coefficient $\kappa_{ij}=\delta_{i,j}$. Then, the non-periodic excess of rotation of the i-th layer has the same expression that the excess rotation in the case of a homogeneous body, with γ_i instead of γ

$$\nu_i^{(stat)}=\frac{12n\gamma_i^2e^2}{\gamma_i^2+n^2}+\mathcal{O}(e^4). \qquad (4.66)$$

In the case $n/\gamma_1\gg 1$, $n/\gamma_2\gg 1$, an elementary calculation shows that each coefficient κ_{ij} becomes independent of the friction parameter μ, depending only on the internal structure and on the relaxation factors γ_1 and γ_2, with f_{ij} tending to

$$f_{ij}=\delta_{i,j}\frac{\mathcal{T}C_1C_2}{C}\frac{\mathcal{H}_1\mathcal{H}_2R_2^5}{R_2^5-R_1^5}+\frac{\mathcal{D}_j\gamma_i}{\gamma_j}\frac{(1+\lambda_i)K}{(1+\lambda_1)(1+\lambda_2)}. \qquad (4.67)$$

In the case $n/\gamma_1 \ll 1$, $n/\gamma_2 \ll 1$, each coefficient κ_{ij} becomes independent of $\mathcal{T}$, K and μ, depending only on the internal structure and on the relaxation factors γ_1 and γ_2, tending to

$$\kappa_{ij} = \frac{\mathcal{D}_j \gamma_i}{\mathcal{D}_1 \gamma_1 + \mathcal{D}_2 \gamma_2}, \tag{4.68}$$

and the stationary solution tends to synchronous rotation.

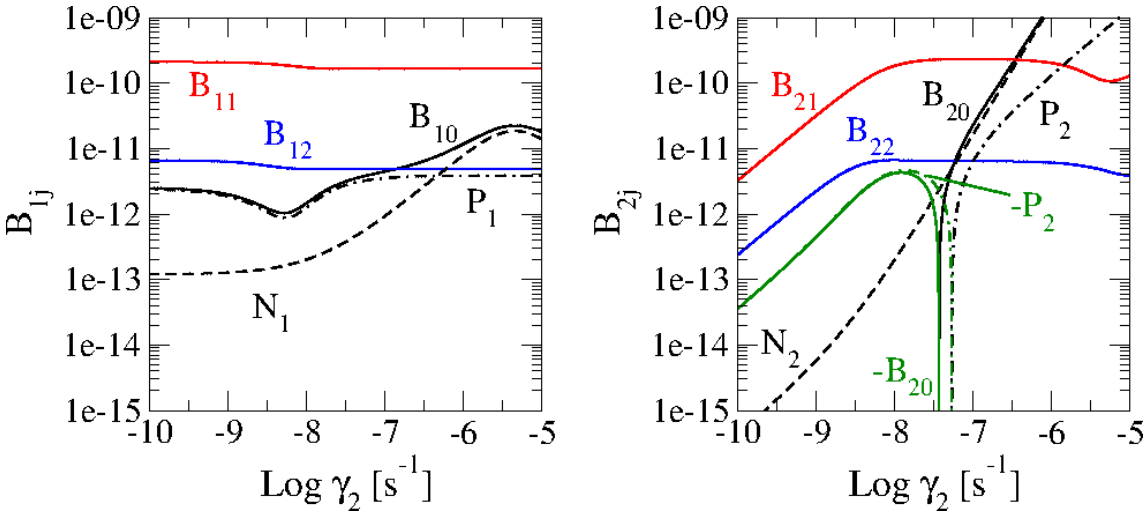

Figure 4.11: The tidal drift B_{i0} (black solid lines), the contribution of the non-periodic terms N_i (black dashed lines) and the periodic terms P_i (black dotted lines) to the tidal drift, and the amplitudes of oscillation of the periodic terms B_{i1} (red solid lines) and B_{i2} (blue solid lines), of the Titan's core and shell in function of the shell relaxation factor γ_2. The core relaxation factor is $\gamma_1 = 10^{-8}$ s^{-1} and the ocean's viscosity and thickness are $\eta_o = 10^{-3}$ Pa s and $h = 178$ km, respectively (see Tables 5.1-5.4). *Left*: The parameter of the core. *Right*: The parameters of the shell. We also plot the negative values of B_{20} (green solid line) and P_2 (green dotted line).

The periodic terms have amplitudes B_{i1} and B_{i2}, given by the Eq. (4.59). The coefficients c_{ij} and s_{ij} gives rise to intricate analytical expressions, but are easy to calculate numerically. Fig. 4.11 shows one example for the Titan's core and the shell constants B_{1j} and B_{2j}, respectively, in function of the shell relaxation factor γ_2 (see Table 5.1-5.4). We use that the core relaxation factor is $\gamma_1 = 10^{-8}$ s^{-1}, and fix the ocean's viscosity and thickness values to $\eta_o = 10^{-3}$ Pa s and $h = 178$ km, respectively. We also plot the non-periodic N_i and periodic P_i terms, separately, and the total tidal drift $B_{i0} = N_i + P_i$. We can observe that if $\gamma_2 \gtrsim 10^{7.5}$ s^{-1}, the shell oscillates around the super-synchronous rotation. When $\gamma_2 \lesssim 10^{7.5}$ s^{-1}, the tidal drift B_{20} becomes negative and tends to zero, that is, the shell oscillates around the synchronous rotation, with a period of oscillation equal to the orbital period. The negative sign of the tidal drift B_{20}, is due to the contribution of the

periodic terms P_2, which becomes negative and $|P_2| \gg N_2$. Finally, if $\gamma_2 \lesssim 10^8$ s^{-1}, the amplitude of the shell rotation decreases, tending to zero when γ_2 decreases. On the other hand, the core oscillates around the synchronous rotation, with a period of oscillation equal to the orbital period, independently of the shell relaxation factor.

This behavior is confirmed by the numerical simulations of non-approximate system. In Fig. 4.12, we show the comparison of the Titan's shell rotation in the complete non-linear system given by Eq. (4.36) and in the approximate analytical solution given by Eq. (4.58), for some values of the core's relaxation factor γ_c and ocean thickness h. The dashed red lines show the maximum and minimum values of $\Omega_s - n$ given by the approximate solution, taking into account only the first harmonic ($|j| \leq 1$), while the solid black lines show the maximum and minimum values of $\Omega_s - n$ when the complete non-linear system is integrated (using $|j| \leq 7$). The approximate solution is in excellent agreement with numerical integration of the equations.

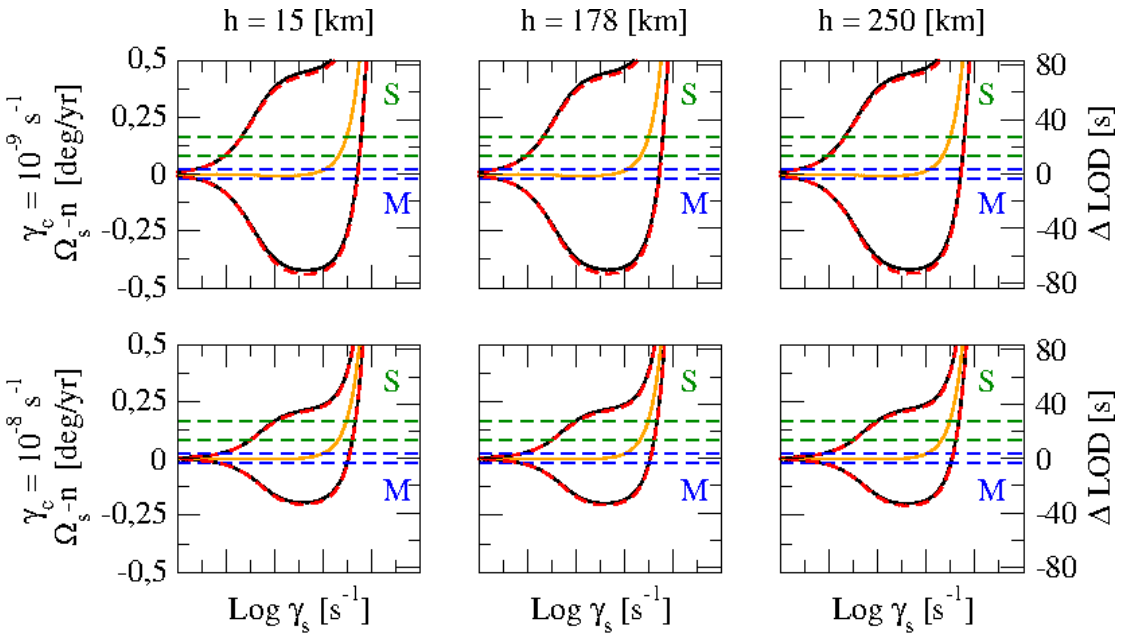

Figure 4.12: Comparison of the amplitudes of the shell rotation and corresponding length-of-day variation of Titan, between the numerical integration of the system Eq. (4.35) (solid black lines) and the analytical solution $\nu_i \simeq B_{i0} + B_{i1} \sin(\ell + \phi_{i1})$ (dashed red lines). We also plot the stationary solution given by B_{i0} (solid orange line). The core relaxation factor γ_c increases from *top* to *bottom* and the ocean thickness h increases from *left* to *right*. The ocean viscosity is $\eta_o = 10^{-3}$ Pa s. The horizontal dashed lines show the confidence interval of the observed values, as determined by Meriggiola (2012) (blue) and by Stiles et al. (2010) (green).

Chapter 5

Application to Titan's rotation

5.1 Introduction

Before the Cassini-Huygens mission, the spin rate of Titan was assumed as a synchronous rotation equal to the mean motion $n = 22.5769768$ deg/day. The first results of this mission, showed a super-synchronous rotation $\Omega_s = 22.5780$ deg/day (Lorenz et al., 2008), or, equivalently, an excess of rotation $\Omega_s - n = 0.38$ deg/yr. Using the Cassini spacecraft's radar images, the super-synchronous rotation value was corrected later by Stiles et al. (2010), to $\Omega_s = 22.57731$ deg/day, or, equivalently, an excess of rotation $\Omega_s - n = 0.122$ deg/yr. These values are far from the synchronous rotation expected to one rocky satellite. These values of the excess of rotation were interpreted as an evidence of a subsurface ocean. Tokano and Neubauer (2005) showed that the exchange of a certain amount of angular momentum between the surface and the atmosphere may be important, and the presence of an internal ocean (as was modeled by Tobie et al., 2005; Sohl et al., 2014) may decouple rotationally the crust from the interior (Karatekin et al., 2008). The rotation of the crust has been studied by Van Hoolst et al. (2009) using the static tide and internal effects, as gravitational coupling and pressure torques. They found that the crust rotation is influenced, mainly by the atmosphere and the Saturn torque, and claim that the viscous crust deformation and the non-hydrostatic effects, could play an important role in the amplitude of the crust oscillation. Recently, Meriggiola et al. (2016) estimated Titan's spin rate to $\Omega_s = 22.57693$ deg/day, with a residual non-synchronus rotation of $\Omega_s - n = \pm 0.02$ deg/yr compatible with a synchronous rotation, and in agreement with Goldreich and Mitchell (2010) and Van Hoolst et al. (2013). These results were interpreted as a differentiated Titan with a relatively thin crust of 10-50 km of thickness. In this

chapter we apply the non-homogeneous creep tide theory to Titan, adding the torque due to the exchange of angular momentum between the surface and the atmosphere.

5.2 The model

Titan's interior was largely discussed in many papers (e.g. Tobie et al., 2005; Castillo-Rogez and Lunine, 2010; McKinnon and Bland, 2011; Fortes, 2012). The existing general data of the Titan-Saturn system is given in Table 5.1. In this section, we assume the interior model given by Sohl et al. (2014) (hereafter *reference model*, see Fig. 5.1), and is given in Table 5.2. In this model, Titan is formed by four homogeneous layers: i) an inner hydrated silicate core (inner core); ii) a layer of high-pressure ice (outer core); iii) a subsurface water-ammonia ocean and iv) a thin ice crust. For the sake of simplicity, we construct one two-layer equivalent model, where the *core* is a layer formed by the inner core and the high-pressure ice layer, and the *shell* is a layer formed by the subsurface ocean and the ice crust, but keeping some features of the four-layer model (e.g. axial moments of inertia and Clairaut numbers). In this way, we can use the rotational equations (4.35), retaining the main features of the realistic reference model. This simplified model is given in Table 5.3, and some calculated parameters of each layer are listed in Table 5.4.

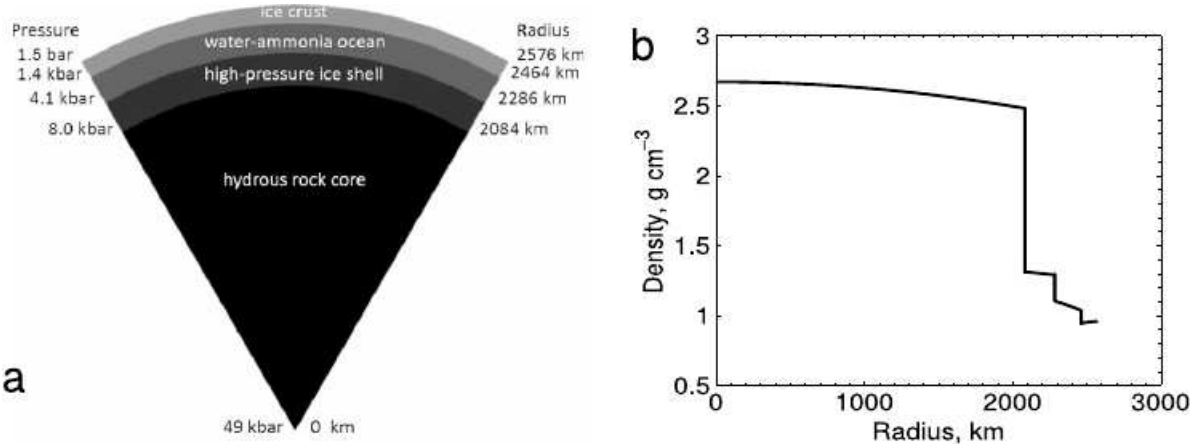

Figure 5.1: Titan's interior for the reference model. *Left*: Scheme of Titan's interior. *Right*: Titan's density profile. Figure extracted of Sohl et al. (2014).

In order to estimate the relative height of the elastic tide λ_s, we assume that the difference between the observed surface flattening ϵ_s' with the tidal flattening $\epsilon_s = \mathcal{H}_s \bar{\epsilon}_J E_{2,0} \cos\sigma_{s0}$ $\approx \mathcal{H}_s \bar{\epsilon}_J \cos\sigma_{s0}$ (calculated) is due to the existence of an elastic component, with flattening

$\epsilon_s^{el} = \lambda_s \mathcal{H}_s \bar{\epsilon}_J$. If we use Eq. (4.23), and assume that near to the synchronous rotation $\cos^2 \sigma_{s0} \approx 1$, we obtain

$$\lambda_s \approx \frac{\epsilon_s'}{\mathcal{H}_s \bar{\epsilon}_J} - 1. \tag{5.1}$$

For the relative heights of the elastic tide λ_c, we assume $\lambda_c \approx \lambda_s \overset{\text{def}}{=} \lambda$.

Mass (10^{22}kg)[1]	m_T	13.45
Eccentricity[2]	e	0.028
Semi-major axis (AU)[3]	a	0.00816825
Mean motion (deg/day)[1]	n	22.5769768
(id.) (10^{-6} s^{-1})		4.560678013
Orbital period (day)[1]	$2\pi/n$	15.9454476
Differential Rotation (deg/yr)	$\Omega_s - n$	0.122 ± 0.040 [4]
		$0.00^{+0.02}_{-0.02}$ [5]
Titan's ellipsoid semi-major axes (km)[6]	a	2575.152 ± 0.048
	b	2574.715 ± 0.048
	c	2574.406 ± 0.044
Titan's mean equatorial radius (km)[6]	R_s	2574.933 ± 0.033
Titan's equatorial prolateness (10^{-4})[6]	ϵ_s'	1.70 ± 0.26
Saturn's mass (10^{26} kg)[7]	M	5.68326
Saturn's mean-motion (10^{-9} s^{-1})[7]	$n_\odot$	6.713428
Titan's tidal parameter (10^{-15} s^{-2})†	$\mathcal{T}$	4.63

[1]Seidelmann et al. (2007); [2] Iess et al. (2012); [3]TASS 1.8‡ (Jan.1,2000); [4]Stiles et al. (2010); [5]Meriggiola et al. (2012; 2016); [6]Mitri et al. (2014); [7]Jacobson et al. (2006); † calculated parameter; ‡ See Vienne and Duriez, (1995).

Table 5.1 - Basic data of Titan.

Layer	Outer radius (km)	Density (g/cm^3)	Viscosity (Pa s)†
Ice I shell	2575	0.951	$10^{14} - 10^{16}$
Ocean	2464	1.07	$10^{-3} - 10^{9}$ §
High-pressure ice	2286	1.30	$10^{15} - 10^{20}$
Rock and iron core	2084	2.55	10^{20}

† Mitri et al., 2014; § adopted values.

Table 5.2 - Titan's four-layer reference model.

Layer	Outer radius (km)	Density (g/cm^3)	Mass (10^{22}kg)
Shell (crust + ocean)	2575	1.02	2.19
Core (rock + HP ice mantle)	2286	2.25	11.26

Table 5.3 - Titan's two-layer equivalent model.

5.3 Atmospheric influence on Titan's rotation

The seasonal variation in the mean and zonal wind speed and direction in Titan's lower troposphere causes the exchange of a substantial amount of angular momentum between the surface and the atmosphere. The variation calculated from the observed zonal wind speeds shows that the atmosphere angular momentum undergoes a periodic oscillation between 3×10^{18} and $3 \times 10^{19}\,\mathrm{kg\,km^2 s^{-1}}$ (Tokano and Neubauer, 2005, hereafter TN05) with a period equal to half Saturn's orbital period and maxima at Titan's equinoxes (when the Sun is in the satellite's equatorial plane).

The angular momentum of the atmosphere may be written as $L_{\rm atm} = L_0 + L_1 \cos 2\alpha_\odot$ where $L_0 = 1.65{\times}10^{19}$ kg km^2 s^{-1}, $L_1 = 1.35{\times}10^{19}$ kg km^2 s^{-1} and $\alpha_\odot$ is the Saturnian right ascension of the Sun. The variation of the angular momentum is $\dot{L}_{\rm atm} = -2L_1 n_\odot \sin 2\alpha_\odot$. If we neglect external effects (as atmospheric tides), this variation may be compensated by an equal variation in the shell's angular momentum: $\delta\dot{L}_s = -\dot{L}_{\rm atm}$, which corresponds to an additional shell acceleration

$$\delta\dot{\Omega}_s = \frac{2L_1 n_\odot}{C_k} \sin 2\alpha_\odot = A_\odot \sin 2\alpha_\odot. \tag{5.2}$$

We must emphasize that we have considered in these calculations the moment of inertia of the ice crust C_k, since the winds are acting on the crust and do not have direct action on the liquid part of the shell.

In a more recent work, Richard et al. (2014) (hereafter R14) re-calculate the amplitude of the variation of the angular momentum with the Titan IPSL GCM (Institut Pierre-Simon Laplace General Circulation models) (Lebonnois et al., 2012). They obtain $L_1 = 8.20{\times}10^{17}$ kg km^2 s^{-1}, which is ~ 16.5 times less than the TN05 value.

		Core	Shell
Clairaut number	$\mathcal{H}_i$	0.772	0.806
Parameter of Eq. (3.46)	$\mathcal{Q}_i$	0.308	0.484
Axial moment of inertia (10^{29}kg km^2)	C_i	2.183	0.866
Equatorial flattening (tidal) (10^{-4})	ϵ_i	1.15	1.20
Relative height of the elastic tide	λ_i	0.42	0.42
Gravitational coupling constant (10^{-15}s^{-2})	K/C_i	2.65	6.69
Friction parameter (10^{-17}s^{-1})§	μ/C_i	0.59	1.48
Atmospheric parameter (10^{-18}s^{-2})†	$2L_1 n_\odot/C_k$	-	5.08
	$2L_1 n_\odot/C_s$	-	0.31

§ Assuming $\eta_o = 10^{-3}$ Pa s; † $L_1 = 1.35 \times 10^{19}$ kg km^2 s^{-1} (Tokano and Neubauer, 2015).

Table 5.4 - Titan's calculated parameters in the two-layer model.

5.4 The results

We fix the outer radius of the inner core R_{ic} and the outer radius of the high-pressure ice layer R_{oc}, the densities of the inner and outer cores d_{ic} and d_{oc} and the density of the crust d_k, to the reference model values in Table 5.2. The density of the inner core is calculated so as to verify the value of Titan's mass $m_T = 13.45 \times 10^{22}$ kg. Fig. 5.2 shows

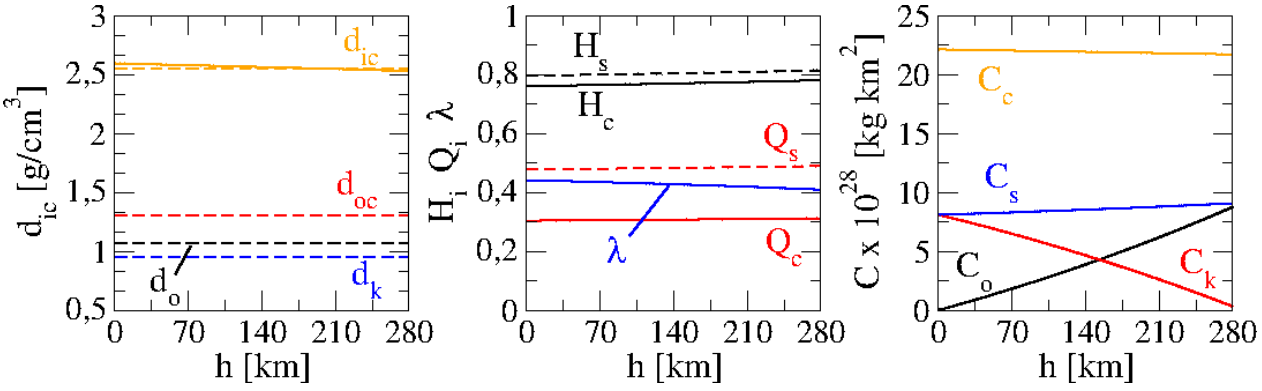

Figure 5.2: Dependence of some parameters on the thickness of the ocean h. *Left*: Density of the inner core d_{ic} (solid orange) and the densities of the reference model (dashed lines). *Middle*: Clairaut parameters $\mathcal{H}_i$ (black), the coefficients $\mathcal{D}_i$ (red), and the maximum relative height of the elastic tide λ (blue). *Right*: The axial moments of inertia of the ocean C_o (black), the crust C_k (red), the shell $C_s = C_o + C_k$ (blue) and the core $C_c = C_{ic} + C_{oc}$ (orange).

the weak dependence of the parameters on the thickness of the ocean h: the density of the inner core d_{ic} (solid orange line) and densities of the reference model (*left* panel); the

parameters $\mathcal{D}_c$, $\mathcal{D}_s$ and the Clairaut numbers $\mathcal{H}_c$, $\mathcal{H}_s$ (*middle* panel); the axial moments of inertia C_c and C_s (*right* panel).

The main consequece of the weak dependence of these parameters with the thickness of the subsurface ocean, is that both the effect of the tide and the gravitational coupling parameter also depend weakly on h. The strength of the acceleration of the rotation, due to the tide, is given by the product $T_{ij}\mathcal{T}_k$ (see Eqs. (4.3) and (4.2)). While the parameter T_{ij} only depends on the internal structure of Titan, the function $\mathcal{T}_k$ do not depend on h. The *left* panel of Fig. 5.3 shows T_{ij} and the gravitational coupling amplitude $K_i = K/C_i$, as function of h. We also observe taht the thickness of the ocean does not have any relevant role. Then, for the tide and the gravitational coupling, the rotational evolution is driven by the ratios n/γ_c, n/γ_s and the orbital eccentricity e.

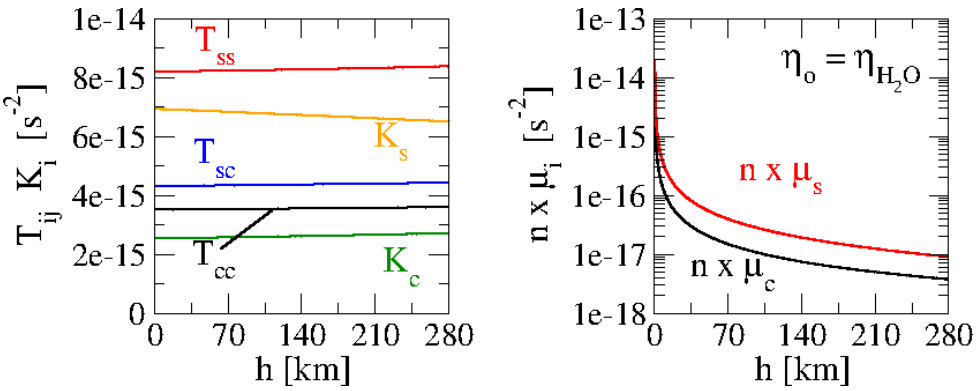

Figure 5.3: Dependence of some parameters with the thickness of the ocean h. *Left*: Tidal parameter T_{ij} and gravitational coupling constant $K_i = K/C_i$. *Right*: The coefficient $n \times \mu_i$, where $\mu_i = \mu/C_i$, for a typical ocean viscosity $\eta_o = \eta_{H_2O} \approx 10^{-3}$ Pa s.

The *right* panel of Fig. 5.3 shows the quantity $n\mu_i = n\mu/C_i$ as function of the thickness h, when we consider the realistic ocean viscosity $\eta_o = \eta_{H_2O} \approx 10^{-3}$ Pa s. The rotational acceleration of each layer, due to the friction, is $\mu_i(\Omega_s - \Omega_c)$. In super-synchronous rotation, the excess of rotation of each layer is of order ne^2, then

$$\mu_i(\Omega_s - \Omega_c) \ll n\mu_i \ll T_{ij}, K_i.$$

Therefore, in Titan's case, the friction term is negligible compared with the tide and the gravitational coupling terms, independently of the h value.

Eqs. (4.35) and (5.2), allow us to calculate the velocities of rotation of the shell and the core of Titan for a wide range of relaxation factors γ_c and γ_s, when different effects

are considered. For that sake, we have to adopt the values of the involved parameters. We use four different values for the viscosity of the subsurface ocean: a realistic value $\eta_o = \eta_{H_2O} = 10^{-3}$ Pa s, a moderate value $\eta_o = 10^0$ Pa s and two very high values $\eta_o = 10^6$ Pa s and $\eta_o = 10^9$ Pa s. For the thickness of the ocean, we use the values $h = 15$, 178 and 250 km, and for the variation of the atmospheric angular momentum, we use the values given by Tokano and Neubauer (2005) and Richard et al. (2014). When we integrate the rotational equations, assuming the values of relaxation factor typical for rock bodies ($\gamma_i < n$), the results show that the excess of rotation of the shell is damped quickly and the final state is an oscillation around the synchronous motion with a period of ~ 15 days, equal to the orbital period (Fig. 5.4). The amplitude of this oscillation depends on the relaxation factors and the ocean thickness, mainly.

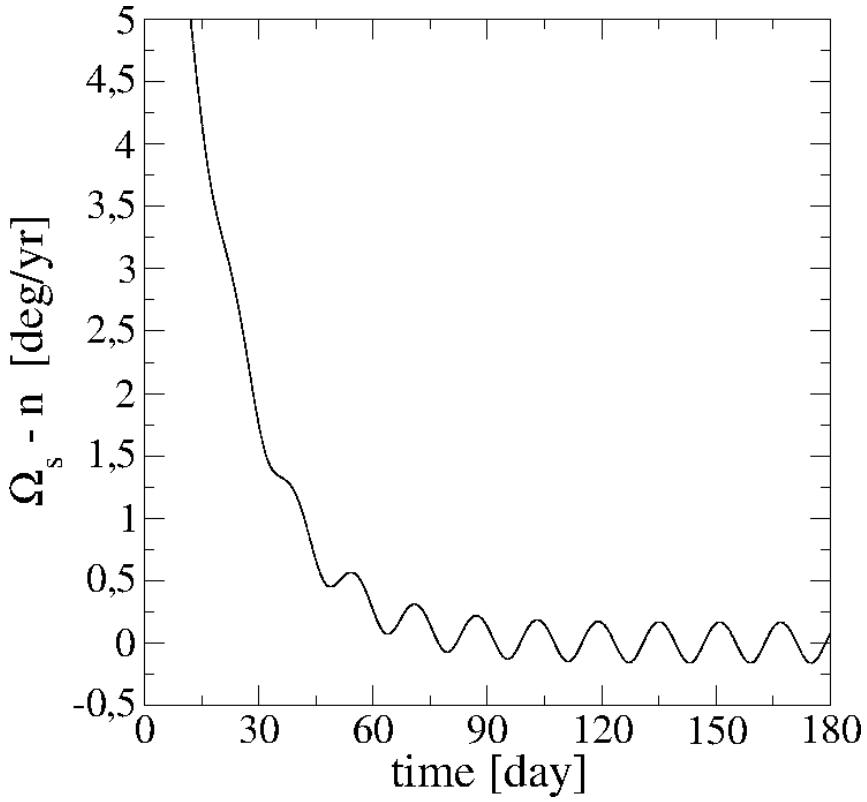

Figure 5.4: Time evolution of $\Omega_s - n$, when $\gamma_c = \gamma_s = 10^{-8}$ s^{-1}, $\eta = 10^{-3}$ Pa s and $h = 178$ km.

These results are compatible with the analytical approximate solution:

$$\nu_i \simeq B_{i0} + B_{i1} \sin(\ell + \phi_{i1}) + B_{i2} \sin(2\ell + \phi_{i1}), \tag{5.3}$$

where the constants B_{ij} and the phases ϕ_{ij} are given by Eqs. (4.59) (see Chap. 4.6.1). Fig.

5.5 shows one example for the Titan's core and shell constants B_{cj} and B_{sj}, in function of the shell relaxation factor, when the core relaxation factor is $\gamma_c = 10^{-8}$ s^{-1} and the ocean's viscosity and thickness are $\eta_o = 10^{-3}$ Pa s and $h = 178$ km, respectively.

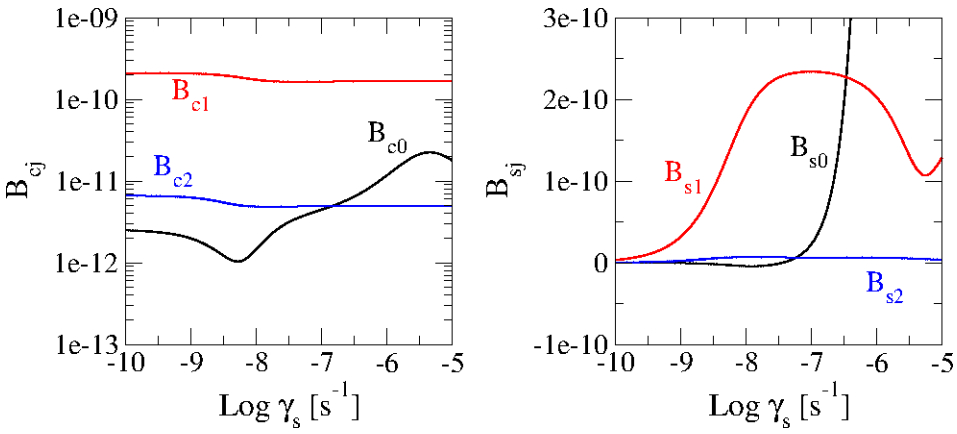

Figure 5.5: Tidal drift and amplitudes of oscillation of the periodic terms of the Titan's core and shell in function of the shell relaxation factor γ_s. The core relaxation factor is $\gamma_c = 10^{-8}$ s^{-1} and the ocean's viscosity and thickness are $\eta_o = 10^{-3}$ Pa s and $h = 178$ km, respectively. *Left*: Core's parameters B_{c0}, B_{c1} and B_{c2}. *Right*: Shell's parameters B_{s0}, B_{s1} and B_{s2}.

In Fig. 5.6, fixing $\eta_o = 10^{-3}$ Pa s and $L_1 = 1.35 \times 10^{19}$ kg km^2 s^{-1} (TN05), we plot the resulting the maximum and minimum of the final oscillation of the shell rotation $\Omega_s - n$, or, equivalently, the length-of-day variation

$$\Delta \text{ LOD} = \frac{2\pi}{n} - \frac{2\pi}{\Omega_s}, \tag{5.4}$$

in function of γ_s, for two dynamical models: i) tidal forces, gravitational coupling and linear friction (solid black lines); and ii) tidal forces, gravitational coupling, linear friction and the atmospheric influence (dashed red lines). The horizontal lines show the intervals corresponding to 1σ uncertainties of the observed values: the blue dashed lines, labelled `M`, correspond to Meriggiola (2012) and Meriggiola et al. (2016) and green dashed lines, labelled `S`, correspond to the Stiles et al. (2010). The core relaxation factor γ_c increases from $\gamma_c = 10^{-9}$ s^{-1} (*top* panels) to 10^{-6} s^{-1} (*bottom* panels) and the ocean thickness h increases from 15 km (*left* panels) to 250 km (*right* panels).

Figure 5.6 shows that if $\gamma_s < 10^{-7}$ s^{-1}, the shell's rotation oscillate around the synchronous motion and the amplitude of oscillation depends on the relaxation factors and the ocean thickness. The average rotation (central orange line) is synchronous; it only becomes

supersynchronous for relaxation values larger than $\sim 10^{-7}$ s^{-1}. We also observe that when $\gamma_s < 10^{-8}$ s^{-1}, independently of the values of γ_c and h, the amplitude of oscillation of the shell tends to zero when the relaxation factor γ_s decreases. Particularly, if $\gamma_s < 10^{-9}$ s^{-1}, the amplitude of the oscillation of the excess of rotation reproduces the dispersion of the Ω_s value of ± 0.02 deg/yr around the synchronous value, observed as reported by Meriggiola (2012) and Merigiolla et al. (2016). The results are not consistent with the previous drift reported by Stiles et al. (2008; 2010). We note that for larger values of the relaxation, e.g. 10^{-8} s^{-1}, the large short period oscillation due to the tide would be much larger than the reported values and would introduce big dispersion in the measurements, much larger than the reported dispersion due to the difficulties in the precise localization of Titan's features. On the other hand, the effect of the atmospheric torque is completely negligible in the range of possible γ_s that reproduces the observed values of the shell rotation, even for the high value of L_1 given Tokano and Neubauer (2005). When we consider the amplitude of the variation of the angular momentum given by Richard et al. (2014), the contribution to the rotation variations tends to zero.

The results shown in Fig. 5.6, remain virtually unchanged when the ocean viscosity is increased up to a value of $\eta_o = 10^6$ Pa s. But, if the ocean viscosity is increased to $\eta_o = 10^9$ Pa s, the transfer of angular momentum between the shell and the core induces in the shell accelerations of the same order as the rotational acceleration due to the others forces. As a consequence, the shell rotation will follow closely the core rotation (which is shown in Fig. 5.7). This high value of η_o can be interpreted as the ocean thickness tending to zero. In this case, to obtain the dispersion of Titan's observed rotation as determined by Meriggiola et al. (2016) we should have a value of γ_s yet smaller than the values obtained in the previous cases, where a low viscosity ocean was assumed between the shell and the core. It is worth noting yet that, in this case, the observed dispersion could also be obtained taking for γ_c an extremely low value (10^{-9} s^{-1}) and for γ_s a much larger and unexpected value (10^{-5} s^{-1}).

It is important to note that, in any case, the rotational constraint does not allow us to estimate the value of the core relaxation factor γ_c. For realistic values of the ocean viscosity ($\eta_o = 10^{-3} - 10^6$ Pa s), the shell relaxation factor may be such that $\gamma_s \lesssim 10^{-9}$ s^{-1}. The actual value will depend on the values of h and γ_c and on the interpretation of the

dispersion determined by Meriggiola, which may include the forced short-period oscillation of Ω_s. Equivalently, using Eq. (3.2), the shell viscosity may be such that $\eta_s \gtrsim 10^{18}$ Pa s. These values remain without significant changes if $\eta_o < 10^9$ Pa s. For the case in which a subsurface ocean does not exist, the shell relaxation factor may be such that $\gamma_s \lesssim 10^{-10}$ s^{-1}, one order less that when an ocean is considered. Equivalently, the shell viscosity may be such that $\eta_s \gtrsim 10^{19}$ Pa s. It is worth noting that in this case, when $\gamma_s \lesssim 10^{-7}$ s^{-1}, the rotation of the core remains stuck to the rotation of the shell even when γ_c is larger, notwithstanding the larger moment of inertia of the core (Fig. 5.8).

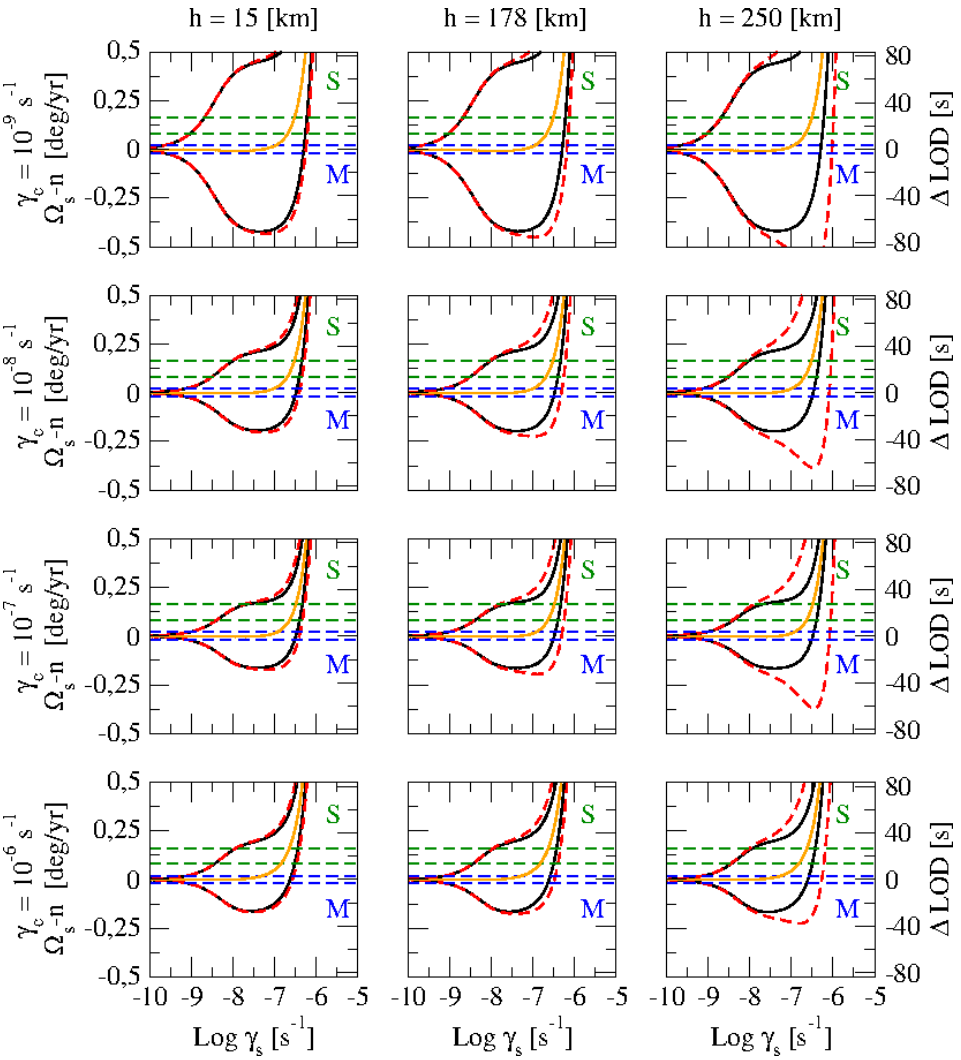

Figure 5.6: Shell rotation and corresponding length-of-day variation of Titan in function of the relaxation factors, when $\eta_o = 10^{-3}$ Pa s and $L_1 = 1.35 \times 10^{19}$ kg km^2 s^{-1}. The core relaxation factor γ_c increases from *top* to *bottom* and the ocean thickness h increases from *left* to *right*. We consider two dynamical models: The pair of solid black lines, indicate the maximum and minimum of the shell rotation when the tidal forces, the gravitational coupling and the linear friction are taken in account, and the pair of dashed red lines, indicate the maximum and minimum of the shell rotation when the angular momentum exchange with the atmosphere is added. The orange solid line, indicates the analytical stationary rotation B_{s0}. The horizontal dashed lines show the confidence interval of the observed values, as determined by Meriggiola (2012) (blue) and by Stiles et al. (2010) (green).

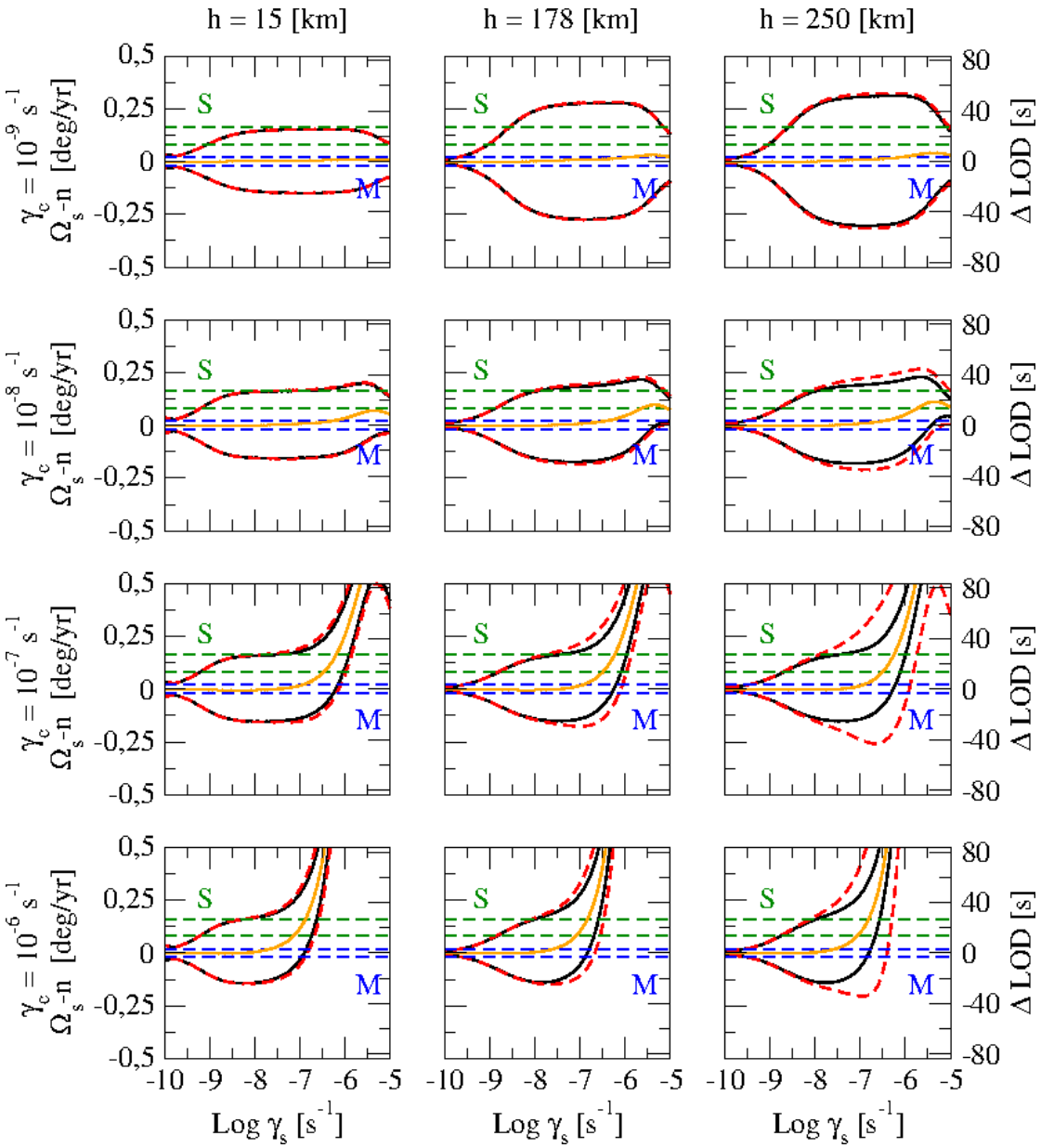

Figure 5.7: Same as Fig. 5.6 for $\eta = 10^9$ Pa s.

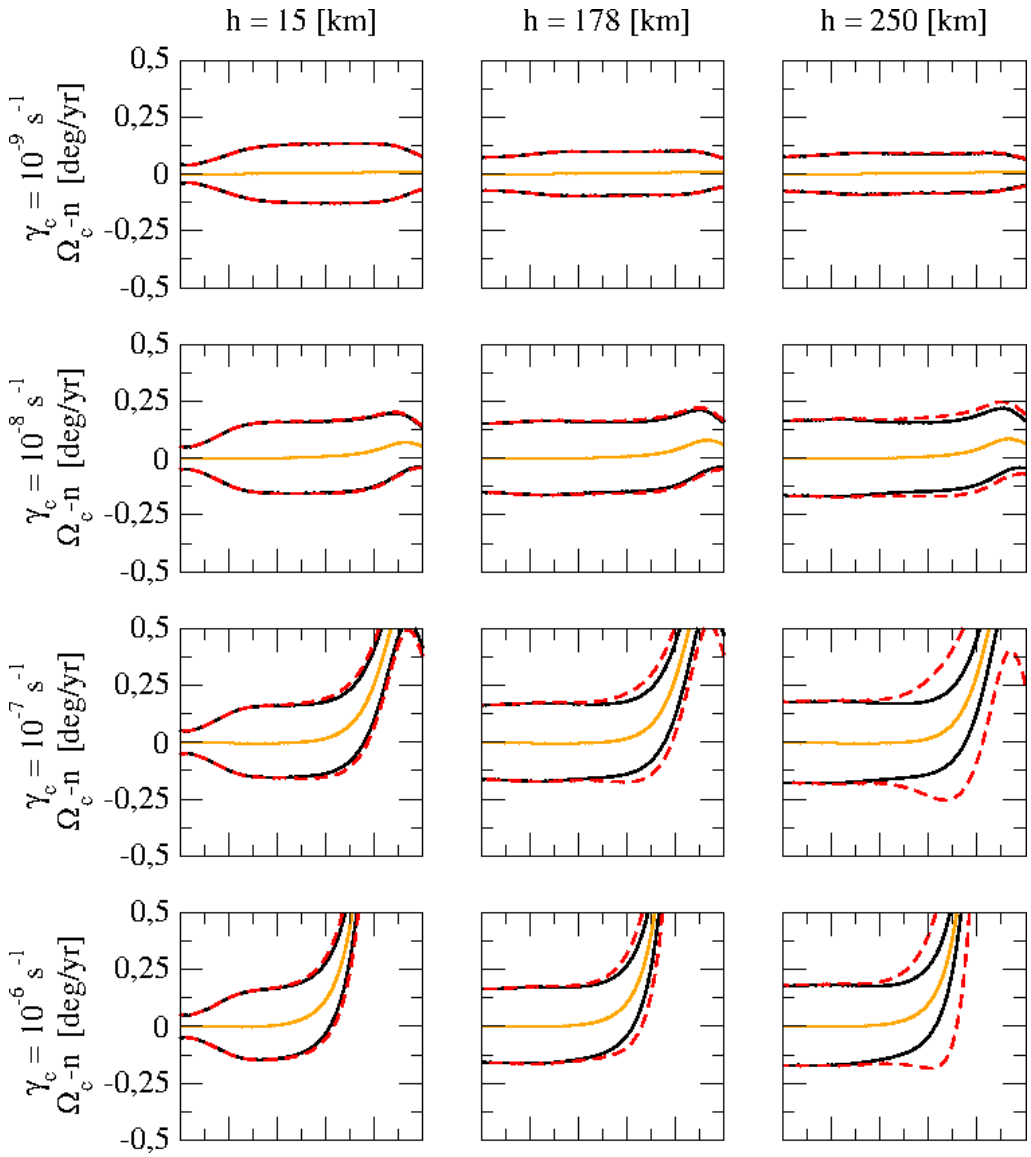

Figure 5.8: Core rotation of Titan in function of the relaxation factors, when $\eta_o = 10^9$ Pa s and $L_1 = 1.35 \times 10^{19}$ kg km^2 s^{-1}. The core relaxation factor γ_c increases from *top* to *bottom* and the ocean thickness h increases from *left* to *right*. We consider two dynamical models: The pair of solid black lines, indicate the maximum and minimum of the core rotation when the tidal forces, the gravitational coupling and the linear friction are taken in account, and the pair of dashed red lines, indicate the maximum and minimum of the core rotation when the angular momentum exchange with the atmosphere is added. The orange solid line, indicates the analytical stationary rotation B_{c0}.

5.5 Near-synchronous solution of the rotational equations

When we consider the effect of the atmosphere, using the convention 1 = *core* and 2 = *shell*, the rotational system (4.36) becomes

$$\begin{aligned} \dot{y}_1 &= -T_{11}\mathcal{T}_1 + \mathcal{K}_1 \sin 2\xi + \mathcal{F}_1(\gamma_2 y_2 - \gamma_1 y_1) \\ \dot{y}_2 &= T_{21}\mathcal{T}_1 - T_{22}\mathcal{T}_2 - \mathcal{K}_2 \sin 2\xi - \mathcal{F}_2(\gamma_2 y_2 - \gamma_1 y_1) + \mathcal{A}_\odot \sin 2\alpha_\odot. \end{aligned} \tag{5.5}$$

where

$$\mathcal{A}_\odot = \frac{2A_\odot}{\gamma_2}. \tag{5.6}$$

We assume that the particular solution

$$\begin{aligned} y_{1\odot} &= c_{1\odot}\cos 2\alpha_\odot + s_{1\odot}\sin 2\alpha_\odot \\ y_{2\odot} &= c_{2\odot}\cos 2\alpha_\odot + s_{2\odot}\sin 2\alpha_\odot, \end{aligned} \tag{5.7}$$

can be added to (4.40) to obtain the general solutions of the complete equation. $c_{j\odot}$ and $s_{j\odot}$ are undetermined coefficients to be obtained by substitution of the parts of the solution into Eq. (5.5) and identification.

The derivative of (5.7) is

$$\begin{aligned} \dot{y}_{1\odot} &= -2n_\odot c_{1\odot}\sin 2\alpha_\odot + 2n_\odot s_{1\odot}\cos 2\alpha_\odot \\ \dot{y}_{2\odot} &= -2n_\odot c_{2\odot}\sin 2\alpha_\odot + 2n_\odot s_{2\odot}\cos 2\alpha_\odot. \end{aligned} \tag{5.8}$$

The tidal function can be approximated by

$$\mathcal{T}_i \simeq c_{i\odot}\cos 2\alpha_\odot + s_{i\odot}\sin 2\alpha_\odot, \tag{5.9}$$

the trigonometric function of the gravitational coupling can be approximated by

$$\sin 2\xi \simeq \left(\frac{c_{2\odot}}{1+\lambda_2} - \frac{c_{1\odot}}{1+\lambda_1}\right)\cos 2\alpha_\odot + \left(\frac{s_{2\odot}}{1+\lambda_2} - \frac{s_{1\odot}}{1+\lambda_1}\right)e^2 \sin 2\alpha_\odot, \tag{5.10}$$

and the friction term is

$$\gamma_2 y_2 - \gamma_1 y_1 \simeq (\gamma_2 c_{2\odot} - \gamma_1 c_{1\odot})\cos 2\alpha_\odot + (\gamma_2 s_{2\odot} - \gamma_1 s_{1\odot})\sin 2\alpha_\odot. \tag{5.11}$$

Defining the constant matrix

$$\mathsf{D}_\odot = \begin{bmatrix} a_{11} & 2n_\odot & a_{12} & 0 \\ -2n_\odot & a_{11} & 0 & a_{12} \\ a_{21} & 0 & a_{22} & 2n_\odot \\ 0 & a_{21} & -2n_\odot & a_{22} \end{bmatrix}, \tag{5.12}$$

and the constant vectors

$$\Lambda_{\odot} = \begin{bmatrix} c_{1\odot} \\ s_{1\odot} \\ c_{2\odot} \\ s_{2\odot} \end{bmatrix}; \qquad \mathsf{P}_{\odot} = \mathcal{A}_{\odot} \begin{bmatrix} 0 \\ 0 \\ 0 \\ 1 \end{bmatrix}, \tag{5.13}$$

the undetermined coefficient vector is

$$\Lambda_{\odot} = \mathsf{D}_{\odot}^{-1} \mathsf{P}_{\odot}. \tag{5.14}$$

Finally, the rotational solutions can be written as

$$\begin{aligned} \nu_1 &= B_{10} + B_{11} \sin(\ell + \phi_{11}) + B_{12} \sin(2\ell + \phi_{12}) + B_{1\odot} \sin(2\alpha_{\odot} + \phi_{1\odot}) \\ \nu_2 &= B_{20} + B_{21} \sin(\ell + \phi_{21}) + B_{22} \sin(2\ell + \phi_{22}) + B_{2\odot} \sin(2\alpha_{\odot} + \phi_{2\odot}), \end{aligned} \tag{5.15}$$

where the constants $B_{i\odot}$ and the phases $\phi_{i\odot}$ are

$$\begin{aligned} B_{i\odot} &= \gamma_i \sqrt{c_{i\odot}^2 + s_{i\odot}^2} \\ \phi_{i\odot} &= \tan^{-1}(c_{i\odot}/s_{i\odot}). \end{aligned} \tag{5.16}$$

In Fig. 5.9, we show the same comparison of the Titan's shell rotation between the complete non-linear system and the approximate analytical solution of the above section. The approximate solution, also is in excellent agreement with numerical integration. It is important to note that the fact that the approximate solution of the non-linear system (5.5) can be expressed as the sum of solutions (4.40) and (5.7), it means that this system has a behavior quasi-linear, at least for the Titan's problem.

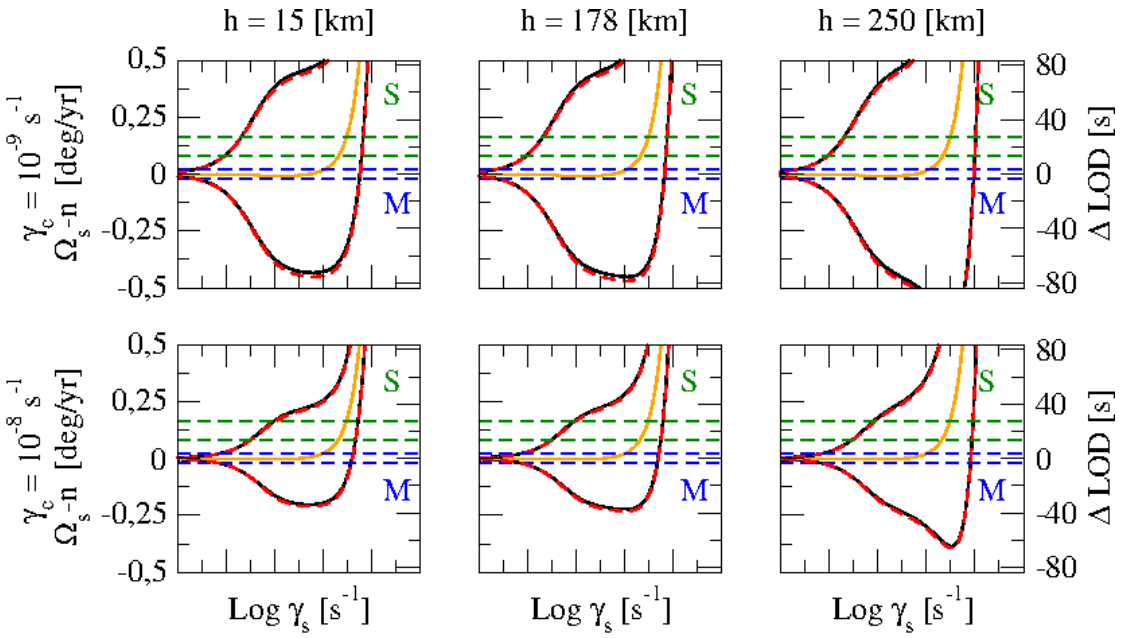

Figure 5.9: Comparison of the amplitudes of the shell rotation and corresponding length-of-day variation of Titan, between the numerical integration of the system Eq. (4.35) (solid black lines) and the analytical solution $\nu_i \simeq B_{i0} + B_{i1}\sin(\ell + \phi_{i1}) + B_{i\odot}\sin(2\alpha_\odot + \phi_{i\odot})$ (dashed red lines), including the atmospheric influence. We also plot the stationary solution given by B_{i0} (solid orange line). The core relaxation factor γ_c increases from *top* to *bottom* and the ocean thickness h increases from *left* to *right*. The ocean viscosity is $\eta_o = 10^{-3}$ Pa s. The horizontal dashed lines show the confidence interval of the observed values, as determined by Meriggiola (2012) (blue) and by Stiles et al. (2010) (green).

Chapter 6

Non-homogeneous Darwin theory

In this Chapter, we extend the Darwin tidal theory, revisited in Ferraz-Mello et al. (2008) (hereafter FRH), to the case of one differentiated body m. The resulting equations that describe this theory are compared to the equations of the creep tide theory, given in Chap. 3.

6.1 Darwin tide theory

We consider one differentiated body m of mass m_T, disturbing to one mass point M of mass M orbiting at a distance r from the center of m, as in the Chap. 2. We assume that m is composed of N homogeneous layers of density d_i $(i = 1, \cdots, N)$ and angular velocity $\mathbf{\Omega}_i = \Omega_i \widehat{\mathbf{k}}$, perpendicular to the orbital plane. We also assume that each layer has an outer ellipsoidal shape with semi axes a_i, b_i and c_i, where the semi-major axis a_i is pointing towards M and c_i is the axis of rotation (see Fig. 2.1 in Chap. 2).

We choose a spherical coordinate system so that $\mathbf{r} = (r, \theta, \varphi)$ and $\mathbf{r}^* = (r^*, \theta^*, \varphi^*)$ are the position vectors of M and an arbitrary point of the space M^*, respectively, relative to the center of the differentiated body m. The angles θ, θ^* are their co-latitudes and φ, φ^* are their longitudes (Fig. 6.1).

The disturbing potential generated by the i-th layer of the deformed body m, at the arbitrary point $\mathbf{r}^*$, can be written as

$$\delta U_i = -\frac{k_i G M R_i^5}{2 r^{*3} r^3}(3\cos^2\psi - 1) + \frac{k_i' \Omega_i^2 R_i^5}{6 r^{*3}}(3\cos^2\theta^* - 1), \tag{6.1}$$

(see Appendix E for the details of this calculation), where ψ is the angle formed by the positions vectors $\mathbf{r}$ and $\mathbf{r}^*$. The constants k_i and k_i' are the tidal and rotational fluid Love

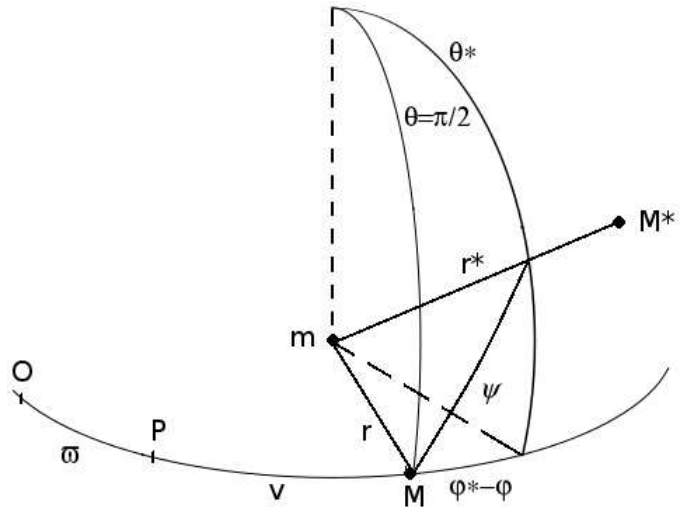

Figure 6.1: Spherical coordinate system with origin at the m and its equator as reference plane.

numbers of the i-th layer, respectively:

$$k_i = \widehat{k}_i \mathcal{L}_i; \qquad k'_i = \widehat{k}_i \frac{n^2 \mathcal{L}'_i}{\Omega_i^2}, \tag{6.2}$$

where

$$\widehat{k}_i = \frac{15 C_i}{4 m_T R_i^2} \frac{R_N^3}{R_i^3}, \tag{6.3}$$

C_i is the axial moment of inertia of this layer, and the parameter

$$\mathcal{L}_i = \frac{\mathcal{H}_i R_i^5 - \mathcal{H}_{i-1} R_{i-1}^5}{R_i^5 - R_{i-1}^5}; \qquad \mathcal{L}'_i = \frac{\mathcal{G}_i R_i^5 - \mathcal{G}_{i-1} R_{i-1}^5}{R_i^5 - R_{i-1}^5}. \tag{6.4}$$

In order to proceed, we consider the two-body motion. The equations of the Keplerian motion to M, orbiting to m, are

$$r = \frac{a(1-e^2)}{1 + e\cos v}, \tag{6.5}$$

and

$$v = \ell + \left(2e - \frac{e^3}{4}\right)\sin\ell + \frac{5e^2}{4}\sin 2\ell + \frac{13e^2}{12}\sin 3\ell + \mathcal{O}(e^4), \tag{6.6}$$

where a is the semi-major axis, e is the eccentricity and the angles v and ℓ are the true and mean anomaly, respectively, of the body M. In the planar case, we have $\theta = \frac{\pi}{2}$ and $\varphi = v + \varpi$, where ϖ is the longitude of the periapsis. By solving the spherical triangle, we obtain

$$\cos\psi = \sin\theta^* \cos(\varphi^* - \varpi - v), \tag{6.7}$$

the disturbing potential of the i-th layer, after Fourier expansion, becomes

$$\begin{aligned}\delta U_i &= -\frac{3k_i GMR_i^5}{4r^{*3}a^3}\sin^2\theta^* \sum_{k\in\mathbb{Z}} E_{2,k}\cos\Theta_k^* + \\ &\frac{k_i GMR_i^5}{4r^{*3}a^3}(3\cos^2\theta^*-1)\sum_{k\in\mathbb{Z}} E_{0,k}\cos k\ell + \frac{k_i'\Omega_i^2 R_i^5}{6r^{*3}}(3\cos^2\theta^*-1),\end{aligned} \tag{6.8}$$

where the argument Θ_k^* is given by Eq. (3.22) and the coefficients of the Fourier series $E_{q,p}$ are the Cayley functions given by Eq; (3.12).

6.2 The tidal phase lags

In Darwin's theory, for each periodic term of the potential δU_i, a delay is introduced in the form of a *lag angle* (Darwin, 1880). The trigonometric functions, in the potential (6.8), are expanded to first order in the lag in the following way

$$\begin{aligned}\cos(2\varphi^* - 2\varpi + (k-2)\ell - \alpha_{ik}) &\approx \cos\Theta_k^* + \alpha_{ik}\sin\Theta_k^* \\ \sin(2\varphi^* - 2\varpi + (k-2)\ell - \alpha_{ik}) &\approx \sin\Theta_k^* - \alpha_{ik}\cos\Theta_k^*,\end{aligned} \tag{6.9}$$

and

$$\begin{aligned}\cos(k\ell - \beta_{ik}) &\approx \cos k\ell + \beta_{ik}\sin k\ell \\ \sin(k\ell - \beta_{ik}) &\approx \sin k\ell - \beta_{ik}\cos k\ell,\end{aligned} \tag{6.10}$$

According to this definition, α_{ik} denote the lag corresponding to the k-th sectorial term of the i-th layer, and β_{ik} denote the lag corresponding to the k-th radial term of the i-th layer. The lags are small quantities.

6.3 The Love numbers

In the homogeneous tidal theories using Love's theory to obtain the disturbing potential δU, the only Love number appearing is k_i. In Darwin's theory (and in all theories introducing lags individually after a Fourier decomposition of δU), we may consider that the surface of the body does not respond instantaneously to the tidal potential and does not reach the deformation predicted in the equilibrium figure theory. In order to take into

account this effect, instead of the Love number $\widehat{k}_i\mathcal{L}_i$ for the i-th layer, we may introduce two different dynamics Love numbers, one for each layer boundary and tidal harmonic:

$$\widehat{k}_i\frac{\mathcal{H}_i R_i^5}{R_i^5-R_{i-1}^5}k_{ik}^*; \qquad \widehat{k}_i\frac{\mathcal{H}_{i-1} R_{i-1}^5}{R_i^5-R_{i-1}^5}k_{i-1k}^*,$$

for the outer and the inner surface, respectively. The coefficient k_{ik}^*, take into account the non-instantaneous response of the outer surface of the layer and k_{i-1k}^* the non-instantaneous response of the inner surface. These coefficients do not depend on the layer, but only the surface considered (e.g. the outer surface of the i-th layer has the same coefficient for the inner surface of the $(i+1)$-th layer).

In FRH, for the sake of simplicity, only one value k_d corresponding to the main tide harmonic is used, while the others are merged with the corresponding lag ε_j. In the present work, we have introduced the delay parameters corresponding to the outer surface

$$\alpha'_{ik}=k_{ik}^*\alpha_{ik}; \qquad \beta'_{ik}=\kappa_{ik}^*\beta_{ik}, \tag{6.11}$$

where α_{ik},β_{ik} are the lags of the frequency-dependent tide harmonics of the outer boundary of the i-th layer and k_{ik}^*,κ_{ik}^* are the frequency-dependent dynamics counterparts of k_i for the sectorial and radial terms, respectively. For the inner surface we have similar expressions.

The scheme used to include the dynamic Love numbers in the sectorial terms is

$$\begin{aligned}
k_i\cos\Theta_k^* &= \widehat{k}_i\frac{\mathcal{H}_i R_i^5}{R_i^5-R_{i-1}^5}\cos\Theta_k^* - \widehat{k}_i\frac{\mathcal{H}_{i-1} R_{i-1}^5}{R_i^5-R_{i-1}^5}\cos\Theta_k^* \\
&\longrightarrow \widehat{k}_i k_{ik}^*\frac{\mathcal{H}_i R_i^5}{R_i^5-R_{i-1}^5}\cos\left(\Theta_k^*-\alpha_{ik}\right) - \widehat{k}_i k_{i-1k}^*\frac{\mathcal{H}_{i-1} R_{i-1}^5}{R_i^5-R_{i-1}^5}\cos\left(\Theta_k^*-\alpha_{i-1k}\right) \\
&\simeq \widehat{k}_i\frac{\Delta\left(\mathcal{H}_i R_i^5 k_{ik}^*\right)}{R_i^5-R_{i-1}^5}\cos\Theta_k^* + \widehat{k}_i\frac{\Delta\left(\mathcal{H}_i R_i^5\alpha'_{ik}\right)}{R_i^5-R_{i-1}^5}\sin\Theta_k^*,
\end{aligned} \tag{6.12}$$

and for the radial terms

$$\begin{aligned}
k_i\cos k\ell &= \widehat{k}_i\frac{\mathcal{H}_i R_i^5}{R_i^5-R_{i-1}^5}\cos k\ell - \widehat{k}_i\frac{\mathcal{H}_{i-1} R_{i-1}^5}{R_i^5-R_{i-1}^5}\cos k\ell \\
&\longrightarrow \widehat{k}_i\kappa_{ik}^*\frac{\mathcal{H}_i R_i^5}{R_i^5-R_{i-1}^5}\cos\left(k\ell-\beta_{ik}\right) - \widehat{k}_i\kappa_{i-1k}^*\frac{\mathcal{H}_{i-1} R_{i-1}^5}{R_i^5-R_{i-1}^5}\cos\left(k\ell-\beta_{i-1k}\right) \\
&\simeq \widehat{k}_i\frac{\Delta\left(\mathcal{H}_i R_i^5\kappa_{ik}^*\right)}{R_i^5-R_{i-1}^5}\cos k\ell + \widehat{k}_i\frac{\Delta\left(\mathcal{H}_i R_i^5\beta'_{ik}\right)}{R_i^5-R_{i-1}^5}\sin k\ell.
\end{aligned} \tag{6.13}$$

where $\Delta(f_i)=f_i-f_{i-1}$, denotes the increment of one function f_i, between the inner and the outer boundaries of this layer.

We assume that the viscosity does not affect the rotational axial terms and the rotational static equilibrium figure remains without change. The orbital motion of M change tha angular velocity motion rotational fluid Love number k_i' remains without change.

6.4 Delayed potential, forces and torques

When we introduce the lags in the trigonometric functions, we can write the delayed tidal potential of the i-th layer as $\delta U_i^{(del)}$, is given by

$$\begin{aligned}\delta U_i^{(del)} &= -\frac{3\widehat{k}_i GMR_i^5}{4r^{*3}a^3}\sin^2\theta^*\sum_{k\in\mathbb{Z}}E_{2,k}\Big(\mathcal{A}_{ik}\sin\Theta_k^* + \mathcal{B}_{ik}\cos\Theta_k^*\Big) + \\ &+\frac{\widehat{k}_i GMR_i^5}{4r^{*3}a^3}(3\cos^2\theta^*-1)\sum_{k\in\mathbb{Z}}E_{0,k}\Big(\mathcal{A}''_{ik}\sin k\ell + \mathcal{B}''_{ik}\cos k\ell\Big) + \\ &+\frac{\widehat{k}_i\mathcal{L}_i' n^2R_i^5}{6r^{*3}}(3\cos^2\theta^*-1),\end{aligned} \tag{6.14}$$

where

$$\mathcal{A}_{ik} = \frac{\Delta\left(\mathcal{H}_i R_i^5\alpha'_{ik}\right)}{R_i^5 - R_{i-1}^5}; \qquad \mathcal{B}_{ik} = \frac{\Delta\left(\mathcal{H}_i R_i^5 k^*_{ik}\right)}{R_i^5 - R_{i-1}^5}. \tag{6.15}$$

and

$$\mathcal{A}''_{ik} = \frac{\Delta\left(\mathcal{H}_i R_i^5\beta'_{ik}\right)}{R_i^5 - R_{i-1}^5}; \qquad \mathcal{B}''_{ik} = \frac{\Delta\left(\mathcal{H}_i R_i^5\kappa^*_{ik}\right)}{R_i^5 - R_{i-1}^5}. \tag{6.16}$$

To obtain the force generated by the i-th layer, acting on one mass M^*, located in $\mathsf{M}^*(r^*,\theta^*,\varphi^*)$, we have to take the negative gradient of the potential of this layer at the

point and multiply it by the mass placed in the point, $\mathbf{F}_i = -M^* \nabla_{\mathbf{r}^*} \delta U_i^{(del)}$

$$\begin{aligned}
F_{1i} &= -\frac{9\widehat{k}_i G M M^* R_i^5}{4r^{*4}a^3} \sin^2\theta^* \sum_{k\in\mathbb{Z}} E_{2,k}\Big(\mathcal{A}_{ik}\sin\Theta_k^* + \mathcal{B}_{ik}\cos\Theta_k^*\Big) + \\
&+\frac{3\widehat{k}_i G M M^* R_i^5}{4r^{*4}a^3}(3\cos^2\theta^* - 1)\sum_{k\in\mathbb{Z}} E_{0,k}\Big(\mathcal{A}''_{ik}\sin k\ell + \mathcal{B}''_{ik}\cos k\ell\Big) + \\
&+\frac{\widehat{k}_i M^* \mathcal{L}'_i n^2 R_i^5}{2r^{*4}}(3\cos^2\theta^* - 1) \\
F_{2i} &= \frac{3\widehat{k}_i G M M^* R_i^5}{4r^{*4}a^3}\sin 2\theta^* \sum_{k\in\mathbb{Z}} E_{2,k}\Big(\mathcal{A}_{ik}\sin\Theta_k^* + \mathcal{B}_{ik}\cos\Theta_k^*\Big) + \\
&+\frac{3\widehat{k}_i G M M^* R_i^5}{4r^{*4}a^3}\sin 2\theta^* \sum_{k\in\mathbb{Z}} E_{2,k}\Big(\mathcal{A}''_{ik}\sin k\ell + \mathcal{B}''_{ik}\cos k\ell\Big) + \\
&+\frac{\widehat{k}_i M^* \mathcal{L}'_i n^2 R_i^5}{2r^{*4}}\sin 2\theta^* \\
F_{3i} &= \frac{3\widehat{k}_i G M M^* R_i^5}{2r^{*4}a^3}\sin\theta^* \sum_{k\in\mathbb{Z}} E_{2,k}\Big(\mathcal{A}_{ik}\cos\Theta_k^* - \mathcal{B}_{ik}\sin\Theta_k^*\Big).
\end{aligned} \tag{6.17}$$

The corresponding torque is $\mathbf{M}_i = \mathbf{r}^* \times \mathbf{F}_i$, or, since, $\mathbf{r}^* = (r^*, 0, 0)$:

$$M_{1i} = 0; \qquad M_{2i} = -r^* F_{3i}; \qquad M_{3i} = r^* F_{2i}, \tag{6.18}$$

that is

$$\begin{aligned}
M_{2i} &= -\frac{3\widehat{k}_i G M M^* R_i^5}{2r^{*3}a^3}\sin\theta^* \sum_{k\in\mathbb{Z}} E_{2,k}\Big(\mathcal{A}_{ik}\cos\Theta_k^* - \mathcal{B}_{ik}\sin\Theta_k^*\Big) \\
M_{3i} &= \frac{3\widehat{k}_i G M M^* R_i^5}{4r^{*3}a^3}\sin 2\theta^* \sum_{k\in\mathbb{Z}} E_{2,k}\Big(\mathcal{A}_{ik}\sin\Theta_k^* + \mathcal{B}_{ik}\cos\Theta_k^*\Big) + \\
&+\frac{3\widehat{k}_i G M M^* R_i^5}{4r^{*3}a^3}\sin 2\theta^* \sum_{k\in\mathbb{Z}} E_{2,k}\Big(\mathcal{A}''_{ik}\sin k\ell + \mathcal{B}''_{ik}\cos k\ell\Big) + \\
&+\frac{\widehat{k}_i M^* \mathcal{L}'_i n^2 R_i^5}{2r^{*3}}\sin 2\theta^*.
\end{aligned} \tag{6.19}$$

6.5 Forces and torques acting on M

Since we are interested in the force acting on M due to the tidal deformation of m, we must substitute $(M^*, r^*, \theta^*, \varphi^*)$ by $(M, r, \frac{\pi}{2}, \varpi + v)$. The forces, then are

$$\begin{aligned} F_{1i} &= -\frac{9\widehat{k}_i G M^2 R_i^5}{4r^4 a^3} \sum_{k\in\mathbb{Z}} E_{2,k}\Big(\mathcal{A}_{ik}\sin\Upsilon_k + \mathcal{B}_{ik}\cos\Upsilon_k\Big) - \\ &\quad -\frac{3\widehat{k}_i G M^2 R_i^5}{4r^4 a^3} \sum_{k\in\mathbb{Z}} E_{0,k}\Big(\mathcal{A}''_{ik}\sin k\ell + \mathcal{B}''_{ik}\cos k\ell\Big) - \frac{\widehat{k}_i M \mathcal{L}'_i n^2 R_i^5}{2r^4} \\ F_{2i} &= 0 \\ F_{3i} &= \frac{3\widehat{k}_i G M^2 R_i^5}{2r^4 a^3} \sum_{k\in\mathbb{Z}} E_{2,k}\Big(\mathcal{A}_{ik}\cos\Upsilon_k - \mathcal{B}_{ik}\sin\Upsilon_k\Big). \end{aligned} \tag{6.20}$$

where the angle Υ_k is defined be the Eq. (3.32).

The corresponding torques are

$$\begin{aligned} M_{2i} &= -\frac{3\widehat{k}_i G M^2 R_i^5}{2r^3 a^3} \sum_{k\in\mathbb{Z}} E_{2,k}\Big(\mathcal{A}_{ik}\cos\Upsilon_k - \mathcal{B}_{ik}\sin\Upsilon_k\Big) \\ M_{3i} &= 0. \end{aligned} \tag{6.21}$$

After Fourier expansion, the torque along to the axis z ($M_{zi} = -M_{2i}$) can be written as

$$M_{zi} = \frac{3\widehat{k}_i G M^2 R_i^5}{2a^6} \sum_{k,j\in\mathbb{Z}} E_{2,k} E_{2,k+j} \mathcal{B}_{ik}\cos j\ell. \tag{6.22}$$

Finally, the time average of the total torque over one period is $\langle M_{zi}\rangle = \frac{1}{2\pi}\int_0^{2\pi} M_{zi} d\ell$, therefore

$$\langle M_{zi}\rangle = \frac{3\widehat{k}_i G M^2 R_i^5}{2a^6} \sum_{k\in\mathbb{Z}} E_{2,k}^2 \mathcal{B}_{ik}. \tag{6.23}$$

As it was explained in Section 3.6, the above expression for the time average, which is equivalent to take into account only the terms with $j = 0$, only is valid if α'_{ik} can be considered as constant. In the opposite case, in which α'_{ik} depends on the time, this fact must be taken into account when computing the time average.

6.6 Work done by the tidal forces acting on M

The time rate of the work done by the tidal forces due to the i-th layer is $\dot{W}^{(i)}_{orb} = \mathbf{F}_i \cdot \mathbf{v}$, where $\mathbf{v}$ is the relative velocity vector of the external body, whose components in spherical

coordinates are

$$v_1 = \frac{nae\sin v}{\sqrt{1-e^2}}; \qquad v_2 = 0; \qquad v_3 = \frac{na^2\sqrt{1-e^2}}{r}. \tag{6.24}$$

Using the tidal force given by the Eq. (6.20), the rate of the work corresponding to the i-th layer is

$$\begin{aligned}
\frac{dW^{(i)}_{orb}}{dt} &= -\frac{3\widehat{k}_i GM^2R_i^5 n}{2a^6}\sum_{k\in\mathbb{Z}}\Bigg\{E_{2,k}\times \\
&\times\Bigg[\mathcal{A}_{ik}\left(\frac{3e}{2\sqrt{1-e^2}}\left(\frac{a}{r}\right)^4\sin v\sin\Upsilon_k - \sqrt{1-e^2}\left(\frac{a}{r}\right)^5\cos\Upsilon_k\right)+ \\
&+\mathcal{B}_{ik}\left(\frac{3e}{2\sqrt{1-e^2}}\left(\frac{a}{r}\right)^4\sin v\cos\Upsilon_k + \sqrt{1-e^2}\left(\frac{a}{r}\right)^5\sin\Upsilon_k\right)\Bigg]+ \\
&+\frac{E_{0,k}}{3}\frac{3e}{2\sqrt{1-e^2}}\left(\frac{a}{r}\right)^4\sin v\Big(\mathcal{A}''_{ik}\sin k\ell + 2\mathcal{B}''_{ik}\cos k\ell\Big)\Bigg\}- \\
&-\frac{\widehat{k}_i MR_i^5 ne}{2a^3\sqrt{1-e^2}}n^2\mathcal{L}'_i\left(\frac{a}{r}\right)^4\sin v,
\end{aligned} \tag{6.25}$$

or, after Fourier expansion of the tidal terms[1],

$$\begin{aligned}
\frac{dW^{(i)}_{orb}}{dt} &= \frac{3\widehat{k}_i GM^2R_i^5 n}{4a^6}\sum_{k,j\in\mathbb{Z}}\Bigg((2-k-j)E_{2,k}E_{2,k+j}\Big(\mathcal{A}_{ik}\cos j\ell + \mathcal{B}_{ik}\sin j\ell\Big)- \\
&-\frac{(k+j)}{3}E_{0,k}E_{0,k+j}\Big(\mathcal{A}''_{ik}\cos j\ell + \mathcal{B}''_{ik}\sin j\ell\Big)\Bigg)- \\
&-\frac{\widehat{k}_i MR_i^5 ne}{2a^3\sqrt{1-e^2}}n^2\mathcal{L}'_i\left(\frac{a}{r}\right)^4\sin v,
\end{aligned} \tag{6.26}$$

and its time-average over one period is

$$\left\langle\frac{dW^{(i)}_{orb}}{dt}\right\rangle = \frac{3\widehat{k}_i GM^2R_i^5 n}{4a^6}\sum_{k\in\mathbb{Z}}\left((2-k)E_{2,k}^2\mathcal{A}_{ik} - \frac{k}{3}E_{0,k}^2\mathcal{A}''_{ik}\right). \tag{6.27}$$

The average of the last term of Eq. (6.26) is

$$\frac{1}{2\pi}\int_0^{2\pi} n^2\mathcal{L}'_i\left(\frac{a}{r}\right)^4\sin v\,d\ell = \sum_{j=1}^{N}\frac{\Delta\big(R_i^5(\mathsf{E}^{-1})_{ij}x_j^3\big)}{R_i^5-R_{i-1}^5}\frac{1}{2\pi}\int_0^{2\pi}\Omega_j^2\left(\frac{a}{r}\right)^4\sin v\,d\ell = 0, \tag{6.28}$$

(see Appendix D).

[1] For the details of this calculation, see Appendix F.

6.7 Variations in semi-major axis and eccentricity

In this section, we calculate the variation in semi-major axis and eccentricity. For this sake, we use the same equations of the Section 3.8.

Using Eqs. (3.41) and (6.21) and summing over all layers, we obtain the equation for the variation in semi-major axis:

$$\begin{aligned}\dot{a} &= \sum_{i=1}^{N}\frac{3\widehat{k}_i M R_i^5 n}{2m_T a^4}\sum_{k,j\in\mathbb{Z}}\Bigg((2-k-j)E_{2,k}E_{2,k+j}\Big(\mathcal{A}_{ik}\cos j\ell+\mathcal{B}_{ik}\sin j\ell\Big)-\\ &\quad-\frac{(k+j)}{3}E_{0,k}E_{0,k+j}\Big(\mathcal{A}''_{ik}\cos j\ell+\mathcal{B}''_{ik}\sin j\ell\Big)\Bigg)-\\ &\quad-\sum_{i=1}^{N}\frac{\widehat{k}_i R_i^5 ne}{Gm_T a\sqrt{1-e^2}}n^2\mathcal{L}'_i\left(\frac{a}{r}\right)^4\sin v, \end{aligned}\tag{6.29}$$

After the time-average over one period, we obtain that the variation in semi-major axes is

$$\langle\dot{a}\rangle = \sum_{i=1}^{N}\frac{3\widehat{k}_i M R_i^5 n}{2m_T a^4}\sum_{k\in\mathbb{Z}}\left((2-k)E_{2,k}^2\mathcal{A}_{ik}-\frac{k}{3}E_{0,k}^2\mathcal{A}''_{ik}\right).\tag{6.30}$$

In the same way, using the Eq. (3.42), replacing $\mathcal{M}_z$ and $\dot{W}_{orb}$ by the Eqs. (6.21) and (6.26), and summing over all layers, we obtain

$$\begin{aligned}\dot{e} &= \sum_{i=1}^{N}\frac{3\widehat{k}_i M R_i^5 n}{2m_T a^4}\frac{(1-e^2)}{2ae}\sum_{k,j\in\mathbb{Z}}\Bigg(\Big(\frac{2}{\sqrt{1-e^2}}-(2-k-j)\Big)E_{2,k}E_{2,k+j}\times\\ &\quad\times\Big(\mathcal{A}_{ik}\cos j\ell+\mathcal{B}_{ik}\sin j\ell\Big)-\frac{(k+j)}{3}E_{0,k}E_{0,k+j}\Big(\mathcal{A}''_{ik}\cos j\ell+\mathcal{B}''_{ik}\sin j\ell\Big)\Bigg)-\\ &\quad-\sum_{i=1}^{N}\frac{\widehat{k}_i R_i^5 n}{Gm_T a}\frac{\sqrt{1-e^2}}{2a}n^2\mathcal{L}'_i\left(\frac{a}{r}\right)^4\sin v, \end{aligned}\tag{6.31}$$

Finally, after the time-average over one period, we obtain that the variation in eccentricity is

$$\langle\dot{e}\rangle = \sum_{i=1}^{N}\frac{3\widehat{k}_i M R_i^5 n}{2m_T a^4}\frac{(1-e^2)}{2ae}\sum_{k\in\mathbb{Z}}\left(\Big(\frac{2}{\sqrt{1-e^2}}-(2-k)\Big)E_{2,k}^2\mathcal{A}_{ik}-\frac{k}{3}E_{0,k}^2\mathcal{A}''_{ik}\right).\tag{6.32}$$

6.8 Comparison with the creep tide theory

In the previous sections, we develop the extension of the non-homogeneous case of the Darwin tidal theory. The resulting equations that describe this theory with the equations

given by the creep tide theory are significantly similar, being that the methods by which they are obtained differ considerably.

Considering that $\widehat{k}_{ik}$ is constant, defined by the Eq. (6.3), the delayed disturbing potential of the Darwin's theory (6.14), can be written as

$$\begin{aligned}\delta U_i^{(del)} &= -\frac{45GMR_N^3C_i}{16m_Tr^{*3}a^3}\sin^2\theta^*\sum_{k\in\mathbb{Z}}E_{2,k}\Big(\mathcal{A}_{ik}\sin\Theta_k^*+\mathcal{B}_{ik}\cos\Theta_k^*\Big)+\\ &+\frac{15GMR_N^3C_i}{16m_Tr^{*3}a^3}(3\cos^2\theta^*-1)\sum_{k\in\mathbb{Z}}E_{0,k}\Big(\mathcal{A}''_{ik}\sin k\ell+\mathcal{B}''_{ik}\cos k\ell\Big)+\\ &+\frac{5R_N^3n^2\mathcal{L}'_iC_i}{8m_Tr^{*3}}(3\cos^2\theta^*-1),\end{aligned}\tag{6.33}$$

which is identical to the disturbing potential of the creep tide (3.21), with $\mathcal{A}_{ik}$, $\mathcal{B}_{ik}$, $\mathcal{A}''_{ik}$ and $\mathcal{B}''_{ik}$ instead $\mathcal{C}_{ik}$, $\mathcal{D}_{ik}$, $\mathcal{C}''_{ik}$ and $\mathcal{D}''_{ik}$, respectively. Considering the equality between these coefficients, we obtain that

$$\begin{aligned}\alpha'_{ik} &= k^*_{ik}\alpha_{ik}=\frac{\sin 2\sigma_{ik}}{2}; & k^*_{ik}&=\cos^2\sigma_{ik}\\ \beta'_{ik} &= \kappa^*_{ik}\beta'_{ik}=\frac{\sin 2\sigma''_{ik}}{2}; & \kappa^*_{ik}&=\cos^2\sigma''_{ik},\end{aligned}\tag{6.34}$$

or, using the Eqs. (3.26) and (3.27), we obtain

$$\begin{aligned}\alpha_{ik} &= \frac{\nu_i+kn}{\gamma_i}; & k^*_{ik}&=\frac{\gamma_i^2}{\gamma_i^2+(\nu_i+kn)^2}\\ \beta_{ik} &= \frac{kn}{\gamma_i}; & \kappa^*_{ik}&=\frac{\gamma_i^2}{\gamma_i^2+(kn)^2}.\end{aligned}\tag{6.35}$$

In other words, the creep tide theory is equivalent to propose a linear-frequency law for the lags α_{ik} and β_{ik}, and a frequency-dependent sectorial and radial dynamic Love numbers $\widehat{k}_ik^*_{ik}$ and $\widehat{k}_i\kappa^*_{ik}$.

However, this equivalence between both theories is only valid if $\alpha_{ik}\ll 1$ and $\beta_{ik}\ll 1$, or $n/\gamma_i\ll 1$. This corresponds to the case of bodies with low viscosity, such as stars and gas giant planets. In order to overcome this limitation, we modify the scheme used to include the dynamic Love numbers in the sectorial and radial terms, without any ad hoc hypothesis for the lags:

$$\begin{aligned}k_i\cos\Theta_k^* &\longrightarrow \widehat{k}_ik^*_{ik}\frac{\mathcal{H}_iR_i^5}{R_i^5-R_{i-1}^5}\cos\left(\Theta_k^*-\alpha_{ik}\right)-\widehat{k}_ik^*_{i-1k}\frac{\mathcal{H}_{i-1}R_{i-1}^5}{R_i^5-R_{i-1}^5}\cos\left(\Theta_k^*-\alpha_{i-1k}\right)\\ &\simeq \widehat{k}_i\frac{\Delta\left(\mathcal{H}_iR_i^5k^*_{ik}\cos\alpha_{ik}\right)}{R_i^5-R_{i-1}^5}\cos\Theta_k^*+\widehat{k}_i\frac{\Delta\left(\mathcal{H}_iR_i^5k^*_{ik}\sin\alpha_{ik}\right)}{R_i^5-R_{i-1}^5}\sin\Theta_k^*,\end{aligned}\tag{6.36}$$

and

$$k_i \cos k\ell \longrightarrow \widehat{k}_i \kappa^*_{ik} \frac{\mathcal{H}_i R_i^5}{R_i^5 - R_{i-1}^5} \cos\left(k\ell - \beta_{ik}\right) - \widehat{k}_i \kappa^*_{i-1k} \frac{\mathcal{H}_{i-1} R_{i-1}^5}{R_i^5 - R_{i-1}^5} \cos\left(k\ell - \beta_{i-1k}\right)$$
$$\simeq \widehat{k}_i \frac{\Delta\left(\mathcal{H}_i R_i^5 \kappa^*_{ik} \cos\beta_{ik}\right)}{R_i^5 - R_{i-1}^5} \cos k\ell + \widehat{k}_i \frac{\Delta\left(\mathcal{H}_i R_i^5 \kappa^*_{ik} \sin\beta_{ik}\right)}{R_i^5 - R_{i-1}^5} \sin k\ell. \tag{6.37}$$

The new coefficients are

$$\begin{aligned} \mathcal{A}_{ik} &= \frac{\Delta\left(\mathcal{H}_i R_i^5 k^*_{ik} \sin\alpha_{ik}\right)}{R_i^5 - R_{i-1}^5}; \qquad \mathcal{B}_{ik} = \frac{\Delta\left(\mathcal{H}_i R_i^5 k^*_{ik} \cos\alpha_{ik}\right)}{R_i^5 - R_{i-1}^5}, \\ \mathcal{A}''_{ik} &= \frac{\Delta\left(\mathcal{H}_i R_i^5 \kappa^*_{ik} \sin\beta_{ik}\right)}{R_i^5 - R_{i-1}^5}; \qquad \mathcal{B}''_{ik} = \frac{\Delta\left(\mathcal{H}_i R_i^5 \kappa^*_{ik} \cos\beta_{ik}\right)}{R_i^5 - R_{i-1}^5}. \end{aligned} \tag{6.38}$$

Considering the equality between these coefficients with the coefficients given by the creep tide, we obtain

$$\begin{aligned} \alpha_{ik} &= \sigma_{ik}; \qquad k^*_{ik} = \cos\sigma_{ik} \\ \beta_{ik} &= \sigma''_{ik}; \qquad \kappa^*_{ik} = \cos\sigma''_{ik}. \end{aligned} \tag{6.39}$$

Therefore, the creep tide theory can be interpreted as one particular case of the generalized Darwin's theory, where the lags and the dynamical tidal Love numbers depend on the frequencies and the viscosities as Eq. (6.39). It is worth emphasizing that while the generalized Darwinian is an analytical free-parameters theory, the creep tide theory is equivalent to fix these free parameter with one specific rheophysical law.

It is important not to confuse these lags α and β (or σ and σ'') with the *geodetic lags* of the surface of each layer. The geodetic lags are the observed lags of each surface, and result of the composition of the elastic and anelastic tidal components. The creep tide use the rheology of one viscous fluid, through the Navier-Stokes's equation. In order to introduce the elastic component we can use two methods: the ad hoc method, proposed in FM13 (Sec. 10) or using the one Maxwellian rheology, as in Correia et al. (2014). These methods, though they are very different, are completely equivalent (see Ferraz-Mello, 2015b).

Chapter 7

Conclusion

In this thesis, we extended the creep tide theory, presented in Ferraz-Mello (2013) and Ferraz-Mello (2015a), to a differentiated non-homogeneous body formed by N homogeneous layers with differential rotation. For this sake, first we have extended the classical results on non-homogeneous rotating figures of equilibrium to the case in which the body is also under the action of a tidal potential due to the presence of an external body, assuming differential rotation. The only assumptions in this work are a body formed by N homogeneous ellipsoidal layers in equilibrium and small enough tidal and rotational deformations with symmetry axes perpendicular to each other (remember that, in the second order, the figure ceases to be an ellipsoid). We have calculated the $2N$ equilibrium equations for small flattenings and we have found that the equatorial and the polar flattenings $\epsilon_\rho^{(k)}$ and $\epsilon_z^{(k)}$ are linearly related, both being proportional to the homogeneous reference values with the factors of proportionality $\mathcal{H}_k$ and $\mathcal{G}_k$, respectively. The equatorial deformations propagate towards the interior of the body in the same way depending, in the first approximation, only on the density profile; it does not depend on the origin of the two considered deformations. Then the problem of finding the $2N$ flattenings corresponds to finding the $2N$ coefficients $\mathcal{H}_k$ and $\mathcal{G}_k$ with $2N$ equilibrium equations. An important consequence of this approach is that the flattening profile $\mathcal{H}_k$ is the same no matter if the rotation of the body is synchronous or non-synchronous and the results for $\mathcal{H}_k$ are the same found by Tricarico (2014).

We have also studied the continuous case as the limit for a very large number of layers of infinitesimal thickness, which leads to the Clairaut's differential equation for the function $\mathcal{H}(x)$. This result was expected because the coefficients of the Clairaut equation only

depend on the internal distribution of matter $\rho(x)$. Therefore, the differential equation that generates the functional form of the profile flattening $\mathcal{H}(x)$ does not change when we change the nature of the deformation, provided that it is small. For densities decreasing monotonically with the radius, we have found that, at the surface, $\mathcal{H}_n$ takes values larger than 0.4 (see Eq. (2.24)) and takes the limit value 1 in the homogeneous case. This means that the surface flattenings of a differentiated body are always smaller than the flattening of the corresponding homogeneous ellipsoids, but always larger than 40% of it.

Using this static equilibrium figure, we found the creep tide equation for the outer surface of each layer. Once solved the creep equations, we obtained the tidal equilibrium figure, and thereby we calculated the potential and the forces which act on the external mass producing the tide, as well as the variations in semi-major axis and eccentricity, produced by the tidal forces.

In order to apply the theory to satellites of our Solar System, we calculated the explicit expression in the particular case of one body formed by two layers. We may remember that the number of free parameters and independent variables increases quickly when the number of layers increases. The simplest version of the non-homogeneous creep tide theory (the two-layer model), allow us to obtain the main features due to the non-homogenity of the body, by introducing a minimal quantity of free parameters. In the used model, we have also calculated the tidal torque which acts on each layer and also the possible interaction torques, as the gravitational coupling and the friction at the interface between the contiguous layers (general developement of these effects are given in Appendices 3 and 4). The friction was modeled assuming two homogeneous contiguous layers separated by one thin Newtonian fluid layer. This model of friction is particularly appropriate for differentiated satellites with one subsurface ocean, as are various satellites of our Solar System (e.g. Titan, Enceladus and Europa).

The two-layer was compared with the homogeneous case. For that sake, we fixed the free parameters of Titan and studied the main features of the stationary solution of this model in function of a few parameters, such as the relaxation factors γ_i, the friction parameter μ and the eccentricity e. When $\gamma_c \approx \gamma_s$, the behavior of the stationary rotations turned out to be identical to the homogeneous case. When $\gamma_c \approx \gamma_s \ll n$, the stationary solutions oscillate around the super-synchronous rotation. When γ_c and γ_s increase, the

oscillation tends to zero. Finally, if $\gamma_c \approx \gamma_s \gg n$, the stationary solution is damped to synchronous rotation. We have also calculated the possible atractors when the eccentricity and the friction parameter μ are varied. We recovered the resonances trapping in commensurabilities $\Omega_c \approx \Omega_s \approx \frac{2+k}{2}n$ (where $k = 1, 2, 3, \cdots \in \mathbb{N}$) as shown in Ferraz-Mello (2015a) and Correia et al. (2014) for the homogeneous case, and we found that if friction remains low, the non-zero diferential rotation commensurabilities $\Omega_c \sim \frac{2+i}{2}n$ and $\Omega_s \sim \frac{2+j}{2}n$, with $i, j = 1, 2, 3, \cdots \in \mathbb{N}$ and $i \neq j$, are possible. When the friction increases, the resonances with higher differential rotation are destroyed. If μ continues increasing, only survive the resonances in which core and shell have the same rotation.

The two-layer model was applied to Titan, but adding to it the torques due to the exchange of angular momentum between the surface and the atmosphere, as modeled by Tokano and Neubauer (2005) and by Richard et al. (2014), and the results were compared to the determinations of Titan's rotational velocity as determined from Cassini observations by Stiles et al. (2010) and Meriggiola et al. (2016). These comparisons allowed us to constrain the relaxation factor of the shell to $\gamma_s \lesssim 10^{-9}$ s^{-1}. The integrations show that for $\gamma_s \lesssim 10^{-7}$ s^{-1} the shell may oscillate around the synchronous rotation, with a period of oscillation equal to the orbital period, and the amplitude of this oscillation depends on the relaxation factors γ_c and γ_s and the ocean's thickness and viscosity. The tidal drift tends to zero and the rotation is dominated by the main periodic term.

The main result was that the rotational constraint does not allow us to confirm or reject the existence of a subsurface ocean on Titan. Only the maximum shell's relaxation factor γ_s can be determined, or equivalently, the minimum shell's viscosity η_s. When a subsurface ocean is considered, the maximum shell's relaxation factor is such that $\gamma_s \lesssim 10^{-9}$ s^{-1}, depending on the ocean's thickness and viscosity values considered. Equivalently, this maximum value of γ_s, corresponds with a minimum shell's viscosity $\eta_s \gtrsim 10^{18}$ Pa s, some orders of magnitude higher than the modeled by Mitri et al. (2014). When the non-ocean case is considered, the maximum shell's relaxation factor is such that $\gamma_s \lesssim 10^{-10}$ s^{-1} and the corresponding minimum shell's viscosity is $\eta_s \gtrsim 10^{19}$ Pa s. For these values of γ_s, the amplitude of the oscillation of the excess of rotation reproduces the dispersion of the Ω_s value of ± 0.02 deg/yr around the synchronous value, observed as reported by Meriggiola (2012) and Merigiolla et al. (2016). It is important to note that in all the cases studied,

the influence of the atmosphere can be neglected, since it does not affect the results in the ranges of γ_c and γ_s where the excess of rotation calculated is compatible with the excess of rotation observed.

Finally, we extended the Darwin theory to a differentiated non-homogeneous body formed by N homogeneous layers with differential rotation, and compared the resulting equations that describe this theory with the equations given by the creep tide theory. The main result of this comparisons, was that the creep tide theory can be interpreted as one particular case of the generalized Darwin's theory, where the lags and the dynamical tidal Love number depends on the frequencies and the viscosities. While the generalized Darwinian is an analytical free-parameters theory, the creep tide theory is equivalent to fix these free parameters with one specific rheophysical law (the rheology of one viscous fluid, through the Navier-Stokes's equation).

Bibliography

Bizyaev, I.A., Borisov, A.V. and Mamaev, I.S.: "Figures of equilibrium of an inhomogeneous self-gravitating fluid. "Nelineinaya Dinamika. **10**, 73â100 (2014). (In Russian)

Borisov, A.V., Mamaev, I.S. and Kilin, A.A.: "The Hamiltonian dynamics of self-gravitating liquid and gas ellipsoids."Regul. Chaotic Dyn. **14**, 179-217 (2009).

Boué, G., Correia, A. C. M., B Laskar, J.: "Complete spin and orbital evolution of close-in bodies using a Maxwell viscoelastic rheology."Celest. Mech. Dyn. Astron. **126**, 31 (2016).

Buffett, B.A.: "Gravitational oscillations of the length of day. "Geoph. Res. Lett. **23**, 2279-2282 (1996).

Bullen, K.E.: "The Earth's density", (Chapman and Hall, London) (1975).

Chandrasekhar, S.: "Ellipsoidal Figures of Equilibrium", (Yale Univ. Press, New Haven) (1969).

Callegari, N., Batista Ribeiro, F.: "The spin-orbit resonant problem including core-mantle gravitational coupling."Comp. Appl. Math. **34**, 423-435 (2015).

Castillo-Rogez, J.C., Lunine, J.I.: "Evolution of Titan's rocky core constrained by Cassini observations."Geophys. Res. Lett. **37**, L20205 (2010).

Cayley, A.: "Tables of developments of functions in the theory of elliptic motion."Mem. Roy. Astron. Soc. **29**, 191-306 (1861).

Clairaut, A.C.: "Théorie de la Figure de la Terre, Tirée des Principes de l'Hydrostratique", (Paris Courcier, Paris) (1743).

Collins, G.W.: "The fundamentals of stellar astrophysics ", (W.H. Freeman and Co., New York) (1989).

Correia, A. and Rodríguez, A.: "On the equilibrium figure of close-in planets and satellites."Astrophys. J. **767**, 128-132 (2013).

Correia, A. C. M., Boué, G., Laskar, J., Rodríguez, A.: "Deformation and tidal evolution of close-in planets and satellites using a Maxwell viscoelastic rheology."Astron. Astrophys. **571**, A50 (2014).

Darwin, G.H.:"On the secular change in the elements of the orbit of a satellite revolving about a tidally distorted planet."Philos. Trans. **171**, 713-891 (1880). (repr. Scientific Papers, Cambridge, Vol. II, 1908).

Efroimsky, M., Lainey, V.: "Physics of bodily tides in terrestrial planets and the appropriate scales of dynamical evolution."J. Geophys. Res. (Planets) **112**(E11), E12003 (2007).

Efroimsky, M., Williams, J.G.: "Tidal torques. I. A critical review of some techniques."Celest. Mech. Dyn. Astron. **104**, 257-289 (2009).

Esteban, E.P. and Vazquez, S.: "Rotating stratified heterogeneous oblate spheroid in newtonian physics."Celest. Mech. Dyn. Astron. **81**, 299-312 (2001).

Ferraz-Mello, S., Rodríguez, A. and Hussmann, H.: "Tidal frition in close-in satellites and exoplanets. The Darwin theory re-visited. "Celest. Mech. Dyn. Astron. **101**, 171-201 (2008). Errata: **104**, 319-320 (2009).

Ferraz-Mello, S.: "Tidal synchronization of close-in satellites and exoplanets. A rheophysical approach."Celest. Mech. Dyn. Astron. **116**, 109-140 (2013).

Ferraz-Mello, S.: "Tidal synchronization of close-in satellites and exoplanets. II. Spin dynamics and extension to Mercury and exoplanets host stars."Celest. Mech. Dyn. Astron. **122**, 359-389 (2015a).

Ferraz-Mello, S.: "The small and large lags of the elastic and anelastic tides. The virtual identity of two rheophysical theories."Astron. Astrophys. **579**, A97 (2015b).

Folonier, H., Ferraz-Mello, S., Kholshevnikov, K.: "The flattenings of the layers of rotating planets and satellites deformed by a tidal potential." Celest. Mech. Dyn. Astron. **122**, 183-198 (2015).

Fortes, A.D.: "Titan's internal structure and the evolutionary consequences." Planetary and Space Science **60**, 10â17 (2012).

Frouard, J., Quillen, A.C., Efroimsky, M., Giannella, D.: "Numerical simulation of tidal evolution of a viscoelastic body modelled with a mass-spring network." Mon. Not. R. Astron. Soc. **458**, 2890-2901 (2016).

Gavrilov, S.V., Zharkov, V.N. and Leontev, V.V.: "Influence of tides on the gravitational field of Jupiter." Soviet Astronomy, **19**, 618-621 (1976).

Goldreich, P.: "Final spin states of planets and satellites." Astron. J. **71**, 1-7 (1966).

Goldreich, P.M., Mitchell, J.L.: "Elastic ice shells of synchronous Moons: Implications for cracks on Europa and non-synchronous rotation of Titan." Icarus **209**, 631-638 (2010).

Henning, W.G., OâConnell, R.J., Sasselov, D.D.: "Tidally heated terrestrial exoplanets: viscoelastic response models." Astrophys. J. **707**, 1000-1015 (2009). arXiv:0912.1907

Hubbard, W.B.: "Gravitational field of a rotating planet with a polytropic index of unity." Sov. Astron. **18**, 621-624 (1975).

Hubbard, W.B.: "Concentric Maclaurin spheroid models of rotating liquid planets." Astrophys. J. **768**, 43 (2013).

Iess, L., Jacobson, R.A., Ducci, M., Stevenson, D.J., Lunine, J.I., et al.: "The tides of Titan." Science **337**, 457-459 (2012).

Jacobson, R.A., Antreasian, P.G., Bordi, J.J., Criddle, K.E., Ionasescu, R., et al.: "The gravity field of the Saturnian system from satellite observations and spacecraft tracking data." Astrophys. J. **132**, 2520-2526 (2006).

Jardetzky, W.S.: "Theories of Figures of Celestial Bodies", (Interscience Publ. New York; repr. Dover, Mineola, NY, 2005) (1958).

Jeans, J.: "Astronomy and Cosmogony" (Cambridge Univ. Press, Cambridge; repr. Dover, New York, 1961) (1929).

Jeffreys, H.S.: "The figures of rotating planets." Mon. Not. R. astr. Soc. **113**, 97 (1953).

Karatekin, Ö., Van Hoolst, T., Tokano, T.: "Effect of internal gravitational coupling on Titan's non-synchronous rotation." Geophys. Res. Lett. **38**, L16202 (2008).

Kaula, W.M.: "Tidal dissipation by solid friction and the resulting orbital evolution." Rev. Geophys. **3**, 661-685 (1964).

Khurana, K.K., Kivelson, M.G., Stevenson, D.J., Schubert, G., Russell, C.T., Walker, R.J., Polanskey, C.: "Induced magnetic fields as evidence for subsurface oceans in Europa and Callisto." Nature **395**, 777â780 (1998).

Kong, D., Zhang, K. and Schubert, G.: "Shapes of two-layer models of rotating planets." J. Geophys. Res. **115**, 12003 (2010).

Lebonnois, S., Burgalat, J., Rannou, P., Charnay, B.: "Titan global climate model: a new 3-dimensional version of the IPSL Titan GCM." Icarus **218**, 707-722 (2012).

Leconte, J., Lai, D. and Chabrier, G.: "Distorted, non-spherical transiting planets: impact on the transit depth and on the radius determination." Astronomy & Astrophysics **528**, A41. Erratum: Astronomy & Astrophysics, **536**, C1 (2011).

Lorenz, R.D., Stiles, B.W., Kirk, R.L., Allison, M.D., Persi del Marmo, P., Iess, L., Lunine, J.I., Ostro, S.J., Hensley, S.: "Titan's rotation reveals an internal ocean and changing sonal winds." Science **319**, 1649-1651 (2008).

Lyapounov, A.: "Sur certaines séries de figures d'equilibre d'un liquide héterogène en rotation.*Acad. Sci. URSS*, Part I, (1925) and Part II (1927).

MacDonald, G.J.F.: "Tidal friction." Rev. Geophys. Space Phys. **2**, 467-541 (1964).

McKinnon, W.B., Bland, M.T.: "Core evolution in icy satellites and Kuiper belt objects." Lunar and Planetary Institute Science Conference Abstracts, 2768 (2011).

Meriggiola, R.: "The Determination of the Rotational State of Celestial Bodies."Ph.D.Thesis, La Sapienza, Roma (2012).

Meriggiola, R., Iess, L., Stiles, B.W., Lunine, J., Mitri, G.: "The rotational dynamics of Titan from Cassini RADAR images."Icarus **275**, 183-192 (2016).

Mignard, F.: "The evolution of the lunar orbit revisited - I."Moon and Planets **20**, 301-315 (1979).

Mitri, G., Meriggiola, R., Hayes, A., Lefevre, A., Tobie, G., Genova, A., Lunine, J.I., Zebker, H.: "Shape, topography, gravity anomalies and tidal deformation of Titan."Icarus **236**, 169-177 (2014).

Montalvo, D., Martínez, F.J. and Cisneros, J.: "On equilibrium figures of ideal fluids in the form of confocal spheroids rotating with common and different angular velocities."Rev. Mexicana Astron. Astrof. **5**, 293-300 (1983).

Munk, W.H., MacDonald, G.J.F.: "The Rotation of the Earth: A Geophysical Discussion.", Cambridge Univ. Press, Cambridge (1960).

Nimmo, F., Spencer, J.R., Pappalardo, R.T., Mullen, M.E.: "Shear heating as the origin of the plumes and heat flux on Enceladus.", Nature **447**, 289-291 (2007).

Papanastasious, T., Georgiou, G., Alexandrou, A.: "Viscous fluid flow "CRC Press LLC, Boca Raton (2000).

Poincaré, H.: "Figures d'equilibre d'una masse fluide "(Leçons professées à la Sorbenne en 1900) *Paris, Gauthier-Villars* (1902).

Porco, C.C., Helfenstein, P., Thomas, P.C., Ingersoll, A.P., Wisdom, J., et al.: "Cassini observes the active south pole of Enceladus."Science **311**, 1393-1401 (2006).

Richard, A., Rambaux, N., Charnay, B.: "Librational response of a deformed 3-layer Titan perturbed by non-Keplerian orbit and atmospheric couplings."Planetary and Space Science **93-94**, 22â34 (2014).

Seidelmann, P.K., Archinal, B.A., A'Hearn, M.F., Conrad, A., Consolmagno, G. J., Hestroffer, D., Hilton, J.L., Krasinsky, G.A., Neumann, G., Oberst, J., Stooke, P., Tedesco,

E.F., Tholen, D.J., Thomas, P.C., Williams, I.P.: "Report of the IAU/IAG Working Group on cartographic coordinates and rotational elements: 2006." Celest. Mech. Dyn. Astron. **98**, 155-180 (2007).

Sohl, F., Solomonidou, A., Wagner, F.W., Coustenis, A.H., Hussmann, A., Schulze-Makuch, D.: "Structural and tidal models of Titan and inferences on cryovolcanism." J. Geophys. Res. Planets, **119**, 1013-1036 (2014).

Stiles, B.W., Kirk, R.L., Lorenz, R.D., Hensley, S., Lee, E., et al.: "Determining Titan's Spin State from Cassini RADAR Images." Astron. J. **135**, 1669-1680 (2008) and Erratum: Astron. J., **139**, 311 (2010).

Tisserand, F.: "Traité de Mécanique Céleste", Tome II, (Gauthier-Villars, Paris) (1891).

Tricarico, P.: "Multi-layer hidrostatic equilibrium of planets and synchronous moons: Theory and application to Ceres and Solar System moons." Astrophys. J. **782**, 12 (2014).

Tobie, G., Grasset, O., Lunine, J.I., Mocquet, A., Sotin, C.: "Titan's internal structure inferred from a coupled thermal-orbital model." Icarus **175**, 496-502 (2005).

Tokano, T., Neubauer, F.M.: "Wind-induced seasonal angular momentum exchange at Titan's surface and its influence on Titan's length-of-day." Geophys. Res. Lett. **32**, L24203 (2005).

Van Hoolst, T., Rambaux, N., Karatekin, Ö., Dehant, V., Rivoldini, A.: "The librations, shape, and icy shell of Europa. " Icarus **195**, 386-399 (2008).

Van Hoolst, T., Baland, R.M., Trinh, A.: "On the librations and tides of large icy satellites." Icarus **226**, 299-315 (2013).

Vienne, A., Duriez, L.: "TASS 1.6: Ephemerides of the major Saturnian satellites." Astron. Astrophys. **297**, 588-605 (1995).

Wahl, S.M., Hubbard, W.B., Militzer, B.: "The Concentric Maclaurin Spheroid method with tides and a rotational enhancement of Saturn's tidal response." Preprint: http://arxiv.org/abs/1602.07350 (2016).

Wahr, J.M., Zuber, M.T., Smith, D.E., Lunine, J.I.: "Tides on Europa, and the thickness of Europa's icy shell." J. Geophys. Res. **111**, E12005 (2006).

Wavre, R.: "Figures planétaries et Géodesie ", (Gauthier-Villars et cie, Paris) (1932).

Zharkov, V.N. and Trubitsyn, V.P.: "Figures planétaries et Géodesie ", (Astronomy and Astrophysics Series, Tucson: Pachart 1978) (1978).

Appendix

Appendix A

Shape and gravitational potential of one ellipsoid and one ellipsoidal layer

A.1 Homogeneous ellipsoid

Let us consider a homogeneous triaxial ellipsoid with density d, semi axes $a > b > c$, equatorial mean radius $R = \sqrt{ab}$ and equatorial and polar flattenings defined as

$$\epsilon_\rho = \frac{a-b}{R}; \qquad \epsilon_z = \frac{b-c}{R}. \tag{A.1}$$

Then, the semi axes of this ellipsoid can be written as

$$\begin{aligned} a &= R\left[\sqrt{1+\left(\frac{\epsilon_\rho}{2}\right)^2}+\frac{\epsilon_\rho}{2}\right] \approx R\left[1+\frac{\epsilon_\rho}{2}\right] \\ b &= R\left[\sqrt{1+\left(\frac{\epsilon_\rho}{2}\right)^2}-\frac{\epsilon_\rho}{2}\right] \approx R\left[1-\frac{\epsilon_\rho}{2}\right] \\ c &= R\left[\sqrt{1+\left(\frac{\epsilon_\rho}{2}\right)^2}-\frac{\epsilon_\rho}{2}-\epsilon_z\right] \approx R\left[1-\frac{\epsilon_\rho}{2}-\epsilon_z\right], \end{aligned} \tag{A.2}$$

Let us also consider the equation of surface of this homogeneous triaxial ellipsoid, in a reference system where the semi axes a, b and c are aligned to the coordinates axes x, y and z, respectively:

$$\frac{x^2}{a^2}+\frac{y^2}{b^2}+\frac{z^2}{c^2} = 1. \tag{A.3}$$

If we use the semi axes (A.2), the spherical coordinates

$$x = \rho\sin\theta\cos\varphi; \qquad y = \rho\sin\theta\sin\varphi; \qquad z = \rho\cos\theta, \tag{A.4}$$

and expand to first order in the flattenings, we obtain

$$\rho = R\left(1+\frac{\epsilon_\rho}{2}\sin^2\theta\cos 2\varphi-\left[\frac{\epsilon_\rho}{2}+\epsilon_z\right]\cos^2\theta\right). \tag{A.5}$$

The mass of this ellipsoids is

$$m = \frac{4\pi}{3} d\ abc \approx \frac{4\pi}{3} d\ R^3 \left[1 - \frac{\epsilon_\rho}{2} - \epsilon_z\right]. \tag{A.6}$$

The principal moments of inertia are

$$\begin{aligned} A &= \frac{1}{5}m(b^2 + c^2) \approx \frac{2}{5}mR^2\left[1 - \epsilon_\rho - \epsilon_z\right] \\ B &= \frac{1}{5}m(a^2 + c^2) \approx \frac{2}{5}mR^2\left[1 - \epsilon_z\right] \\ C &= \frac{1}{5}m(a^2 + b^2) \approx \frac{2}{5}mR^2, \end{aligned} \tag{A.7}$$

and its differences are

$$\begin{aligned} C - A &\approx \frac{2}{5}mR^2(\epsilon_\rho + \epsilon_z) \approx C(\epsilon_\rho + \epsilon_z) \\ C - B &\approx \frac{2}{5}mR^2\epsilon_z \approx C\epsilon_z \\ B - A &\approx \frac{2}{5}mR^2\epsilon_\rho \approx C\epsilon_\rho. \end{aligned} \tag{A.8}$$

If we consider that the flattenings are

$$\epsilon_\rho = \epsilon_J; \qquad \epsilon_z = \epsilon_M, \tag{A.9}$$

then, the difference of the principal moments of inertia can be approximated to first order in the flattenings as

$$\begin{aligned} C - A &\approx C(\epsilon_J + \epsilon_M) \\ C - B &\approx C\epsilon_M \\ B - A &\approx C\epsilon_J. \end{aligned} \tag{A.10}$$

The gravitational potential U generated by this ellipsoid, at an external point $\mathbf{r}^* = x^*\hat{\mathbf{x}} + y^*\hat{\mathbf{y}} + z^*\hat{\mathbf{z}}$, may be presented by Laplace series. Neglecting harmonics of degree higher than 2 we have

$$U(\mathbf{r}^*) = -\frac{Gm}{r^*} - \frac{GI}{r^{*3}} + \frac{3G}{2r^{*5}}\Big[I_{xx}x^{*2} + I_{yy}y^{*2} + I_{zz}z^{*2} + 2I_{xy}x^*y^* + 2I_{yz}y^*z^* + 2I_{zz}z^*x^*\Big], \tag{A.11}$$

where $r^* = |\mathbf{r}^*|$, I is the moment of inertia of this ellipsoid, relative to the center of mass and I_{nm} are the components of its inertia tensor (see Beutler, 2005; Murray and

Dermott, 1999). If the reference axes are oriented following the principal axes of inertia, then $I_{nm} = 0$ if $n \neq m$. Because $A = I_{xx}$, $B = I_{yy}$ and $C = I_{zz}$, and hence $2I = A+B+C$, the gravitational potential can be written as

$$U(\mathbf{r}^*) = -\frac{Gm}{r^*} - \frac{G(B-A)}{2r^{*5}}(3x^{*2} - r^{*2}) + \frac{G(C-B)}{2r^5}(3z^{*2} - r^{*2}), \quad (A.12)$$

or, using the Eq. (A.8), we obtain

$$U(\mathbf{r}^*) = -\frac{Gm}{r^*} - \frac{GC}{2r^{*3}}\epsilon_\rho(3\cos^2\varphi^*\sin^2\theta^* - 1) + \frac{GC}{2r^{*3}}\epsilon_z(3\cos^2\theta^* - 1). \quad (A.13)$$

Another useful way to express this gravitational potential is

$$U(\mathbf{r}^*) = -\frac{Gm}{r^*} - \frac{3GC}{4r^{*3}}\epsilon_\rho\sin^2\theta^*\cos 2\varphi^* + \frac{GC}{2r^{*3}}\left(\frac{\epsilon_\rho}{2} + \epsilon_z\right)(3\cos^2\theta - 1). \quad (A.14)$$

It is worth emphasizing that both the surface equation (A.5) as the gravitational potential (A.13) are valid in a reference system where the semi axes (or, equivalently, the principal axes of inertia) are aligned to the coordinates axes x, y and z. In a reference system rotated, around to the axis z, at an angle ϕ_r, these equations remains valid if we use the longitude transformations $\varphi \longrightarrow \varphi' - \phi_r$ and $\varphi^* \longrightarrow \varphi'^* - \phi_r$, and the co-latitude transformations $\theta \longrightarrow \theta'$ and $\theta^* \longrightarrow \theta'^*$. That is

$$\rho = R\left(1 + \frac{\epsilon_\rho}{2}\sin^2\theta'\cos(2\varphi' - 2\phi_r) - \left[\frac{\epsilon_\rho}{2} + \epsilon_z\right]\cos^2\theta'\right), \quad (A.15)$$

and

$$U(\mathbf{r}^*) = -\frac{Gm}{r^*} - \frac{GC}{2r^{*3}}\epsilon_\rho(3\cos^2(\varphi'^* - \phi_r)\sin^2\theta'^* - 1) + \frac{GC}{2r^{*3}}\epsilon_z(3\cos^2\theta'^* - 1), \quad (A.16)$$

or

$$U(\mathbf{r}^*) = -\frac{Gm}{r^*} - \frac{3GC}{4r^{*3}}\epsilon_\rho\sin^2\theta^*\cos(2\varphi^* - 2\phi_r) + \frac{GC}{2r^{*3}}\left(\frac{\epsilon_\rho}{2} + \epsilon_z\right)(3\cos^2\theta - 1). \quad (A.17)$$

A.2 Ellipsoidal layer

Let us consider a homogeneous triaxial ellipsoidal shell with density d_i, outer semi axes $a_i > b_i > c_i$, outer equatorial mean radius $R_i = \sqrt{a_i b_i}$ and outer equatorial and polar flattenings

$$\epsilon_\rho^{(i)} = \frac{a_i - b_i}{R_i}; \qquad \epsilon_z^{(i)} = \frac{b_i - c_i}{R_i}. \quad (A.18)$$

At the inner ellipsoidal boundary, the semi axes are $a_{i-1} > b_{i-1} > c_{i-1}$ (not necessarily aligned with the axes of the outer surface), the inner equatorial mean radius is $R_{i-1} = \sqrt{a_{i-1}b_{i-1}}$ and inner equatorial and polar flattenings are

$$\epsilon_\rho^{(i-1)} = \frac{a_{i-1} - b_{i-1}}{R_{i-1}}; \qquad \epsilon_z^{(i-1)} = \frac{b_{i-1} - c_{i-1}}{R_{i-1}}. \tag{A.19}$$

The semi axes of the outer boundary are

$$\begin{aligned}
a_i &= R_i \left[\sqrt{1 + \left(\frac{\epsilon_\rho^{(i)}}{2} \right)^2} + \frac{\epsilon_\rho^{(i)}}{2} \right] \approx R_i \left[1 + \frac{\epsilon_\rho^{(i)}}{2} \right] \\
b_i &= R_i \left[\sqrt{1 + \left(\frac{\epsilon_\rho^{(i)}}{2} \right)^2} - \frac{\epsilon_\rho^{(i)}}{2} \right] \approx R_i \left[1 - \frac{\epsilon_\rho^{(i)}}{2} \right] \\
c_i &= R_i \left[\sqrt{1 + \left(\frac{\epsilon_\rho^{(i)}}{2} \right)^2} - \frac{\epsilon_\rho^{(i)}}{2} - \epsilon_z^{(i)} \right] \approx R_i \left[1 - \frac{\epsilon_\rho^{(i)}}{2} - \epsilon_z^{(i)} \right].
\end{aligned} \tag{A.20}$$

and the semi axes of the inner boundary are

$$\begin{aligned}
a_{i-1} &= R_{i-1} \left[\sqrt{1 + \left(\frac{\epsilon_\rho^{(i-1)}}{2} \right)^2} + \frac{\epsilon_\rho^{(i-1)}}{2} \right] \approx R_{i-1} \left[1 + \frac{\epsilon_\rho^{(i-1)}}{2} \right] \\
b_{i-1} &= R_{i-1} \left[\sqrt{1 + \left(\frac{\epsilon_\rho^{(i-1)}}{2} \right)^2} - \frac{\epsilon_\rho^{(i-1)}}{2} \right] \approx R_{i-1} \left[1 - \frac{\epsilon_\rho^{(i-1)}}{2} \right] \\
c_{i-1} &= R_{i-1} \left[\sqrt{1 + \left(\frac{\epsilon_\rho^{(i-1)}}{2} \right)^2} - \frac{\epsilon_\rho^{(i-1)}}{2} - \epsilon_z^{(i-1)} \right] \approx R_{i-1} \left[1 - \frac{\epsilon_\rho^{(i-1)}}{2} - \epsilon_z^{(i-1)} \right].
\end{aligned} \tag{A.21}$$

Because the semi-major axes a_i and a_{i-1} are not necessarily aligned, we consider a reference system such that the outer semi-major axis a_i and the inner semi-major axis a_{i-1} are not aligned with the coordinate axis x. In this reference system, using he Eq. (A.15), the surface equation of the outer boundary of the layer is

$$\rho_i = R_i \left(1 + \frac{\epsilon_\rho^{(i)}}{2} \sin^2\theta \cos\left(2\varphi - 2\phi_i\right) - \left[\frac{\epsilon_\rho^{(i)}}{2} + \epsilon_z^{(i)} \right] \cos^2\theta \right), \tag{A.22}$$

and the surface equation of the inner boundary of the layer is

$$\rho_{i-1} = R_{i-1} \left(1 + \frac{\epsilon_\rho^{(i-1)}}{2} \sin^2\theta \cos\left(2\varphi - 2\phi_{i-1}\right) - \left[\frac{\epsilon_\rho^{(i-1)}}{2} + \epsilon_z^{(i-1)} \right] \cos^2\theta \right), \tag{A.23}$$

where ϕ_i and ϕ_{i-1} are the angles formed between the semi-major axes a_i and a_{i-1}, respectively, and the coordinate axis x.

The mass m_i of this layer, can be written as the subtraction of the masses of the two homogeneous ellipsoids of same density d_i: the homogeneous ellipsoid of mass m_i' and same surface as the outer boundary of the layer, less the homogeneous ellipsoid of mass m_i'' and same surface as the inner boundary of the layer (Fig. A.1). The total mass of the layer then is

$$m_i = m_i' - m_i'' \approx \frac{4\pi}{3} d_i \left(R_i^3 \left[1 - \frac{\epsilon_\rho^{(i)}}{2} - \epsilon_z^{(i)} \right] - R_{i-1}^3 \left[1 - \frac{\epsilon_\rho^{(i-1)}}{2} - \epsilon_z^{(i-1)} \right] \right). \qquad \text{(A.24)}$$

Note that this result is independent of the orientation of the ellipsoidal boundaries semi axes. The masses m_i' and m_i'' are

$$\begin{aligned} m_i' &= d_i \frac{4\pi}{3} a_i b_i c_i \approx \frac{m_i R_i^3 \left[1 - \frac{\epsilon_\rho^{(i)}}{2} - \epsilon_z^{(i)} \right]}{R_i^3 \left[1 - \frac{\epsilon_\rho^{(i)}}{2} - \epsilon_z^{(i)} \right] - R_{i-1}^3 \left[1 - \frac{\epsilon_\rho^{(i-1)}}{2} - \epsilon_z^{(i-1)} \right]} \\ m_i'' &= d_i \frac{4\pi}{3} a_{i-1} b_{i-1} c_{i-1} \approx \frac{m_i R_{i-1}^3 \left[1 - \frac{\epsilon_\rho^{(i-1)}}{2} - \epsilon_z^{(i-1)} \right]}{R_i^3 \left[1 - \frac{\epsilon_\rho^{(i)}}{2} - \epsilon_z^{(i)} \right] - R_{i-1}^3 \left[1 - \frac{\epsilon_\rho^{(i-1)}}{2} - \epsilon_z^{(i-1)} \right]}. \end{aligned} \qquad \text{(A.25)}$$

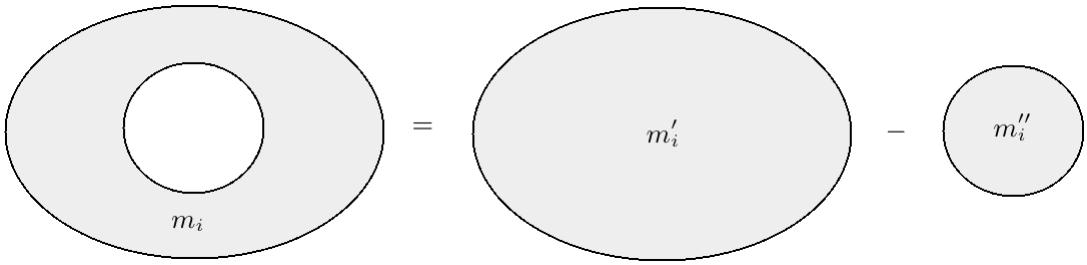

Figure A.1: Scheme for the calculation of the mass, principal moments of inertia and gravitational potential of a homogeneous ellipsoidal layer as the subtraction of two homogeneous ellipsoids of same density d_i.

To calculate the principal moments of inertia A_i, B_i, C_i of a homogeneous triaxial ellipsoidal layer when the inner and the outer boundaries are not aligned is particularly complicated because the orientation of the principal axes of inertia do not coincide with the axes of symmetry of both boundaries. In the sequence we focus in the particular case in which the inner and the outer boundaries are aligned.

In this case, we can use the same scheme used to calculate the mass of the layer. The principal moments of inertia of the layer, can be written as the subtraction of the principal moments of inertia of two homogeneous ellipsoids of same density d_i: the principal moments of inertia of one homogeneous ellipsoid of mass m_i' and the same surface as the outer boundary of the layer, less the principal moments of inertia of the homogeneous ellipsoid of mass m_i'' and the same surface as the inner boundary of the layer. Using the semi axes (A.20) and (A.21), and the masses (A.25), the principal moments of inertia can be approximated to first order in the flattenings as

$$\begin{aligned}
A_i &= \frac{1}{5}m_i'\left(b_i^2+c_i^2\right)-\frac{1}{5}m_i''\left(b_{i-1}^2+c_{i-1}^2\right)\\
&\approx \frac{2}{5}m_i\frac{R_i^5-R_{i-1}^5}{R_i^3-R_{i-1}^3}\left[1+\frac{\Delta(R_i^3\epsilon_\rho^{(i)})}{R_i^3-R_{i-1}^3}+\frac{\Delta(R_i^3\epsilon_z^{(i)})}{R_i^3-R_{i-1}^3}-\frac{3}{2}\frac{\Delta(R_i^5\epsilon_\rho^{(i)})}{R_i^5-R_{i-1}^5}-2\frac{\Delta(R_i^5\epsilon_z^{(i)})}{R_i^5-R_{i-1}^5}\right]\\
B_i &= \frac{1}{5}m_i'\left(a_i^2+c_i^2\right)-\frac{1}{5}m_i''\left(a_{i-1}^2+c_{i-1}^2\right)\\
&\approx \frac{2}{5}m_i\frac{R_i^5-R_{i-1}^5}{R_i^3-R_{i-1}^3}\left[1+\frac{\Delta(R_i^3\epsilon_\rho^{(i)})}{R_i^3-R_{i-1}^3}+\frac{\Delta(R_i^3\epsilon_z^{(i)})}{R_i^3-R_{i-1}^3}-\frac{1}{2}\frac{\Delta(R_i^5\epsilon_\rho^{(i)})}{R_i^5-R_{i-1}^5}-2\frac{\Delta(R_i^5\epsilon_z^{(i)})}{R_i^5-R_{i-1}^5}\right]\\
C_i &= \frac{1}{5}m_i'\left(a_i^2+b_i^2\right)-\frac{1}{5}m_i''\left(a_{i-1}^2+b_{i-1}^2\right)\\
&\approx \frac{2}{5}m_i\frac{R_i^5-R_{i-1}^5}{R_i^3-R_{i-1}^3}\left[1+\frac{\Delta(R_i^3\epsilon_\rho^{(i)})}{R_i^3-R_{i-1}^3}+\frac{\Delta(R_i^3\epsilon_z^{(i)})}{R_i^3-R_{i-1}^3}-\frac{1}{2}\frac{\Delta(R_i^5\epsilon_\rho^{(i)})}{R_i^5-R_{i-1}^5}-\frac{\Delta(R_i^5\epsilon_z^{(i)})}{R_i^5-R_{i-1}^5}\right],
\end{aligned} \tag{A.26}$$

and its differences are

$$\begin{aligned}
C_i-A_i &\approx C_i\left[\frac{\Delta(R_i^5\epsilon_\rho^{(i)})}{R_i^5-R_{i-1}^5}+\frac{\Delta(R_i^5\epsilon_z^{(i)})}{R_i^5-R_{i-1}^5}\right]\\
C_i-B_i &\approx C_i\frac{\Delta(R_i^5\epsilon_z^{(i)})}{R_i^5-R_{i-1}^5}\\
B_i-A_i &\approx C_i\frac{\Delta(R_i^5\epsilon_\rho^{(i)})}{R_i^5-R_{i-1}^5},
\end{aligned} \tag{A.27}$$

where $\Delta(f_i)=f_i-f_{i-1}$, denotes the increment of one function f_i, between the inner and the outer boundaries of this layer.

Using the same scheme used to calculate the mass and the principal moments of inertia, the corresponding gravitational potential of this homogeneous triaxial layer at an external

point $\mathbf{r}^*$ is

$$\begin{aligned} U_i(\mathbf{r}^*) &= -\frac{Gm_i}{r^*} - \frac{G(B_i - A_i)}{2r^{*5}}(3x^{*2} - r^{*2}) + \frac{G(C_i - B_i)}{2r^{*5}}(3z^{*2} - r^{*2}) \\ &\approx -\frac{Gm_i}{r^*} - \frac{GC_i}{2r^{*3}}\frac{\Delta(R_i^5\epsilon_\rho^{(i)})}{R_i^5 - R_{i-1}^5}(3\cos^2\varphi^*\sin^2\theta^* - 1) + \frac{GC_i}{2r^{*3}}\frac{\Delta(R_i^5\epsilon_z^{(i)})}{R_i^5 - R_{i-1}^5}(3\cos^2\theta^* - 1), \end{aligned} \tag{A.28}$$

or

$$\begin{aligned} U_i(\mathbf{r}^*) &= -\frac{Gm_i}{r^*} - \frac{3GC_i}{4r^{*3}}\frac{\Delta(R_i^5\epsilon_\rho^{(i)})}{R_i^5 - R_{i-1}^5}\sin^2\theta^*\cos 2\varphi^* + \\ &\quad + \frac{GC_i}{2r^{*3}}\frac{\Delta\big(R_i^5(\frac{\epsilon_\rho^{(i)}}{2} + \epsilon_z^{(i)})\big)}{R_i^5 - R_{i-1}^5}(3\cos^2\theta^* - 1). \end{aligned} \tag{A.29}$$

If we consider the static equilibrium figure, the flattenings are

$$\epsilon_\rho^{(k)} = \mathcal{H}_k\epsilon_J; \qquad \epsilon_z^{(k)} = \mathcal{G}_k\bar{\epsilon}_M, \tag{A.30}$$

where $\mathcal{H}_k$ and $\mathcal{G}_k$ are the Clairaut numbers (see Eq. 2.12). Then, the difference of the principal moments of inertia can be approximated to first order in the flattenings as

$$\begin{aligned} C_i - A_i &\approx C_i(\mathcal{L}_i\epsilon_J + \mathcal{L}_i'\bar{\epsilon}_M) \\ C_i - B_i &\approx C_i\mathcal{L}_i'\bar{\epsilon}_M \\ B_i - A_i &\approx C_i\mathcal{L}_i\epsilon_J, \end{aligned} \tag{A.31}$$

where the parameters $\mathcal{L}_i$ and $\mathcal{L}_i'$ are

$$\mathcal{L}_i = \frac{\mathcal{H}_iR_i^5 - \mathcal{H}_{i-1}R_{i-1}^5}{R_i^5 - R_{i-1}^5}; \qquad \mathcal{L}_i' = \frac{\mathcal{G}_iR_i^5 - \mathcal{G}_{i-1}R_{i-1}^5}{R_i^5 - R_{i-1}^5}. \tag{A.32}$$

The coefficients $\mathcal{L}_i$ and $\mathcal{L}_i'$ play a role equivalent to the coefficients $\mathcal{H}_i$ and $\mathcal{G}_i$ for the quantities $C_i - A_i$, $C_i - B_i$ and $B_i - A_i$. In this case, the moments of inertia $B_i - A_i$ (resp. $C_i - B_i$) of the i-th layer can be written as the homogeneous moments multiplied by the coefficients $\mathcal{L}_i$ (resp. $\mathcal{L}_i'$), characteristics of this layer. The difference between $\mathcal{L}_i$ and $\mathcal{L}_i'$ comes from the fact that the body has a differential rotation. If we assume a rigid rotation, then $\mathcal{L}_i' = \mathcal{L}_i(\Omega/n)^2$.

The corresponding gravitational potential of this homogeneous triaxial layer at an ex-

ternal point $\mathbf{r}^*$ is

$$\begin{aligned} U_i(\mathbf{r}^*) &= -\frac{Gm_i}{r^*} - \frac{G(B_i - A_i)}{2r^{*5}}(3x^{*2} - r^{*2}) + \frac{G(C_i - B_i)}{2r^{*5}}(3z^{*2} - r^{*2}) \\ &\approx -\frac{Gm_i}{r^*} - \frac{GC_i\mathcal{L}_i}{2r^{*3}}\epsilon_J(3\cos^2\varphi^*\sin^2\theta^* - 1) + \frac{GC_i\mathcal{L}'_i}{2r^{*3}}\bar{\epsilon}_M(3\cos^2\theta^* - 1), \end{aligned} \tag{A.33}$$

or

$$U_i(\mathbf{r}^*) = -\frac{Gm_i}{r^*} - \frac{3GC_i\mathcal{L}_i}{4r^{*3}}\epsilon_J\sin^2\theta^*\cos 2\varphi^* + \frac{GC_i}{2r^{*3}}\left(\mathcal{L}_i\frac{\epsilon_J}{2} + \mathcal{L}'_i\bar{\epsilon}_M\right)(3\cos^2\theta^* - 1). \tag{A.34}$$

Although we do not calculate the principal moments of inertia when the inner and the outer boundaries are not aligned, it is possible to calculate easily the gravitational potential with the same scheme used to calculate the mass of the layer and the principal moments of inertia. The potential of the layer, can be written as the subtraction of the potential of two homogeneous ellipsoids of same density d_i: the potential of one homogeneous ellipsoid of mass m'_i and the same surface as the outer boundary of the layer, given by the Eq. (A.22), less the potential of the homogeneous ellipsoid of mass m''_i and the same surface as the inner boundary of the layer, given by the Eq. (A.23).

The corresponding gravitational potential is

$$\begin{aligned} U_i(\mathbf{r}^*) &= -\frac{Gm_i}{r^*} - \frac{GC_i}{2r^{*3}}\left[\frac{\Delta\left(R_i^5\epsilon_\rho^{(i)}(3\cos^2(\varphi^* - \phi_i)\sin^2\theta^* - 1)\right)}{R_i^5 - R_{i-1}^5} - \right. \\ &\quad \left. - \frac{\Delta\left(R_i^5\epsilon_z^{(i)}(3\cos^2\theta^* - 1)\right)}{R_i^5 - R_{i-1}^5}\right], \end{aligned} \tag{A.35}$$

or

$$\begin{aligned} U_i(\mathbf{r}^*) &= -\frac{Gm_i}{r^*} - \frac{3GC_i}{4r^{*3}}\frac{\Delta(R_i^5\epsilon_\rho^{(i)}\cos(2\varphi^* - 2\phi_i))}{R_i^5 - R_{i-1}^5}\sin^2\theta^* + \\ &\quad + \frac{GC_i}{2r^{*3}}\frac{\Delta\left(R_i^5(\frac{\epsilon_\rho^{(i)}}{2} + \epsilon_z^{(i)})\right)}{R_i^5 - R_{i-1}^5}(3\cos^2\theta^* - 1). \end{aligned} \tag{A.36}$$

Appendix B

The contribution of the gravitational potentials to the equilibrium equations

B.1 The equilibrium equations

In this Appendix, we detail the calculation of the contribution of each gravitational potential to the $2N$ equilibrium equations. For the sake of simplicity, due to the operators $\chi_i^{(1)}$ and $\chi_i^{(2)}$ are linear, the contribution of the gravitational potential of i-th homogeneous layer can be calculated as the subtraction of the contributions of the two homogeneous ellipsoids of same density d_i: the contribution of one homogeneous ellipsoid of mass m_i' and the same surface as the outer boundary of the layer, less the contribution of the homogeneous ellipsoid of mass m_i'' and the same surface as the inner boundary of the layer (see Fig. A.1). Then, the contribution of the i-th layer to the equilibrium equations can be written as

$$\begin{aligned} \chi_i^{(1)}(U_j) &= \chi_i^{(1)}(U_j') - \chi_i^{(1)}(U_j'') \\ \chi_i^{(2)}(U_j) &= \chi_i^{(2)}(U_j') - \chi_i^{(2)}(U_j''). \end{aligned} \tag{B.1}$$

B.2 The contribution of the outer layers

Let us consider the contribution by the j-th layer at one point $\mathbf{r}_i = x_i\hat{\mathbf{x}} + y_i\hat{\mathbf{y}} + z_i\hat{\mathbf{z}}$ on the surface of the i-th layer, assumed interior to it. The gravitational potential U_j' of one ellipsoid with density d_j and the same surface as the outer boundary of the j-th layer is

$$U_j'(\mathbf{r}_i) = U_{0j}' + A_{0x}' x_i^2 + A_{0y}' y_i^2 + A_{0z}' z_i^2, \tag{B.2}$$

where the coefficients U'_{0i}, A'_{0x}, A'_{0y} and A'_{0z} are

$$\begin{aligned}
U'_{0j} &= -\pi G d_j c_j^2 \int_0^\infty \frac{dt}{\sqrt{(1+\alpha_j t)(1+\beta_j t)(1+\gamma_j t)}} \\
A'_{0x} &= \pi G d_j \alpha_j \int_0^\infty \frac{dt}{(1+\alpha_j t)\sqrt{(1+\alpha_j t)(1+\beta_j t)(1+\gamma_j t)}} \\
A'_{0y} &= \pi G d_j \beta_j \int_0^\infty \frac{dt}{(1+\beta_j t)\sqrt{(1+\alpha_j t)(1+\beta_j t)(1+\gamma_j t)}} \\
A'_{0z} &= \pi G d_j \gamma_j \int_0^\infty \frac{dt}{(1+\gamma_j t)\sqrt{(1+\alpha_j t)(1+\beta_j t)(1+\gamma_j t)}},
\end{aligned} \tag{B.3}$$

and G is the gravitational constant (see Tisserand, 1891, Chap. 8 and 13; Jardetzky, 1958, Sec. 2.2). Then the derivatives of the potential are

$$\begin{aligned}
\frac{1}{x_i}\frac{\partial U'_j}{\partial x_i} &= 2\pi G d_j \alpha_j \int_0^\infty \frac{dt}{(1+\alpha_j t)^{3/2}(1+\beta_j t)^{1/2}(1+t)^{1/2}} \\
\frac{1}{y_i}\frac{\partial U'_j}{\partial y_i} &= 2\pi G d_j \beta_j \int_0^\infty \frac{dt}{(1+\alpha_j t)^{1/2}(1+\beta_j t)^{3/2}(1+t)^{1/2}} \\
\frac{1}{z_i}\frac{\partial U'_j}{\partial z_i} &= 2\pi G d_j \int_0^\infty \frac{dt}{(1+\alpha_j t)^{1/2}(1+\beta_j t)^{1/2}(1+t)^{3/2}},
\end{aligned} \tag{B.4}$$

and its contribution to the first equation of equilibrium is

$$\chi_i^{(1)}(U'_j) = 2\pi G d_j \int_0^\infty \frac{\alpha_j(1-\alpha_i)t + (\alpha_j - \alpha_i)}{(1+\alpha_j t)^{3/2}(1+\beta_j t)^{1/2}(1+t)^{3/2}} dt. \tag{B.5}$$

Neglecting terms of order 2 in the flattenings we can write

$$\chi_i^{(1)}(U'_j) = G\frac{4\pi}{3} d_j \left[2\left(\epsilon_\rho^{(i)} + \epsilon_z^{(i)}\right) - \frac{6\left(\epsilon_\rho^{(j)} + \epsilon_z^{(j)}\right)}{5} \right]. \tag{B.6}$$

Similarly, if we consider the potential U''_j of the one ellipsoid with density d_j and the same surface as the inner boundary of the j-th layer, the contribution of this potential to the first equilibrium equation, neglecting terms of order 2 in the flattenings, is

$$\chi_i^{(1)}(U''_j) = G\frac{4\pi}{3} d_j \left[2\left(\epsilon_\rho^{(i)} + \epsilon_z^{(i)}\right) - \frac{6\left(\epsilon_\rho^{(j-1)} + \epsilon_z^{(j-1)}\right)}{5} \right]. \tag{B.7}$$

Then, the total contribution of the outer layers to the first equilibrium equation is

$$\sum_{j=i+1}^{N} \chi_i^{(1)}(U_j) = \sum_{j=i+1}^{N} \chi_i^{(1)}(U'_j) - \sum_{j=i+1}^{N} \chi_i^{(1)}(U''_j), \tag{B.8}$$

and using the above results, we obtain

$$\sum_{j=i+1}^{N} \chi_i^{(1)}(U_j) = G\frac{4\pi}{3} d_{i+1} \frac{6}{5} \left(\epsilon_\rho^{(i)} + \epsilon_z^{(i)}\right) - G\frac{4\pi}{3} \sum_{j=i+1}^{N} (d_j - d_{j+1}) \frac{6}{5} \left(\epsilon_\rho^{(j)} + \epsilon_z^{(j)}\right). \tag{B.9}$$

Analogously, the total contribution of the outer layers to the second equilibrium equation is

$$\sum_{j=i+1}^{N} \chi_i^{(2)}(U_j) = G\frac{4\pi}{3} d_{i+1} \frac{6}{5} \epsilon_z^{(i)} - G\frac{4\pi}{3} \sum_{j=i+1}^{N} (d_j - d_{j+1}) \frac{6}{5} \epsilon_z^{(j)}. \tag{B.10}$$

B.3 The contribution of the inner layers

The gravitational potential U_j' generated by one ellipsoid with density d_j and the same surface as the outer boundary of the j-th layer, at an external point $\mathbf{r}_i = x_i\hat{\mathbf{x}} + y_i\hat{\mathbf{y}} + z_i\hat{\mathbf{z}}$ on the surface of the i-th layer may be presented by Laplace series. Neglecting harmonics of degree higher than 2 we have (see Eq. (A.13))

$$U_j'(\mathbf{r}_i) = -\frac{Gm_j'}{r_i} - \frac{GC_j'}{2r_i^5} \left(\epsilon_\rho^{(j)} + \epsilon_z^{(j)}\right) \left(3x_i^2 - r_i^2\right) - \frac{GC_j'}{2r_i^5} \epsilon_z^{(j)} \left(3y_i^2 - r_i^2\right), \tag{B.11}$$

and its derivatives are

$$\begin{aligned}
\frac{1}{x_i}\frac{\partial U_j'}{\partial x_i} &= \frac{Gm_j'}{r_i^3} + \frac{GC_j'}{2r_i^5}(\epsilon_\rho^{(j)} - 2\epsilon_z^{(j)}) + \\
&\quad + \frac{5GC_j'}{2r_i^7}(\epsilon_\rho^{(j)} + \epsilon_z^{(j)}) \left(3x_i^2 - r_i^2\right) + \frac{5GC_j'}{2r_i^7} \epsilon_z^{(j)} \left(3y_i^2 - r_i^2\right) \\
\frac{1}{y_i}\frac{\partial U_j'}{\partial y_i} &= \frac{Gm_j'}{r_i^3} + \frac{GC_j'}{2r_i^5}(7\epsilon_\rho^{(j)} - 2\epsilon_z^{(j)}) + \\
&\quad + \frac{5GC_j'}{2r_i^7}(\epsilon_\rho^{(j)} + \epsilon_z^{(j)}) \left(3x_i^2 - r_i^2\right) + \frac{5GC_j'}{2r_i^7} \epsilon_z^{(j)} \left(3y_i^2 - r_i^2\right) \\
\frac{1}{z_i}\frac{\partial U_j'}{\partial z_i} &= \frac{Gm_j'}{r_i^3} + \frac{GC_j'}{2r_i^5}(7\epsilon_\rho^{(j)} + 4\epsilon_z^{(j)}) + \\
&\quad + \frac{5GC_j'}{2r_i^7}(\epsilon_\rho^{(j)} + \epsilon_z^{(j)}) \left(3x_i^2 - r_i^2\right) + \frac{5GC_j'}{2r_i^7} \epsilon_z^{(j)} \left(3y_i^2 - r_i^2\right).
\end{aligned} \tag{B.12}$$

Making the approximation $r_i \simeq R_i$, the contribution to the first equilibrium equation, to first order in flattenings, is

$$\chi_i^{(1)}(U_j') = G\frac{4\pi}{3}\frac{R_j^3}{R_i^3} \left[2\left(\epsilon_\rho^{(i)} + \epsilon_z^{(i)}\right) - \frac{6R_j^2}{5R_i^2}\left(\epsilon_\rho^{(j)} + \epsilon_z^{(j)}\right)\right]. \tag{B.13}$$

Similarly, if we consider the potential U_j'' of the one ellipsoid with density d_j and the same surface as the inner boundary of the j-th, its contribution to the first equilibrium

equation, neglecting terms of order 2 in the flattenings, is

$$\chi_i^{(1)}(U_j'') = G\frac{4\pi}{3}\frac{R_{j-1}^3}{R_i^3}\left[2\left(\epsilon_\rho^{(i)}+\epsilon_z^{(i)}\right)-\frac{6R_{j-1}^2}{5R_i^2}\left(\epsilon_\rho^{(j-1)}+\epsilon_z^{(j-1)}\right)\right]. \tag{B.14}$$

Then, the total contribution of the inner layers to the first equilibrium equation is

$$\begin{aligned}\sum_{j=1}^{i}\chi_i^{(1)}(U_j) &= G\frac{4\pi}{3}\left[2d_i-\frac{6}{5}d_i+\sum_{j=1}^{i-1}2(d_j-d_{j+1})\frac{R_j^3}{R_i^3}\right]\left(\epsilon_\rho^{(i)}+\epsilon_z^{(i)}\right)- \\ &\quad -G\frac{4\pi}{3}\sum_{j=1}^{i-1}\frac{6}{5}(d_j-d_{j+1})\frac{R_j^5}{R_i^5}\left(\epsilon_\rho^{(j)}+\epsilon_z^{(j)}\right),\end{aligned} \tag{B.15}$$

or, using that

$$\sum_{j=1}^{N}\frac{4\pi}{3}(d_j-d_{j+1})R_j^3=\sum_{j=1}^{N}\frac{4\pi}{3}d_j(R_j^3-R_{j-1}^3)=m_T, \tag{B.16}$$

we obtain

$$\begin{aligned}\sum_{j=1}^{i}\chi_i^{(1)}(U_j) &= G\frac{4\pi}{3}\left[\frac{3m_T}{2\pi R_i^3}-\frac{6d_i}{5}-\sum_{j=i+1}^{N}2(d_j-d_{j+1})\frac{R_j^3-R_i^3}{R_i^3}\right]\left(\epsilon_\rho^{(i)}+\epsilon_z^{(i)}\right)- \\ &\quad -G\frac{4\pi}{3}\sum_{j=1}^{i-1}\frac{6}{5}(d_j-d_{j+1})\frac{R_j^5}{R_i^5}\left(\epsilon_\rho^{(j)}+\epsilon_z^{(j)}\right).\end{aligned} \tag{B.17}$$

Analogously, the total contribution of the inner layers to the second equilibrium equation is

$$\begin{aligned}\sum_{j=1}^{i}\chi_i^{(2)}(U_j) &= G\frac{4\pi}{3}\left[\frac{3m_T}{2\pi R_i^3}-\frac{6d_i}{5}-\sum_{j=i+1}^{N}2(d_j-d_{j+1})\frac{R_j^3-R_i^3}{R_i^3}\right]\epsilon_z^{(i)}- \\ &\quad -G\frac{4\pi}{3}\sum_{j=1}^{i-1}\frac{6}{5}(d_j-d_{j+1})\frac{R_j^5}{R_i^5}\epsilon_z^{(j)}.\end{aligned} \tag{B.18}$$

B.4 The contribution of the tidal potential

If $\mathbf{r}=r\hat{x}$ is the position of the mass M, the tidal potential, to second order, at a point $\mathbf{r}_i=x_i\hat{\mathbf{x}}+y_i\hat{\mathbf{y}}+z_i\hat{\mathbf{z}}$ on the surface of the i-th layer is (Lambeck 1980)

$$U_{tid}=-\frac{GMr_i^2}{r^3}P_2(\hat{\mathbf{r}}\cdot\hat{\mathbf{r}}_i) \tag{B.19}$$

where P_2 is the Legendre polynomial of degree two. The differential acceleration of this point is

$$-\nabla_{\mathbf{r}_i}U_{tid}=-\frac{GM}{r^3}\left[\mathbf{r}_i-\frac{3(\mathbf{r}_i\cdot\mathbf{r})}{r^2}\mathbf{r}\right]=-\frac{GM}{r^3}\begin{bmatrix}-2x_i\\ y_i\\ z_i\end{bmatrix}, \tag{B.20}$$

therefore their derivatives are

$$\begin{aligned}\frac{1}{x_i}\frac{\partial U_{tid}}{\partial x_i} &= -\frac{2GM}{r^3}\\ \frac{1}{y_i}\frac{\partial U_{tid}}{\partial y_i} &= \frac{GM}{r^3}\\ \frac{1}{z_i}\frac{\partial U_{tid}}{\partial z_i} &= \frac{GM}{r^3}.\end{aligned} \tag{B.21}$$

Finally, the contribution of the tide in the equilibrium equations of the i-th surface is

$$\begin{aligned}\chi_i^{(1)}(U_{tid}) &= -\frac{3GM}{r^3} + \frac{4GM}{r^3}\left(\epsilon_\rho^{(i)} + \epsilon_z^{(i)}\right)\\ \chi_i^{(2)}(U_{tid}) &= \frac{4GM}{r^3}\epsilon_z^{(i)}.\end{aligned} \tag{B.22}$$

However, we discard terms which containing $\epsilon_\rho^{(i)}, \epsilon_z^{(i)}$, because when we calculate the flattenings of each layer, they appear multiplied by a factor of the same order as $\epsilon_\rho^{(k)}, \epsilon_z^{(k)}$, therefore we obtain

$$\begin{aligned}\chi_i^{(1)}(U_{tid}) &= -\frac{3GM}{r^3}\\ \chi_i^{(2)}(U_{tid}) &= 0.\end{aligned} \tag{B.23}$$

Appendix C

The relaxation factor

Let us consider the equilibrium surface $\rho_i(\phi, \theta)$ between two adjacent homogeneous layers of the body m whose densities are d_i (inner) and d_{i+1} (outer). We consider that at a given instant, the actual surface between the two layers $\zeta_i(\phi, \theta)$ does not coincide with the equilibrium surface (Fig. C.1). In some parts, the separation surface is above the equilibrium surface (as in region I) and in other parts it is below the equilibrium surface (as in the region II). Let us now consider one small element of the equilibrium surface in region I. The pressure in the base of this element is positive because the weight of the column above the element is larger than its weight in the equilibrium configuration. Note that the column is now partly occupied by the fluid with density d_i and $d_i > d_{i+1}$. The pressure surplus is given by

$$p_I = \Delta w h, \tag{C.1}$$

where $\Delta w = (d_i - d_{i+1})g$ is the difference of the specific weight of the two columns in the neighborhood of the separation surface, and h is the distance of the element of the equilibrium surface to the actual separation surface. g is the local acceleration of gravity.

The radial flow in the considered element is ruled by the Navier-Stokes equation:

$$0 = F_{ext} - \nabla p_I + \eta_i \boldsymbol{\Delta} \mathbf{u} \tag{C.2}$$

where F_{ext} is the external force per unit volume (equal to zero if no other external forces are acting on the fluid), u is the radial velocity and η_i is the viscosity of the layer i (assuming $\eta_i > \eta_{i+1}$). We notice that $\boldsymbol{\Delta}$ is operating on a vector, contrary to the usual Δ. Actually in this pseudo-vectorial notation, the formula refers to the components of $\mathbf{u}$ and means the vector formed by the operation of the classical Δ on the three components of the vector

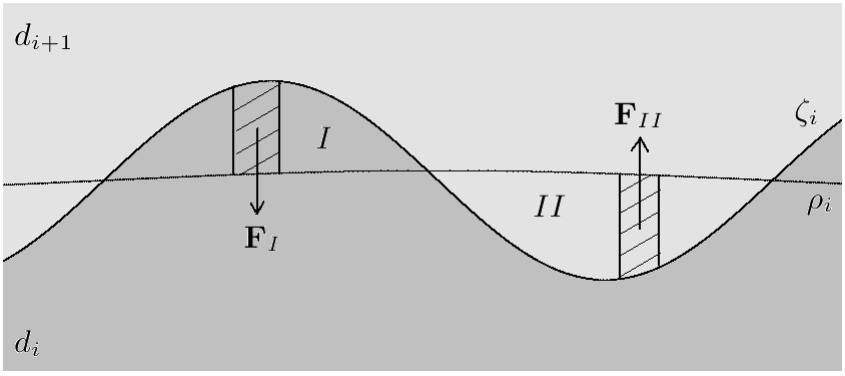

Figure C.1: Interface between two adjacent homogeneous layers of m whose densities are d_i (inner) and d_{i+1} (outer). $\zeta_i(\phi,\theta)$ and $\rho_i(\phi,\theta)$ are the actual and the equilibrium surfaces, respectively, of the outer boundary of the i-th layer. I (resp. II) is the region where the actual surface is above (resp. below) the equilibrium surface. $\mathbf{F}_I$ (resp. $\mathbf{F}_{II}$) is the force acting on one small element of the equilibrium surface in the region I (resp. region II) due to the pressure surplus (resp. pressure deficit).

$\mathbf{u}$. We assume that the flow, respect to the equilibrium surface, is radial and thus $\mathbf{u}$ is restricted to its radial component u_r. That is

$$0 \approx \Delta w + \eta_i \, \nabla^2 u_r. \tag{C.3}$$

Then

$$\nabla^2 u_r = \frac{\partial^2 u_r}{\partial r^2} + \frac{2}{r}\frac{\partial u_r}{\partial r} - \frac{2u_r}{r^2} = -\frac{\Delta w}{\eta_i}. \tag{C.4}$$

The general solution of this equation is

$$u_r(r) = C_1 r + \frac{C_2}{r^2} - \frac{\Delta w}{4\eta_i} r^2, \tag{C.5}$$

where C_1 and C_2 are integration constants. The task of interpreting and determining its integration constants becomes easier if the solution is linearized in the neighborhood of $r = \rho_i$ (i.e. $h = 0$):

$$u_r(r) = u_r(\rho_i) + u_r'(\rho_i)(r-\rho_i) + \frac{1}{2}u_r''(\rho_i)(r-\rho_i)^2 + ... \tag{C.6}$$

Hence $u_r(\rho_i) = 0$, that is, there is no pressure surplus (or deficit) when the actual separation surface coincides with the equilibrium and the linear approximation of the solution is obtained when we assume $u_r''(\rho_i) = 0$.

Therefore

$$\begin{aligned} C_1 &= \rho \Delta w / 6\eta_i \\ C_2 &= \rho^4 \Delta w / 12\eta_i. \end{aligned} \tag{C.7}$$

Hence $u_r'(\rho_i) = \rho_i \Delta w / 2\eta_i$, and the linear approximation corresponding to the Newtonian creep of the fluid is

$$u_r(r) = \gamma_i (r - \rho_i), \tag{C.8}$$

where

$$\gamma_i = u_r'(\rho_i) = \frac{\Delta w \rho_i}{2\eta_i}. \tag{C.9}$$

In the region II the calculation is similar; however, instead of a pressure surplus we have a pressure deficit because the equilibrium assumes one fluid with density d_i below the equilibrium surface, which is now occupied by fluid of density $d_{i+1} < d_i$. The equations are the same as above. We note that in the new equations, the adopted viscosity continues being η_i since we assumed it larger than η_{i+1}. The relaxation of the surface to the equilibrium will be governed by the larger of the viscosities of the two layers.

In the homogeneous case we have one layer body ($N = 1$). If we consider $d_{N+1} = 0$ (neglected the density of the atmosphere), we recover the expression of the relaxation factor of FM13 and FM15

$$\gamma_N \approx \frac{w R_N}{2\eta_N}, \tag{C.10}$$

where $w = d_N g$ is the specific weight and $\rho_N \approx R_N$.

Appendix D

The integral of section 3.7

Proposition:

$$\frac{1}{2\pi}\int_0^{2\pi} \Omega_j^2 \left(\frac{a}{r}\right)^4 \sin v \; d\ell = 0. \tag{D.1}$$

To prove (D.1), we consider only the tidal force. Introducing the adimensinals variables and time

$$y_i = \frac{\nu_i}{\gamma_i}; \qquad x = nt = \ell, \tag{D.2}$$

the rotational system can be written as

$$\begin{aligned}
\dot{y}_1 &= -T_{11}^* \sum_{k,j\in\mathbb{Z}} E_{2,k}E_{2,k+j}\frac{(y_1+P_{1k})\cos(jx)+\sin(jx)}{1+(y_1+P_{1k})^2} \\
\dot{y}_2 &= -T_{22}^* \sum_{k,j\in\mathbb{Z}} E_{2,k}E_{2,k+j}\frac{(y_2+P_{2k})\cos(jx)+\sin(jx)}{1+(y_2+P_{2k})^2} + \\
&\quad +T_{21}^* \sum_{k,j\in\mathbb{Z}} E_{2,k}E_{2,k+j}\frac{(y_1+P_{1k})\cos(jx)+\sin(jx)}{1+(y_1+P_{1k})^2} \\
&\vdots \\
\dot{y}_N &= -T_{NN}^* \sum_{k,j\in\mathbb{Z}} E_{2,k}E_{2,k+j}\frac{(y_N+P_{Nk})\cos(jx)+\sin(jx)}{1+(y_N+P_{Nk})^2} + \\
&\quad +T_{NN-1}^* \sum_{k,j\in\mathbb{Z}} E_{2,k}E_{2,k+j}\frac{(y_{N-1}+P_{N-1k})\cos(jx)+\sin(jx)}{1+(y_{N-1}+P_{N-1k})^2}.
\end{aligned} \tag{D.3}$$

where the constants

$$T_{ij}^* = \frac{2\mathcal{T}}{\gamma_i n}\frac{\mathcal{H}_j R_j^5}{R_i^5 - R_{i-1}^5}; \qquad P_{ik} = \frac{kn}{\gamma_i}. \tag{D.4}$$

In low-γ approximation ($\gamma_i \ll n$), we can neglet the terms $k \neq 0$. If we consider only

the terms $j = 0$, the system becomes

$$\begin{aligned}
\dot{y}_1 &= -\frac{T^*_{11}E^2_{2,0}y_1}{1+y_1^2} \\
\dot{y}_2 &= -\frac{T^*_{22}E^2_{2,0}y_2}{1+y_2^2} + \frac{T^*_{21}E^2_{2,0}y_1}{1+y_1^2} \\
&\vdots \\
\dot{y}_N &= -\frac{T^*_{NN}E^2_{2,0}y_N}{1+y_N^2} + \frac{T^*_{NN-1}E^2_{2,0}y_{N-1}}{1+y_{N-1}^2}.
\end{aligned} \tag{D.5}$$

In the same way in Ferraz-Mello (2015a), each solution of this system tends to zero. The role of the terms $j \neq 0$ that are periodic fluctuations which are the harmonics of the orbital period are added to the solution. If we consider the terms $j \neq 0$, we have that $y_i \ll 1$, and the rotational system is

$$\dot{y}_i = -\sum_{j\in\mathbb{Z}\ j\neq 0} K_{ij}\sin(jx), \tag{D.6}$$

where $K_{ij} = (T^*_{ii} - T^*_{ii-1})E_{2,0}E_{2,j}$.

The solution of this differential equation is

$$y_i(x) = y_{i0} - K_{ij} + \sum_{j\in\mathbb{Z}\ j\neq 0} \frac{K_{ij}}{j}\cos(jx), \tag{D.7}$$

or, in term of the angular velocity, we obtain

$$\Omega_i = \Omega_{i0} - \frac{\gamma_i K_{ij}}{2} + \sum_{j\in\mathbb{Z}\ j\neq 0} \frac{\gamma_i K_{ij}}{2j}\cos(jnt). \tag{D.8}$$

Therefore, the square of the angular velocity of the j-th layer can be written as

$$\Omega_j^2 = \sum_{k=0}^{\infty} A_{jk}\cos k\ell. \tag{D.9}$$

Finally, the integral (D.1) is

$$\begin{aligned}
&\frac{1}{2\pi}\int_0^{2\pi} \Omega_j^2\left(\frac{a}{r}\right)^4 \sin v\ d\ell = \\
&\qquad \sum_{k=0}^{\infty}\frac{A_{jk}}{2}\left(\frac{1}{2\pi}\int_0^{2\pi}\left(\frac{a}{r}\right)^4\sin(v+k\ell)\ d\ell - \frac{1}{2\pi}\int_0^{2\pi}\left(\frac{a}{r}\right)^4\sin(v-k\ell)\ d\ell\right) = 0.
\end{aligned} \tag{D.10}$$

In high-γ approximation ($\gamma_i \gg n$), we can neglet P_{ik}, then, the system can be written as

$$\begin{aligned}
\dot{y}_1 &= -T^*_{11} \sum_{k,j\in\mathbb{Z}} E_{2,k}E_{2,k+j} \frac{y_1 \cos(jx) + \sin(jx)}{1+y_1^2} \\
\dot{y}_2 &= -T^*_{22} \sum_{k,j\in\mathbb{Z}} E_{2,k}E_{2,k+j} \frac{y_2 \cos(jx) + \sin(jx)}{1+y_2^2} + \\
&\quad +T^*_{21} \sum_{k,j\in\mathbb{Z}} E_{2,k}E_{2,k+j} \frac{y_1 \cos(jx) + \sin(jx)}{1+y_1^2} \\
&\vdots \\
\dot{y}_N &= -T^*_{NN} \sum_{k,j\in\mathbb{Z}} E_{2,k}E_{2,k+j} \frac{y_N \cos(jx) + \sin(jx)}{1+y_N^2} + \\
&\quad +T^*_{NN-1} \sum_{k,j\in\mathbb{Z}} E_{2,k}E_{2,k+j} \frac{y_{N-1} \cos(jx) + \sin(jx)}{1+y_{N-1}^2}.
\end{aligned} \tag{D.11}$$

If we consider only the terms $j = 0$, the system becomes

$$\begin{aligned}
\dot{y}_1 &= -T^*_{11} \sum_{k\in\mathbb{Z}} E^2_{2,k} \frac{y_1}{1+y_1^2} \\
\dot{y}_2 &= -T^*_{22} \sum_{k\in\mathbb{Z}} E^2_{2,k} \frac{y_2}{1+y_2^2} + T^*_{21} \sum_{k\in\mathbb{Z}} E^2_{2,k} \frac{y_1}{1+y_1^2} \\
&\vdots \\
\dot{y}_N &= -T^*_{NN} \sum_{k\in\mathbb{Z}} E^2_{2,k} \frac{y_N}{1+y_N^2} + T^*_{NN-1} \sum_{k\in\mathbb{Z}} E^2_{2,k} \frac{y_{N-1}}{1+y_{N-1}^2},
\end{aligned} \tag{D.12}$$

which is identical to the system D.5, with $\sum_{k\in\mathbb{Z}} E^2_{2,k}$ instead of $E^2_{2,0}$. Therefore, each solution of this system tends to zero. As in low-γ approximation, the role of the terms $j \neq 0$ are periodic fluctuations which are the harmonics of the orbital period are added to the solution. If we consider the terms $j \neq 0$, we have that $y_i \ll 1$, and the rotational system is

$$\dot{y}_i = -\sum_{j\in\mathbb{Z}\ j\neq 0} K'_{ij} \sin(jx), \tag{D.13}$$

where $K'_{ij} = (T^*_{ii} - T^*_{ii-1}) \sum_{k\in\mathbb{Z}} E_{2,k}E_{2,k+j}$.

Using the solution of the low-γ approximation, then, the angular velocity is

$$\Omega_i = \Omega_{i0} - \frac{\gamma_i K'_{ij}}{2} + \sum_{j\in\mathbb{Z}\ j\neq 0} \frac{\gamma_i K'_{ij}}{2j} \cos(jnt), \tag{D.14}$$

and the integral (D.1) is zero.

Appendix E

Fluid Love's number of the i-th layer

E.1 The tidal fluid Love number of the i-th layer

The disturbing potential generated by the i-th homogeneous ellipsoidal layer, deformed only by the tide due to a mass point M of mass M orbiting at a distance r, at an external point $\mathbf{r}^*$ is

$$\delta U_i^{(tid)}(\mathbf{r}^*) = -\frac{GC_i\mathcal{L}_i}{2r^{*3}}\epsilon_J(3\cos^2\varphi^*\sin^2\theta^* - 1) = -\frac{15GMR_N^3C_i\mathcal{L}_i}{8m_Tr^3r^{*3}}(3\cos^2\varphi^*\sin^2\theta^* - 1), \tag{E.1}$$

(see Eq. (A.34)).

On the other hand, the tidal potential at the same point $\mathbf{r}^*$ is

$$U_{tid}(\mathbf{r}^*) = -\frac{GMr^{*2}}{2r^3}(3\cos^2\varphi^*\sin^2\theta^* - 1). \tag{E.2}$$

The Love's theorem says that (Munk and MacDonald, 1960; Correia and Rodriguez, 2013)

$$\delta U_i^{(tid)}(R_i) = k_iU_{tid}(R_i), \tag{E.3}$$

therefore, we obtain

$$\boxed{k_i = \frac{15C_i}{4m_TR_i^2}\frac{\mathcal{L}_iR_N^3}{R_i^3}.} \tag{E.4}$$

The constant k_i is tidal fluid Love number of the i-th layer, and can be rewritten as

$$k_i = \widehat{k}_i\mathcal{L}_i, \tag{E.5}$$

where $\mathcal{L}_i$ is given by Eq. (A.32), and

$$\widehat{k}_i = \frac{15C_i}{4m_TR_i^2}\frac{R_N^3}{R_i^3}. \tag{E.6}$$

E.2 The rotational fluid Love number of the i-th layer

The disturbing potential generated by the i-th homogeneous ellipsoidal layer, deformed only by the rotation with angular velocity Ω_i, at an external point $\mathbf{r}^*$ is

$$\begin{aligned} \delta U_i^{(cen)}(\mathbf{r}^*) &= -\frac{GC_i\mathcal{L}'_i}{2r^{*3}}\bar{\epsilon}_M(3\sin^2\theta^* - 2) = -\frac{15R_N^3n^2C_i\mathcal{L}'_i}{8m_Tr^{*3}}\sin^2\theta^* + \frac{5R_N^3n^2C_i\mathcal{L}'_i}{4m_Tr^{*3}} \\ &= \delta U_i^{\prime(cen)}(\mathbf{r}^*) + \frac{5R_N^3n^2C_i\mathcal{L}'_i}{4m_Tr^{*3}}, \end{aligned} \tag{E.7}$$

(see Eq. (A.34)).

The centrifugal potential at the same point $\mathbf{r}^*$ is

$$U_{cen}(\mathbf{r}^*) = -\frac{1}{2}\Omega_i^2r^{*2}\sin^2\theta^*. \tag{E.8}$$

The Love's theorem say that

$$\delta U_i^{\prime(cen)}(R_i) = k'_iU_{cen}(R_i), \tag{E.9}$$

therefore

$$\boxed{k'_i = \frac{15C_i}{4mR_i^2}\frac{n^2\mathcal{L}'_iR_N^3}{\Omega_i^2R_i^3}.} \tag{E.10}$$

The constant k'_i is rotational fluid Love number of the i-th layer, and can be rewritten as

$$k'_i = \widehat{k}_i\frac{n^2\mathcal{L}'_i}{\Omega_i^2}, \tag{E.11}$$

where $\mathcal{L}'_i$ and $\widehat{k}_i$ are given by Eqs. (A.32) and (E.6), respectively.

E.3 Potential of the tidally deformed layer

Finally, using Eqs. (E.5) ana (E.11) in the disturbing potential (A.34), we obtain

$$\boxed{\delta U_i(\mathbf{r}^*) = -\frac{k_iGMR_i^5}{2r^{*3}r^3}(3\cos^2\psi - 1) - \frac{k'_i\Omega_i^2R_i^5}{2r^{*3}}\left(\sin^2\theta^* - \frac{2}{3}\right).} \tag{E.12}$$

Appendix F

The Cayley functions

In this appendix we complete some calculations used in chapters 3 and 6. We also show the Cayley coefficients $E_{0,k}$ and $E_{2,k}$, for $|k| \leq 4$.

F.1 Auxiliary formulas

In this section we complete some calculations used in the Eqs. (3.38) and (6.26). For this sake, we use the Fourier expansion given in the Online Suplement of Ferraz-Mello (2015):

$$\left(\frac{a}{r}\right)^n \sin\left(qv + (p-q)\ell + \Phi\right) = \sum_{j=-\infty}^{\infty} E^{(n)}_{q,p+j} \sin\left(\Phi - j\ell\right), \tag{F.1}$$

and

$$\left(\frac{a}{r}\right)^n \cos\left(qv + (p-q)\ell + \Phi\right) = \sum_{j=-\infty}^{\infty} E^{(n)}_{q,p+j} \cos\left(\Phi - j\ell\right), \tag{F.2}$$

where the more general Cayley function is defined as:

$$E^{(n)}_{q,p}(e) = \frac{1}{2\pi}\int_0^{2\pi} \left(\frac{a}{r}\right)^n \cos\left(qv + (p-q)\ell\right)\, d\ell. \tag{F.3}$$

We also use the auxiliary formulas:

$$kE^{(3)}_{0,k} = \frac{3e}{2\sqrt{1-e^2}}\left(E^{(4)}_{1,1-k} - E^{(4)}_{1,1+k}\right), \tag{F.4}$$

and

$$(2-k)E^{(3)}_{2,k} = \frac{3e}{2\sqrt{1-e^2}}\left(E^{(4)}_{3,k+1} - E^{(4)}_{1,k-1}\right) + 2\sqrt{1-e^2}E^{(5)}_{2,k}, \tag{F.5}$$

(see Online Suplement of Ferraz-Mello (2015) for more details).

Proposition 1:

$$\begin{aligned} F_1 &= \frac{3e}{2\sqrt{1-e^2}}\left(\frac{a}{r}\right)^4 \sin v \sin\left(2v+(k-2)\ell\right) - \sqrt{1-e^2}\left(\frac{a}{r}\right)^5 \cos\left(2v+(k-2)\ell\right) \\ &= -\frac{1}{2}\sum_{j=-\infty}^{\infty}(2-k-j)E^{(3)}_{2,k}\cos j\ell. \end{aligned} \tag{F.6}$$

Using Eq. (F.2), with $\Phi = 0$, we obtain

$$\begin{aligned} \left(\frac{a}{r}\right)^4 \sin v \sin\left(2v+(k-2)\ell\right) &= \frac{1}{2}\left(\frac{a}{r}\right)^4 \Big(\cos\left(v+(k-2)\ell\right) - \cos\left(3v+(k-2)\ell\right)\Big) \\ &= -\frac{1}{2}\sum_{j=-\infty}^{\infty}\left(E^{(4)}_{3,k+j+1} - E^{(4)}_{1,k+j-1}\right)\cos j\ell, \end{aligned} \tag{F.7}$$

and

$$\left(\frac{a}{r}\right)^5 \cos\left(2v+(k-2)\ell\right) = \sum_{j=-\infty}^{\infty} E^{(5)}_{2,k+j}\cos j\ell. \tag{F.8}$$

Then

$$F_1 = -\frac{1}{2}\sum_{j=-\infty}^{\infty}\left(\frac{3e}{2\sqrt{1-e^2}}\left(E^{(4)}_{3,k+j+1} - E^{(4)}_{1,k+j-1}\right) + 2\sqrt{1-e^2}\sum_{j=-\infty}^{\infty}E^{(5)}_{2,k+j}\right)\cos j\ell, \tag{F.9}$$

or, using (F.5), with the transformation $k \longrightarrow k+j$

$$F_1 = -\frac{1}{2}\sum_{j=-\infty}^{\infty}(2-k-j)E^{(3)}_{2,k}\cos j\ell. \tag{F.10}$$

Proposition 2:

$$\begin{aligned} F_2 &= \frac{3e}{2\sqrt{1-e^2}}\left(\frac{a}{r}\right)^4 \sin v \cos\left(2v+(k-2)\ell\right) + \sqrt{1-e^2}\left(\frac{a}{r}\right)^5 \sin\left(2v+(k-2)\ell\right) \\ &= -\frac{1}{2}\sum_{j=-\infty}^{\infty}(2-k-j)E^{(3)}_{2,k}\sin j\ell. \end{aligned} \tag{F.11}$$

Using Eq. (F.1), with $\Phi = 0$, we obtain

$$\begin{aligned} \left(\frac{a}{r}\right)^4 \sin v \cos\left(2v+(k-2)\ell\right) &= \frac{1}{2}\left(\frac{a}{r}\right)^4 \Big(\sin\left(3v+(k-2)\ell\right) - \sin\left(v+(k-2)\ell\right)\Big) \\ &= -\frac{1}{2}\sum_{j=-\infty}^{\infty}\left(E^{(4)}_{3,k+j+1} - E^{(4)}_{1,k+j-1}\right)\sin j\ell, \end{aligned} \tag{F.12}$$

and

$$\left(\frac{a}{r}\right)^5 \cos\left(2v+(k-2)\ell\right) = -\sum_{j=-\infty}^{\infty} E^{(5)}_{2,k+j}\sin j\ell. \tag{F.13}$$

Then

$$F_2 = -\frac{1}{2}\sum_{j=-\infty}^{\infty}\left(\frac{3e}{2\sqrt{1-e^2}}\left(E^{(4)}_{3,k+j+1} - E^{(4)}_{1,k+j-1}\right) + 2\sqrt{1-e^2}\sum_{j=-\infty}^{\infty}E^{(5)}_{2,k+j}\right)\sin j\ell, \tag{F.14}$$

or, using (F.5), with the transformation $k \longrightarrow k+j$

$$F_2 = -\frac{1}{2}\sum_{j=-\infty}^{\infty}(2-k-j)E^{(3)}_{2,k}\sin j\ell. \tag{F.15}$$

Proposition 3:

$$F_3 = \frac{3e}{2\sqrt{1-e^2}}\left(\frac{a}{r}\right)^4 \sin v \sin k\ell = \frac{1}{2}\sum_{j=-\infty}^{\infty}(k+j)E^{(3)}_{0,k}\cos j\ell. \tag{F.16}$$

Using Eq. (F.2), with $\Phi = 0$, we obtain

$$\begin{aligned}\left(\frac{a}{r}\right)^4 \sin v \sin k\ell &= \frac{1}{2}\left(\frac{a}{r}\right)^4\Big(\cos(v-k\ell) - \cos(v+k\ell)\Big)\\ &= \frac{1}{2}\sum_{j=-\infty}^{\infty}\left(E^{(4)}_{1,1-k-j} - E^{(4)}_{1,1+k+j}\right)\cos j\ell.\end{aligned} \tag{F.17}$$

Then

$$F_3 = \frac{1}{2}\frac{3e}{2\sqrt{1-e^2}}\sum_{j=-\infty}^{\infty}\left(E^{(4)}_{1,1-k-j} - E^{(4)}_{1,1+k+j}\right)\cos j\ell. \tag{F.18}$$

or, using (F.4), with the transformation $k \longrightarrow k+j$

$$F_3 = \frac{1}{2}\sum_{j=-\infty}^{\infty}(k+j)E^{(3)}_{0,k}\cos j\ell. \tag{F.19}$$

Proposition 4:

$$F_4 = \frac{3e}{2\sqrt{1-e^2}}\left(\frac{a}{r}\right)^4 \sin v \cos k\ell = \frac{1}{2}\sum_{j=-\infty}^{\infty}(k+j)E^{(3)}_{0,k}\cos j\ell. \tag{F.20}$$

Using Eq. (F.1), with $\Phi = 0$, we obtain

$$\begin{aligned}\left(\frac{a}{r}\right)^4 \sin v \cos k\ell &= \frac{1}{2}\left(\frac{a}{r}\right)^4\Big(\sin(v+k\ell) + \sin(v-k\ell)\Big)\\ &= -\frac{1}{2}\sum_{j=-\infty}^{\infty}\left(E^{(4)}_{1,1+k+j} - E^{(4)}_{1,1-k-j}\right)\sin j\ell.\end{aligned} \tag{F.21}$$

Then

$$F_4 = \frac{1}{2}\frac{3e}{2\sqrt{1-e^2}}\sum_{j=-\infty}^{\infty}\left(E^{(4)}_{1,1-k-j} - E^{(4)}_{1,1+k+j}\right)\sin j\ell. \tag{F.22}$$

or, using (F.4), with the transformation $k \longrightarrow k+j$

$$F_4 = \sum_{j=-\infty}^{\infty}(k+j)E^{(3)}_{0,k}\sin j\ell. \tag{F.23}$$

F.2 Cayley coefficients

$$\begin{aligned} E_{0,0} &= 1 + \frac{3}{2}e^2 + \frac{15}{8}e^4 \\ E_{0,1} &= \frac{3}{2}e + \frac{27}{16}e^3 \\ E_{0,2} &= \frac{9}{4}e^2 + \frac{7}{4}e^4 \\ E_{0,3} &= \frac{53}{16}e^3 \\ E_{0,4} &= \frac{77}{16}e^4 \end{aligned} \tag{F.24}$$

Table F.1 - Cayley coefficients $E_{0,k}$ to $\mathcal{O}(e^4)$. $E_{0,-k} = E_{0,k}$.

$$\begin{aligned} E_{2,-4} &= \frac{533}{16}e^4 \\ E_{2,-3} &= \frac{845}{48}e^3 \\ E_{2,-2} &= \frac{17}{2}e^2 - \frac{115}{6}e^4 \\ E_{2,-1} &= \frac{7}{2}e - \frac{123}{16}e^3 \\ E_{2,0} &= 1 - \frac{5}{2}e^2 + \frac{13}{16}e^4 \\ E_{2,1} &= -\frac{1}{2}e + \frac{1}{16}e^3 \\ E_{2,2} &= 0 \\ E_{2,3} &= \frac{1}{48}e^3 \\ E_{2,4} &= \frac{1}{24}e^4 \end{aligned} \tag{F.25}$$

Table F.2 - Cayley coefficients $E_{2,k}$ to $\mathcal{O}(e^4)$.